Journal of the Geological Survey of Brazil

The Serra do Caparaó Complex, Mantiqueira Province, Brazil, revisited: metamorphic age constraints by U-Pb and Lu-Hf method in zircon by LA-ICP-MS

Thaís G. Faria[1,4], Marcio I. Alves[1], Guilherme L. Potratz[1], Luiz Felipe Romero da Silva[1], Sergio W.O. Rodrigues[2], Maria V. A. Martins[1,3], Mauro C. Geraldes[1,*]

[1]Universidade do Estado do Rio de Janeiro, UERJ, Faculdade de Geologia, Av. São Francisco Xavier, 24, sala 2020A, Maracanã. Rio de Janeiro, RJ, Brazil, CEP: 20550-013
[2]Instituto de Ciências e Tecnologia, Universidade Federal de Goiás-Rua Mucuri s/n. Aparecida de Goiânia, Goiás – Brazil. CEP: 74968-755
[3]Universidade de Aveiro, GeoBioTec, Departamento de Geociências, Campus de Santiago, 3810-193 Aveiro, Portugal
[4]Present Address: IFES - Instituto Federal do Espírito Santo, Campus Cachoeiro do Itapemirim. Rodovia Engenheiro Fabiano Vivácqua, 1568, Morro Grande, Cachoeiro de Itapemirim - ES. CEP 29.322-000

Abstract

The U-Pb method was used in order to understand the high-grade metamorphic rocks in the Ribeira Belt (SE Brazil) and Lu-Hf isotopes were applied to investigate the magmatic photolith sources and the tectonic setting of Serra do Caparaó Complex rocks. The results indicate the existence of two thermal events: the first related to a Paleoproterozoic magmatic event and the second one linked to high-grade metamorphism related to the Brasiliano Orogeny. The U-Pb age interval from 2209 to 2060 Ma obtained in zircon grains from the granulitic orthogneiss with $T_{DMcrustal}$ ages ranging from 2.13 to 3.87 Ga may be interpreted as mantle-derived source with important older crust participation in the magma formation; juvenile arc-related rocks were generated at this time as indicated by the positive ε_{Hf} values. The second group of U-Pb ages ranging from 633 to 584 Ma is interpreted as a metamorphic event, resulting from the collisional process related to the Gondwana assembly.

Article Information

Publication type: Research Papers
Received 1 May 2021
Accepted 27 December 2021
Online pub. 7 January 2022
Editor: Evandro Klein

Keywords:
U-Pb isotopes
Lu-Hf isotopes
LA-ICP-MS
Zircon
Ribeira Belt
Gondwana assembly

*Corresponding author
Mauro C. Geraldes
geraldes@uerj.br

1. Introduction

Geochronological studies have become, in the last decades, an indispensable analytical tool for geosciences studies. U-Pb and Lu-Hf isotope analytical techniques in zircon have been gradually improved, thus enabling the investigation of several geological processes that occur in crustal dynamics (Santosh et al. 2009, Andersen et al. 2002). The study area of this work is located in Serra do Caparaó region (Figure 1), at southern of the Araçuaí Orogen and included in the northern sector of Mantiqueira Province (Pedrosa-Soares et al. 2001). The lithological associations of Serra do Caparaó region were correlated in the literature to the Juiz de Fora Complex and should represent the basement rocks of the Ribeira-Araçuaí belts, of Rhyacian age (≈2.19 Ga), according to Campos Neto and Figueiredo (1990).

The evolution of the basement of the Ribeira-Araçuai belt occurred as a result from the agglutination of Archaean crustal blocks during the Paleoproterozoic orogenic processes, which were evidenced in the period from 2.2 to 2.0 Ga. These Archean-Paleoproterozoic blocks represent, according to Heilbron et al. (2004), remnants of a magmatic arc developed in the Archaean paleocontinent margin, and of one or more additional magmatic arcs, which were dismembered and reworked in the Neoproterozoic era by the Brasiliano Orogeny.

Although the nature of the rocks from Serra do Caparaó region is still a matter of great debate for the scientific community, although these are treated by some authors as a unit of the basement of the orogen (Seidensticker and Wiedmann 1992), other authors believe that it is part of the Juíz de Fora Complex (Campos Neto and Figueiredo 1990). Compositionally, there is an association of charnockite, diorite, and gabbro defined by Horn (2006) as Carapaó Suite, with Paleoproterozoic (2.2 Ga) U/Pb ages (Silva et al. 2002). The migmatitic unit of the Caparaó Suite shows various intensities of partial melt. The

ISSN: 2595-1939
https://doi.org/10.29396/jgsb.2022.v5.n1.1
Open access at jgsb.cprm.gov.br

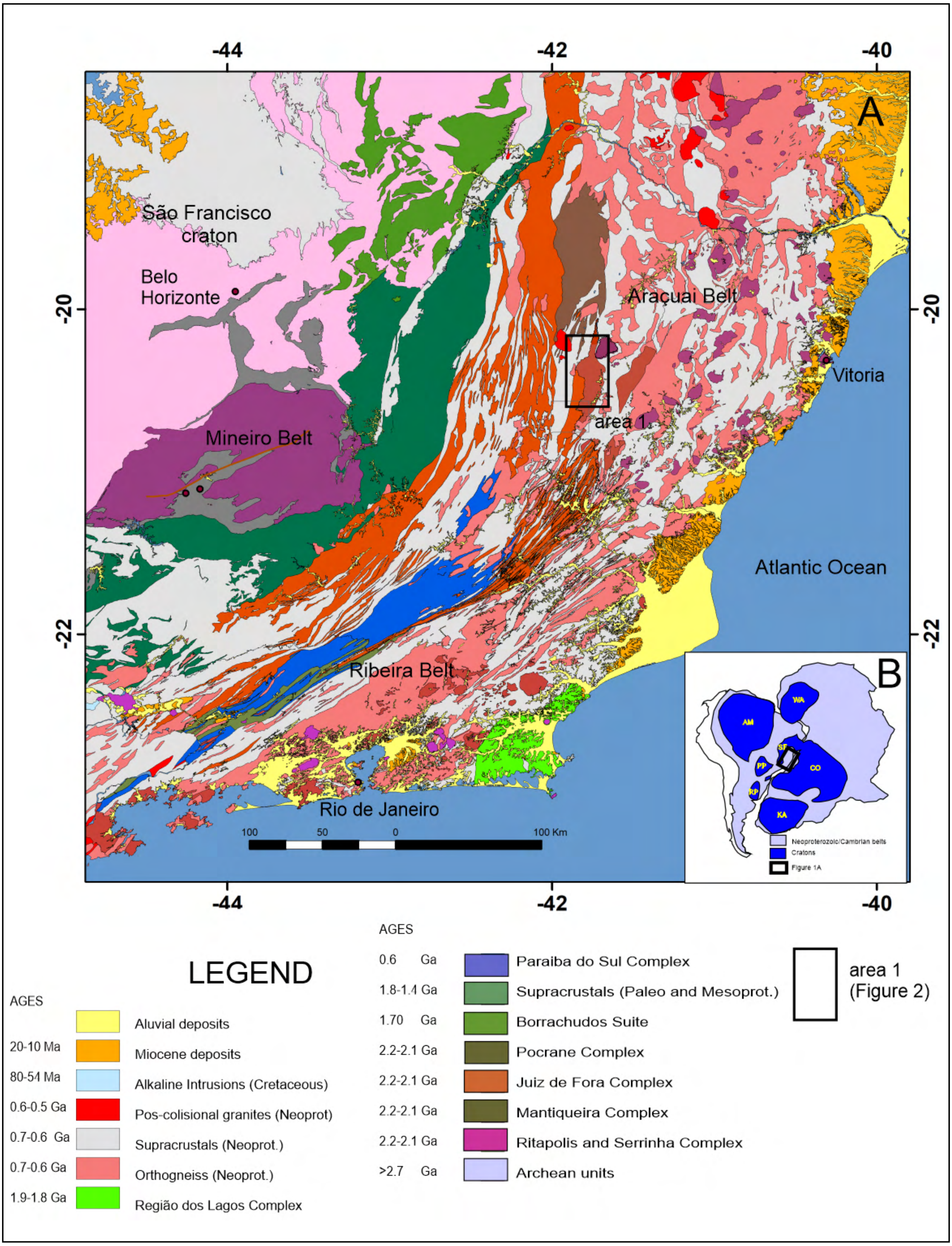

FIGURE 1. (A) Regional geologic map of the studied area in the context of Ribeira and Araçuai belts (adapted from Machado et al. 2021). (B) Paleo reconstruction of West Gondwana. The study area is signed (rectangle).

main migmatitic structures are schlieren, ptigmatic, agmatic and complex folded rocks (Horn 2006). Two events affect the rocks of this unit, the first Paleoproterozoic in age (ca. 2.2-2.1 Ga), which is responsible for the formation of diagnostic paragenesis of granulite facies (orthopyroxene + plagioclase ± clinopyroxene ± hornblende) as reported by Noce et al. (2007) to high-grade metamorphism. This metamorphic event was broadly coeval with the magmatic crystallization. The second event is related to the Brasiliano Orogeny, whose collisional episodes led to the amalgamation of different tectono-stratigraphic terranes that progressively collided against the southeastern margin of São Francisco Craton (SFC) between the Early Ediacaran and the Cambrian (Heilbron et al. 2000, 2004, 2008, 2020; Trouw et al., 2000; Schmitt et al. 2004, 2008, 2016; Freitas et al. 2021), where the regional foliation generated is evidenced by the crystallization of hornblende, biotite and garnet and locally orthopyroxene and clinopyroxene.

The present work aims to investigate the crystallization and metamorphic ages of granulitic rocks of Caparaó Complex, providing information about the crustal evolution of this terrane in the internal tectonic domain of the Araçuaí Orogen. Thus, the aim of the study herein is to contribute to the understanding and characterization of the Paleoproterozoic and Neoproterozoic evolution of the Ribeira-Araçuai belt and the border of the São Francisco Craton, by constraining the U-Pb zircon ages in the Caparaó Complex to define the crystallization ages of the granulitic rocks photoliths. In addition, Lu-Hf analysis were performed to provide the sources of these granulitic lithotypes.

2. Regional Geology

The units observed in the study are included in the Araçuaí Belt as defined by Almeida (1977, 1981) and comprise the eastern portion of the São Francisco Craton (Silva et al. 2002, 2005; Noce et al. 2007; Pedrosa-Soares 1992, 1999, Amorim et al. 2021). Its origin is related to the Brasiliano Cycle, which comprised a series of collisional events, from the Neoproterozoic era lasting to the Paleozoic era, when the passive margin of the São Francisco paleocontinent was amalgamated with the active margin of the Congo paleocontinent (Figure 1B) (Seindensticker and Wiedeman, 1993; Vieira 1997; Horn 2006; Novo et al. 2011; Vieira and Menezes 2014; Pinto and Silva 2014; Vieira and Menezes 2014).

In the study region, the Araçuai Belt has its southern extension represented by rocks from Juiz de Fora/Paraíba do Sul Domain (Pedrosa-Soares et al. 2007; Novo et al. 2011). This Domain occupies an extensive northeast-oriented belt throughout the central-north and western portion of Rio de Janeiro state and SE of Minas Gerais state, subparallel to Rio Paraíba do Sul shear Zone. It consists of kinzigite gneisses, schists, quartzites and marbles from Paraíba do Sul Complex (Angeli 1978), metamorphosed into amphibolite and granulite facies, tectonically intercalated in Paleoproterozoic rocks represented by tonalitic orthogranulites and orthogneisses from Juiz de Fora Complex, and granitic to granodiorite orthogneisses from Quirino Suite.

In the Araçuaí Orogen, several geotectonic components are found, such as: passive margin deposits, ophiolitic splinters, magmatic arc and associated basins, syn-collisional granites, post-collisional granitoids, among others, which together mark the evolution of an accretionary orogen to the collisional orogen stage (Correia Neves et al. 1987; Pedrosa-Soares et al. 2001, 2007). Therefore, the Araçuaí Belt is divided, according to Pedrosa-Soares et al. (2001) in External (West) and Internal (East) domains. The external domain comprises the folding-thrusted belt, of low metamorphic degree, and the internal domain is characterized by the granitoids related to different evolutionary stages, reaching a high metamorphic degree.

The metamorphism associated with the Brasiliano collisional event reworked older rocks with Paleoproterozoic to Archean ages, notably rocks from the Mantiqueira and Juiz de Fora complexes, and from the orthogneisses of the Quirino Unit. These units constitute inliers of the basement of the province, tectonically intercalated with the metasedimentary rocks of the Andrelândia Group.

In the Espera Feliz region, three dominant units can be identified with relative lithological homogeneity: the basement, the Neoproterozoic metasedimentary cover and the Neoproterozoic-Cambrian granitoids (Wiedemann 1993; Noce et al. 2007; De Campos et al. 2004). The study area of this work is focused on the internal domain, with dominant tectonic trends in the NNE directions with a westward vergence. In this domain, the Neoproterozoic and Cambrian granitoid suites are hosted by basement rocks (Pedrosa-Soares et al. 2001, 2007).

3. Local Geology

The Caparaó Complex (Figure 2) comprises a unit formed by granulitic orthogneiss from felsic to intermediate composition which is the predominant lithology in the work area but variations may also occur with clinopyroxene and amphibole and units of mafic composition (Campos Neto and Figueiredo 1990; Pedrosa-Soares et al. 2001, 2007). Metasedimentary rocks are represented by the Andrelandia unit, which is composed of paragneisses and quartzites, and interpreted as deposited in a platformal basin (Paciullo et al. 2000; Ribeiro et al. 2012). Isotropic granites are regionally described as post-orogenic granites and may represent the collapse period of the orogenic process. The post-collisional stage (ca. 530-480 Ma) is formed by G4 and G5 supersuites, which consist from calc-alkaline to alkaline, A and I-type granitoids, without deformation features (Wiedemann et al. 1987; 2002; Pedrosa-Soares et al. 2011; De Campos 2014; De Campos et al. 2016).

The granulitic orthogneisses were divided in two groups according to the mineralogical composition; the first group presents mainly granulitic gneiss with felsic to intermediate composition (charno-enderbitic), occurs with gray to dark gray coloration or grayish when it presents certain degree of weathering. The compositional banding continuity is observed in large outcrops, occurring folded locally with axis filled with melt (Figure 3 A and B). Garnet may be observed as large crystals (Figure 3C) or in banded gneisses with thickness from millimeters to centimeters. Large enclaves are locally observed. In thin sections, banded gneisses are marked by mineral segregation in felsic bands, with quartz, plagioclase, and rare K-feldspar; and in mafic bands, with pyroxene (Figure 4A and B), amphibole, biotite, and garnets. Zircon and oxides are accessory minerals.

A second group of granulitic orthogneiss is comprised of felsic rocks presenting quartz and plagioclase (Figure 3 D) that occur with granoblastic texture and have fine to medium grain size, while K-feldspar occurs as porphyroclasts up to two centimeters. Garnet grains occur mainly in felsic bands as crystals of about 1 centimeter but they may occur agglomerated. Amphibole crystals occur in the felsic bands (Figure 4C and

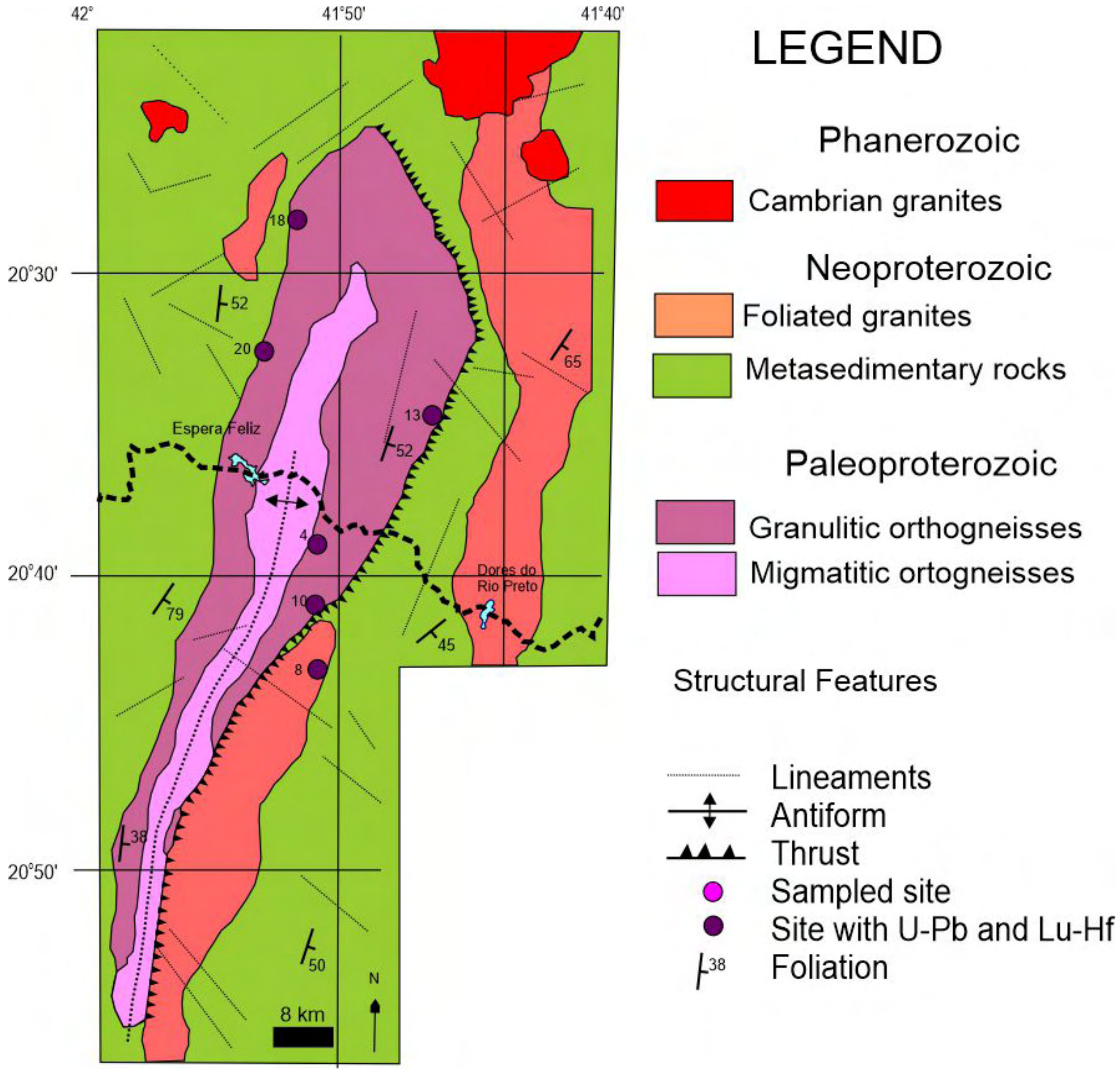

FIGURE 2. Geological map of Serra do Caparaó study area. The sampled points are shown on the map.

D), as porphyroclasts and in the mafic bands the pyroxene occurs with fine to medium-sized with nematoblastic texture. The mafic orthopyroxene gneiss appears mainly in the higher elevations of the Caparaó Complex, as it enclaves in the middle of the orthogneiss migmatized unit, presents dark color and mafic composition, with or without millimetric banding. Centimetric to metric mafic enclaves are often observed (Figure 3 E), locally stretched in the banding direction (Figure 3 F). In contact with other units in the area, the gneissic rocks of the Caparaó Complex develop a complex folded features characterized by open and tight folds (Figure 5 A, B, C and D).

4. Materials and Methods

Seven samples were taken to collect representative rocks of the units observed in Serra do Caparaó region (Fig. 2). In this way, the samples were included in two groups (Table 1): the first is composed of charno-enderbitic gneisses (samples CPR03, CPR04, CPR08 and CPR10) and the second group is composed of felsic orthogneiss (samples CPR13, CPR18 and CPR 20).

4.1. Sample preparation and Scanning Electronic Microscopy (SEM)

Initially all the collected samples were washed and dried to avoid any contamination for geochronological studies. The crushing was performed on a jaw crusher that breaks the rock to sizes of approximately 1 centimeter. This was followed by disc-mill to obtain fined-grained material and then by gravimetric separation is carried out with a ruffled table. This procedure aimed to separate the heavy minerals. Finally, the concentrated heavy minerals were taken to separation in dense liquid and magnetic separation. This procedure was performed to find larger amounts of zircon grains with different magnetic susceptibilities, followed by the epoxy preparation in which the zircon grains were fixed to an epoxy resin. After drying the resin, the samples were sent to the polishing process and then to the Scanning Electron Microscope (SEM) QUANTA 250 using backscattered and cathodoluminescence detectors for imaging of the zircon grains and observation of internal mineral structure and evidence of inherited core, areas of reabsorption, magmatic zoning to guide the subsequent location of the isotopic analysis.

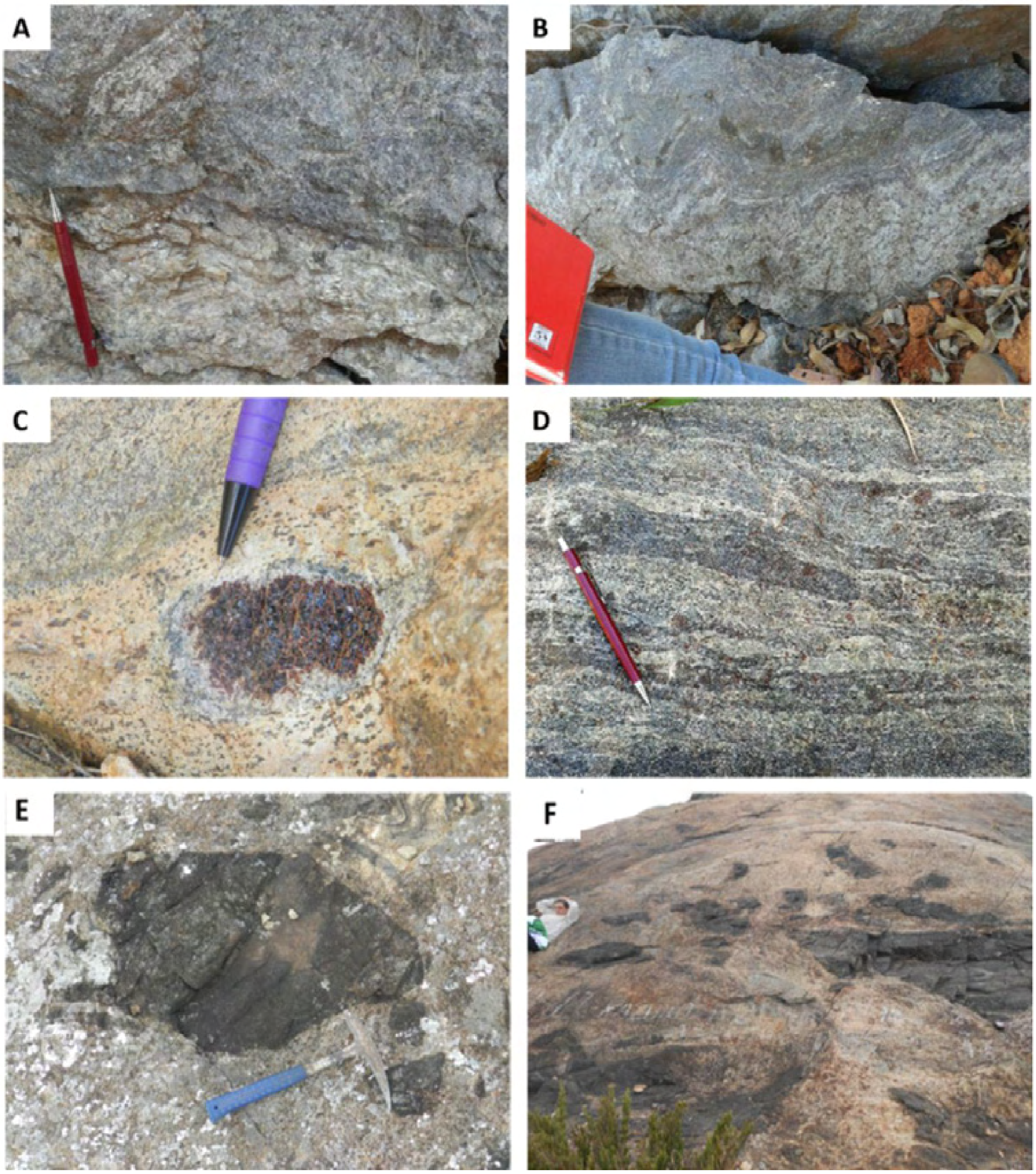

FIGURE 3. Outcrop images of orthogneisses and migmatitic rocks of the Caparaó Complex. (A) and (B) Local melt; fold with axes filled by melt. (C) Garnet; (D) Layers of garnet; (E) and (F) Enclaves observed in banded gneiss.

4.2 U-Pb dating

The spectrometer used to perform the isotopic quantification of the present work was a Neptune plus (Thermo Finnigan) in the MultiLab laboratory, of Rio de Janeiro State University. It is a high-resolution Multi-Collector Induced Coupled Plasma Mass Spectrometer (MC-ICP-MS) for isotopic measurements, with a special configuration to simultaneously detect a wide range of element nuclides using 9 Faraday collectors and 6 ion counters which can be combined in an appropriate configuration for the isotopes of interest for the U-Pb method (Jackson et al. 2004; Geraldes 2010). During the analysis, the collector's geometry (with 2 Faradays and 5 ion count) followed the specifications presented in Table 2. The U-Th-Pb isotope analysis includes ^{204}Pb, ^{206}Pb, ^{207}Pb, ^{208}Pb, ^{232}Th, and ^{238}U. Mercury represents a common contaminant in He and Ar gas and ^{204}Hg interferes with ^{204}Pb mass counts. Mass ^{202}Hg, mass ^{204}(^{204}Pb + ^{204}Hg) as well as ^{206}Pb, ^{207}Pb and ^{208}Pb were detected by the ion counters while ^{238}U and ^{232}Th were measured with a Faraday cup. Isotopic data was obtained using the static mode through 40 cycles of 1.054 seconds acquirement time with a gas inlet flow (Ar) of 15 L / min, auxiliary flow (Ar) 0.8 L / min, in MC-ICP-MS (Table 3).

The acquisition process consisted of a sequence (Figure 6), which began with the analysis of one blank, which is the data measurement performed in the passage of only Ar and

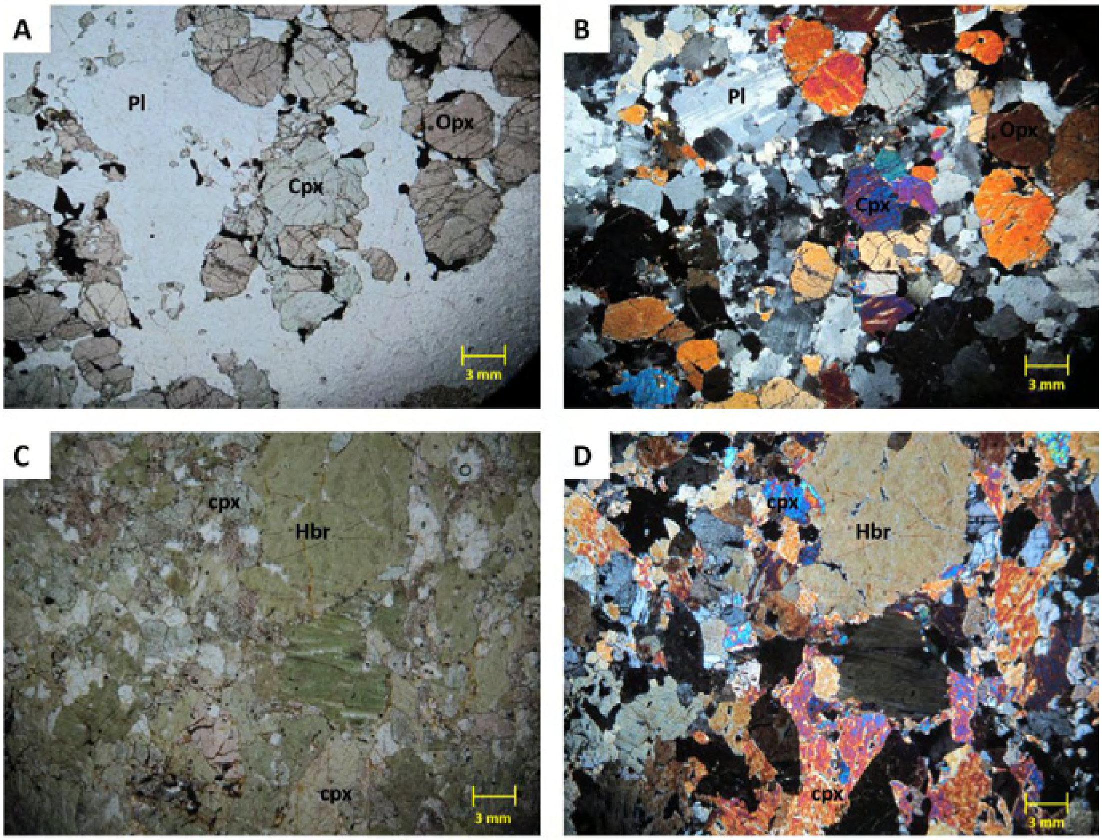

FIGURE 4. Photomicrographs of some points where the clinopyroxene (Cpx) - orthopyroxene (Opx) gneiss variation predominates in the granulite orthogneiss unit. (A) and (B) granoblastic arrangements of Cpx, Opx, plagioclase (Caparaó region sample CPR 04). (C) and (D) Clinopyroxene associated with hornblende. Legend Minerals: Cpx- clinopyroxene;Opx- orthopyroxene; Hbr - hornblende, Pl - plagioclase.

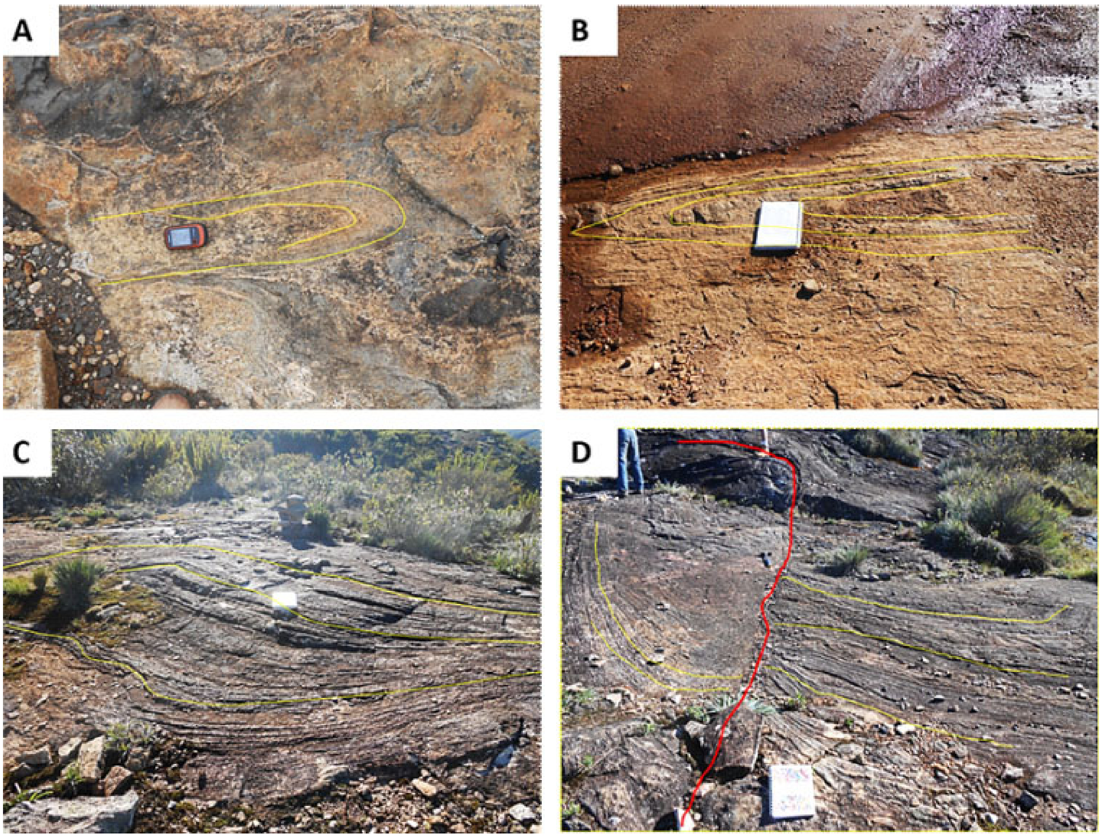

FIGURE 5. Images of outcrops with complex folded features.

TABLE 1. Rock samples and composition

Rock type	samples	description
Granulite	CPR03, CPR04, CPR08, CPR10	Quartz, K-Feldspar, Biotite, and pyroxene
Migmatite	CPR13, CPR18, CPR 20	Quartz, K-Feldspar, Biotite, and amphibole

TABLE 2. Configuration of Faraday and CDD collectors for U-Pb isotopic analyzes.

H4	H3	H2	H1	C	L1	L2	L3	L4	IC1	IC2	IC3	IC4	IC5
^{238}U		^{232}Th											
									^{208}Pb	^{207}Pb	^{206}Pb	^{204}Pb	^{202}Hg

TABLE 3. Operating conditions of LA-ICP-MC-MS in the U-Pb method.

ICP-MC-MS – NEPTUNE PLUS (Termo Scientific	
RF Energy	1200W
Gas flow:	Ar Coll: 15L/min Ar Aux: 0,73 L/min Ar carrier: 0,85 L/min
Analysis Mode:	Static
Detectors:	Faradys + ion counting
Aquisition time:	1,045s
Laser ablation – Machines In. 193 mm	
Crater diameter:	30 μm
Laser pulse energy:	4-7 j/cm^2
Frequence:	6 Hz
Abration time	40 s
Gas flow (He) (A):	0,80 L/min
Gas flow (He) (B):	0,22 L/min

He gases, being measured as a background, followed by the measurement of a shot made on a reference material zircon (GJ-1). If the data are compatible with the true value reported in the literature (Elhlou et al. 2006; Jackson et al. 2004). that is, for $^{206}Pb/2^{07}Pb$ = 0.06389 and $^{206}Pb/^{238}U$ = 0.09812), so the analysis of nine grains of unknown age can be started. The choice of the grain to be analyzed and the crater position was made using the cathodoluminescence images and the image provided by the equipment camera. The laser was positioned at the chosen location and the beam was manually activated, initiating the ablation process; then data acquisition was initiated in 40 cycles. With the completion of the unknown analyzes, data of another reference material (91500) was obtained, ending the spreadsheet with the reading of a second GJ-1 and a blank again. The U-Pb results obtained by LA-ICP-MS were treated in an offline spreadsheet for blank and GJ-01 correction. Finally, the program ISOPLOT (version 4.1.5 of Ludwig 2003) was used to calculate ages and construct concordia diagrams. The decay constant values used in this work were the ones recommended by Steiger and Jäger (1977). All values were referred to as 2σ for all the uncertainties cited in the body of the text.

The data obtained in the mass spectrometer was processed using an Excel spreadsheet, where off-line corrections were performed through the blanket procedure, following the sequence: blank, GJ1 zircon reference material, nine unknown analyzes, the 91500 and GJ1 reference material, and one blank again. The procedure works to correct the average of the final blank and for reference materials.

The abundance determination of the U-Pb isotopes in the zircon grains consisted of reading isotope concentrations where the material volatilization procedure occurs (crater)

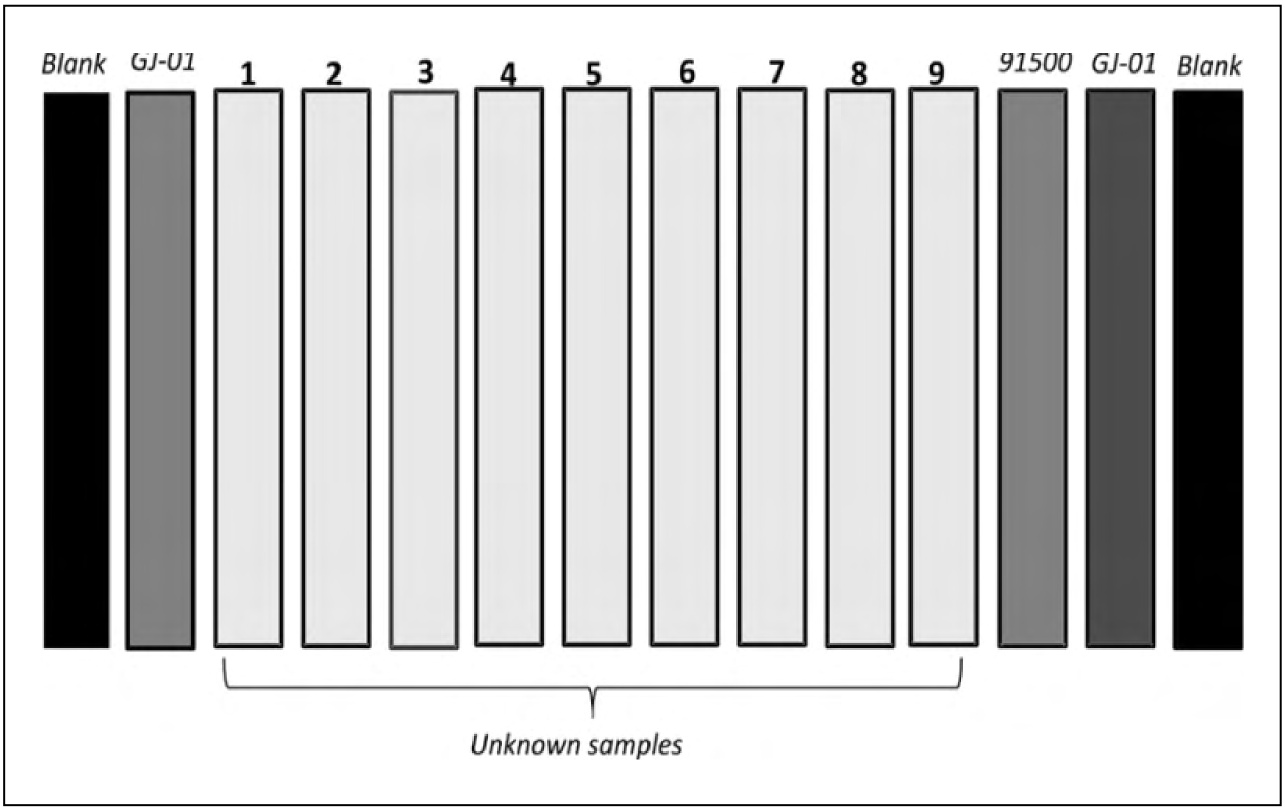

FIGURE 6. Schematically bracketing procedure used for reference material and blank corrections.

through the laser ablation (LA) method. In the isotopic data collection, the sample mount was inserted in the reserved compartment inside the device, together with the reference material. In the U-Pb method, GJ-1 and 91500 were used. Isotopic data were obtained using the static mode through 40 cycles of 1.054 seconds acquirement time with a gas inlet flow (Ar) of 15 L/min, auxiliary flow (Ar) 0.8 L / min, in the MC-ICP-MS.

Data on the GJ-1 zircon standard for a 30µm ablation spot usually yielded 432,000-114,000 cps of ^{206}Pb, 25,000-7,000 cps of ^{207}Pb, 6,500-4,200 cps of ^{208}Pb, 4,400-4,200 cps of ^{202}Hg and 1,060-1,090 cps of ^{204}(Hg+Pb). For ^{232}Th and ^{238}U, measurements on faraday cups the values are 0.78 mV and 6.06 mV, respectively, yielding an age of 610.8 ± 2.6 Ma (Table 4; Figure 7). The GJ-01 reference material comprises a large amount of zircon crystals approximately 1 cm in size from African pegmatites (Elhlou et al. 2006; Morel et al. 2008) with crystallization age of 608.5 ± 0.4Ma (Jackson et al. 2004). Using an Excel spreadsheet, off-line corrections for blank, Hg interference and common lead were performed. In addition, the obtained GJ-1 reference material values (Table 5) were compared with the literature values (Elhlou et al. 2006). Hence, the U-Pb results obtained by LA-ICP-MS were treated in an off-line spreadsheet for blank and GJ-1 correction. A second reference material was used, the 91500 (Figure 8), which represents a single crystal of zircon from a syenite pegmatite from the Renfrew County mine, Canada, crystallized at 1065 ± 6 Ma (Griffin et al. 2006).

4.3. Lu-Hf isotopes

The Lu-Hf isotopic system is one of the most innovative and powerful tools in zircon geochronology (e.g., Amelin et al. 1999; Griffin et al. 2000, 2002; Woodhead et al. 2004; Belousova et al. 2006; Gerdes and Zeh 2006, 2009; Hawkesworth and Kemp 2006; Zeh et al. 2007). The Lu-Hf technique is applied to zircon grains because this mineral has high Hf concentration, because it replaces Zr, and preserves the initial ratios of Hf. The blocking temperature of the Hf in the zircon is about 200 °C higher than the Pb (approximately 1,100 °C), indicating that the Hf isotopic system is closed during almost all thermal events, such as high-grade metamorphism, maintaining the isotopic ratios present in the zircon crystallization (Duchene et al. 1997; Choi et al. 2006; Schmidt et al. 2008). The models of Hf isotopic evolution have been proposed based on the hypothesis of the use of the Hafnium as a marker of the geochemical differentiation between the mantle and the crust (Patchett et al. 1981; Amelin et al. 1999; Vervoort and Blichert-Toft 1999; Hawkesworth and Kemp 2006). In this sense, interpretations of εHfvalues are similar to those of εNd values being able to indicate mantle-derived rocks or rocks originating from crustal magmas (if the values are positive or negative, respectively). It has been widely used for understanding crustal evolution and mantle/crust differentiation.

The acquisition of Lu-Hf data is carried out following a sequence that begins with the choice of the grain to be analyzed and the place where the crater will be made, usually in the place where the U-Pb age was performed, however with a diameter of 40-50µm. For this, the CL images and the image provided by the equipment camera were considered when choosing the location to analyze, then the laser spot was positioned, and the beam was manually activated, initiating the ablation process. The material ablated by laser was carried out using Ar and He gases and it took a few seconds (3-10 s) for the signal to stabilize. In sequence, data acquisition were obtained in 40 cycles (1.045 seconds each cycle).

The collectors were positioned as follows (Table 6): mass ^{176}Hf in the central collector, mass ^{177}Hf in the collector H1, mass ^{178}Hf in H2 and mass ^{179}Hf in H3. In the collectors L1 the mass ^{175}Lu, L2 the mass ^{174}Hf, L3 the mass ^{173}Yb and in L4 the mass ^{171}Yb. The isobaric corrections were installed in the mass spectrometer software, so that the interferences ^{176}Lu and ^{176}Yb had their abundances obtained through the measurements of the masses ^{173}Yb and ^{175}Lu. Thus, the correction factors of 0.795015 and 0.026580 were used, respectively. The correction of the isotopic fractionation of the mass spectrometer is performed from the constant ratios ^{179}Hf/^{177}Hf (true value 0.7325) and ^{171}Yb/^{173}Yb (true value of 1.123456) reported in the literature (Patchett and Tatsumoto 1980, 1981; Morel et al. 2008).

A calibration procedure of Faraday detectors (Table 7) was then performed using the reference material solution (JMC475) through plasma settings and gas (Ar) flows for signal optimization (Woodhead et al. 2004). Isotopic data were obtained using the static mode through 50 cycles of 1.054 seconds acquirement time with a gas inlet flow (Ar) of 15 L/min, auxiliary flow (Ar) 0.8 L/min, in MC-ICP-MS. The laser was connected with two input He streams with volumes of 0.800 l/m and 0.220 l/m, totalizing 1.020 l/m. The laser repetition was at 10 Hz, with 4-7 J / cm^2 (35-60%) output power and 40 µm crater size.

4.4 Lu-Hf Calibrations

The abundances values of the Hf, Lu and Yb isotopes were reliable according to the three reference materials used (GJ-1, Mud Tank and 91500). In the calibration of the Lu-Hf method using laser ablation, the ^{176}Hf/^{177}Hf ratios of the GJ-1 reference material were initially analyzed. The GJ-1 (Figure 9) is used in large scale by geochronology laboratories being a reference material for U-Pb and Lu-Hf isotopic analysis. The isotopic ratios ^{176}Lu/^{177}Hf and ^{176}Hf/^{177}Hf of this reference material were reported in the literature (Woodhead and Hergt 2005; Elhlou et al. 2006; Morel et al. 2008) with values of 0.00025 and 0.282005 ± 5, respectively. In the calibration of the method using laser, the ^{176}Hf/^{177}Hf ratios of the GJ-1 were similar to the published reference material values. The average ratio value was 0.282016 ± 5, which is almost identical to the recommended value in the literature.

A second reference material used during the analysis is comprised of Mud Tank (Figure 9), a natural zircon collected in a carbonatite that outcrops in Strangways, east of Alice Springs (Australia). This carbonatite has an age of 732 Ma and has large amounts of zircon and apatite crystals up to ten centimeters. The obtained isotopic ratios ^{176}Lu/^{177}Hf and ^{176}Hf/^{177}Hf were 0.000042 ± 6 and 0.2882507 ± 6, respectively, which are equivalent to those described in the literature for the Mud Tank reference material (Woodhead and Hergt 2005).

The 91500 (Figure 9) reference material was also used. It was part of the Harvard Museum collection and was carefully prepared as a reference material after a preliminary characterization, including Lu-Hf isotopic analyzes. Zircon 91500 has been widely adopted by many laboratories as

TABLE 4. LA-ICP-MC-MS in the U-Pb results of GJ-1 reference material.

Spot number	ƒ 206a	Pb ppm	Th ppm	U ppm	Th/Ub	$^{207}Pb/^{235}U$	1 s [%]	$^{206}Pb/^{238}U$	1 s [%]	Rhod	$^{207}Pb/^{206}Pb^{e}$	1 s [%]	$^{206}Pb/^{238}U$	1 s abs	$^{207}Pb/^{235}U$	1 s abs	$^{207}Pb/^{206}Pb$	1 s abs	% Concord
003-Sample1	0.005477466	30.06282838	6.081669973	301.9533515	0.020141091	0.824007886	4.052433176	0.099335992	1.834997771	0.452813826	0.060162166	3.613170053	610.5163828	11.20296201	610.2819872	24.73126972	609.4120401	22.01909333	100.1812144
003-Sample1	0.004144864	31.32510126	6.141735653	316.2858571	0.019418306	0.823796581	3.371622299	0.099165922	1.785387642	0.529533703	0.06024989	2.86010977	609.5190274	10.88227739	610.1643517	20.57243735	612.5609202	17.51991473	99.50341383
004-Sample 2	0.005425667	31.87489874	6.458264347	322.9166958	0.019999785	0.816388279	3.39337087	0.098647078	1.764412704	0.519958699	0.06002211	2.898588221	606.4753848	10.70072873	606.0314438	20.56489448	604.3717471	17.51824827	100.3480702
003-Sample1	0.000723882	33.49376938	6.92654484	339.2692516	0.02041607	0.819742823	2.369111315	0.098681867	1.347150792	0.568631277	0.060247495	1.948813271	606.6795053	8.172887761	607.9049449	14.40194484	612.4750257	11.93599459	99.05375401
004-Sample 2	0.001065214	29.70623062	5.67345516	299.9333013	0.018915723	0.820426983	2.826345368	0.099131133	1.734536616	0.613702994	0.060024505	2.231504172	609.3149967	10.56879173	608.2866219	17.19228077	604.4580811	13.4885073	100.8035157
003-Sample1	0.002170495	31.6	6.3	319.6012765	0.019712061	0.820088356	2.440273061	0.0989065	1.410143996	0.577863198	0.060136	1.991588945	607.9973857	8.573638632	608.0977279	14.83924504	608.4716136	12.11825339	99.92206245
003-Sample1	0.003769035	29.03815828	5.728594541	289.5010172	0.019787822	0.844114448	3.417973185	0.101450121	1.359496298	0.397749258	0.060345861	3.135970426	622.9015515	8.46832353	621.4136046	21.23975037	615.9986906	19.31753676	101.1205967
004-Sample 2	0.003769035	29.26287264	5.703050476	289.1737738	0.01972188	0.846452268	3.393735036	0.101661395	1.287540263	0.379387386	0.060387233	3.140012351	624.1379522	8.036027429	622.7000101	21.13278841	617.478364	19.38889689	101.0785136
ARI 17 (D) 01	0.002360413	31.92863133	6.417043187	325.7854435	0.019697145	0.81800087	2.307614603	0.098652597	1.192795377	0.516895402	0.060137306	1.975430167	606.5077648	7.23439658	606.9325015	14.00566303	608.5185664	12.02085933	99.6695579
ARI 17 (C) 01	0.002379237	32.21276906	6.405464223	324.3234968	0.019750232	0.830222278	2.467139778	0.100146822	1.220815209	0.494830175	0.060125117	2.143919054	615.2692669	7.511300785	613.7355157	15.14171304	608.0803156	13.03674975	101.1822371
ARI 17 (C) 02	0.002018368	30.98723094	6.194535777	314.8790561	0.019672746	0.809950713	2.619744015	0.097666178	1.321742064	0.504530999	0.060146883	2.26187016	600.7172922	7.939933135	602.4263739	15.78202887	608.8628152	13.77168633	98.66217433
ARI 17 (B) 02	0.003178273	40.1785558	7.972566628	404.2939044	0.01971973	0.828293715	2.682013354	0.100512535	1.27502357	0.47539792	0.059767194	2.359557274	617.4118448	7.872146544	612.6650104	16.43175739	595.1565998	14.04306084	103.7393931
ARI 17 (A) 01	0.004986568	24.32898541	4.896934876	248.9959986	0.019666721	0.810258523	3.292932808	0.097041422	1.510095343	0.458586746	0.060557116	2.926263579	597.0471561	9.015981298	602.5990412	19.84318153	623.5398328	18.24641903	95.7512455
ARI 17 (A) 02	0.004139965	38.87101459	7.703065124	390.2065543	0.019740994	0.829701603	3.004318594	0.100771578	1.397889975	0.46529352	0.059714884	2.65929198	618.9290462	8.651947091	613.4466115	18.42989062	593.2590141	15.77648938	104.3269519
CA-14-A1	0.002650275	38.45949184	9.406424903	385.8370959	0.024379265	0.830639157	2.403451352	0.099624575	1.605275523	0.667904313	0.060470651	1.788761833	612.2083858	9.827631366	613.9667685	14.7563926	620.4576424	11.0985095	98.67045612
CA-14-A2	0.002694392	24.74050816	3.193575097	253.365457	0.012604619	0.809603822	3.184728489	0.098188425	2.399140715	0.753326609	0.059801349	2.094425788	603.7836331	14.48561897	602.2317494	19.17944609	596.3944081	12.49103828	101.2389829
CA-1-(D) 1	0.002461032	23.41418277	4.962662571	242.0716777	0.020500798	0.813095378	2.119367114	0.098089688	1.031848792	0.486866473	0.060119708	1.851217177	603.2040136	6.224153327	604.1890015	12.804983	607.8857882	11.25328613	99.2298266
CA-1-(D) 2	0.001471668	39.78581723	7.637337429	397.1308752	0.019231286	0.827085004	1.852878085	0.099723312	1.196522318	0.645764191	0.060152292	1.414740803	612.7871963	7.332135566	611.9935046	11.33949353	609.0572229	8.616581047	100.6124176
CA-1-(C)2	0.003336702	30.25869307	5.503206232	301.4031778	0.01825862	0.840478448	2.730154254	0.101107024	1.591227807	0.582834397	0.060289819	2.218498662	620.8932072	9.879825364	619.4096199	16.91083808	613.9921215	13.621407	101.1239697

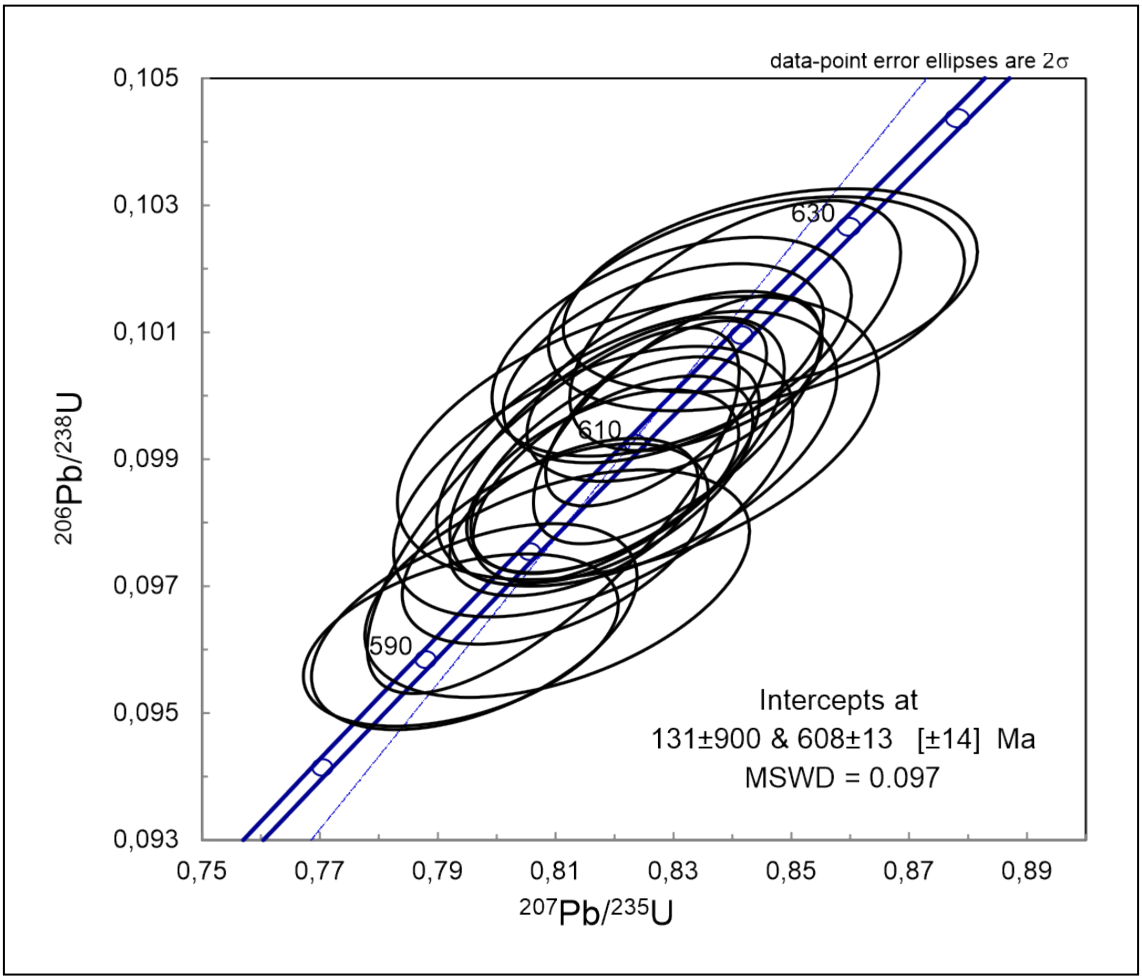

FIGURE 7. Concordia diagram of GJ-1 (reference material) U-Pb isotopic results obtained in the MultiLab laboratory during the analysis of unknown samples reported herein.

reference material for Lu-Hf analyzes. The isotopic ratios values of 0.000311 ± 8 (^{176}Lu/^{177}Hf) and 0.2882305 ± 8 (^{176}Hf/^{177}Hf) were determined and are consistent with the reported values in the literature (Elhlou et al. 2006; Morel et al. 2008).

The data were recorded by computers that are coupled to the mass spectrometer and then transferred to another computer for processing in Excel where the obtained GJ-1 values were compared with the literature values (Elhlou et al. 2006; Morel et al. 2008) to calculate T_{DM} and ε_{Hf} values. Finally, the Excel spreadsheet was used to make the Hf isotopic evolution diagrams. The procedure was used in order to correct the average of the final blank and for reference materials (detailed procedures may be found in Alves et al. 2019). T_{DM} ages and $\mathcal{E}_{Hf}$ were calculated assuming an average crustal ^{176}Lu/^{177}Hf value of 0.01250 (Patchett et al. 1981; Griffin et al. 2000; Chauvel et al. 2014), using an offline Excel spreadsheet (Bertotti et al. 2013). In all the tables and figures, the initial εHf was calculated using present-day CHUR values of ^{176}Hf/^{177}Hf = 0.282785 and ^{176}Lu/^{177}Hf = 0.0336 (Bouvier et al. 2008). For diagrams of the crustal and depleted mantle evolution curves (Patchett and Tatsumoto 1980; Vervoort and Blichert-Toft 1999), the present-day values for ^{176}Hf/^{177}Hf in the depleted mantle and Archean crust are 0.283214 and 0.280554, respectively, and corresponding values for ^{176}Lu/^{177}Hf are 0.0399 and 0.0024.

For all the samples, the U-Pb method was performed and crystallization ages were calculated prior to the Lu-Hf analyses. This procedure was necessary because for the calculations of the ε_{Hf} parameter it is necessary to obtain the crystallization ages. In this sense, 10 zircon grains of each sample were chosen for the analysis; the laser crater of the Lu-Hf analysis was positioned in the same area of the crater produced by the U-Pb method.

5. Results and data analyses

5.1. Banded felsic granulite (Sample CPR 03)

The zircon grains occur with morphology varying from prismatic to elongate and show the length/width ratio ranging from 1:1 to 1:5. In general, the grains show rounded endings and in rare cases pyramidal endings. The cathodoluminescence (CL) images show well-defined oscillatory zoning (with layers varying in thickness), a typical growth texture in magmatic processes (Figure 10A).

For this sample, a total of 19 grains were analyzed, which generated the concordia diagram (Figure 11A). Most of the analyses are concordant, with discordance values <10%. The analyses exhibit Th/U ratios ranging from 0.5 to 1.5 (Table 8), indicating that the zircon grains were derived from magmatic rocks.

For the construction of the concordia diagram and age calculation, the fifteen measurements with the lowest error and the most concordant results were selected. The age

TABLE 5. LA-ICP-MC-MS in the U-Pb results of 91500 reference material

									Isotope ratios						Ages (Ma)				
Spot number	ƒ 206a	Pb ppm	Th ppm	U ppm	Th/Ub	$^{207}Pb/^{235}U$	1 s [%]	$^{206}Pb/^{238}U$	1 s [%]	Rhod	$^{207}Pb/^{206}Pb$e	1 s [%]	$^{206}Pb/^{238}U$	1 s abs	$^{207}Pb/^{235}U$	1 s bs	$^{207}Pb/^{206}Pb$	1 s abs	% Concord
012-91500	0.009961	8.792298	4.853542	46.54754	0.104271	1.835211	4.213146	0.176322	2.739343	0.650189	0.075488	3.201031	1046.848	28.67676	1058.147	44.5813	1081.53	34.62012	96.79322984
012-91500	0.010988	8.596215	-26.8882	42.96674	-0.62579	1.947319	6.306179	0.1874	2.905876	0.460798	0.075364	5.596765	1107.277	32.17609	1097.523	69.21178	1078.233	60.34614	102.6936837
012-91500	0.00739	8.071079	1.06961	39.96361	0.026765	1.890144	3.552354	0.1821	2.849466	0.802135	0.075281	2.121263	1078.436	30.72966	1077.633	38.28132	1076.009	22.82497	100.2255462
012-91500	0.008758	8.399928	6.302696	40.96072	0.153872	1.913471	5.487691	0.183427	3.707488	0.675601	0.075659	4.045897	1085.668	40.251	1085.795	59.58507	1086.05	43.94047	99.96478502
012-91500	0.021059	5.955597	-7.68195	29.2964	-0.26221	1.942041	6.969953	0.187465	5.828175	0.836186	0.075134	3.822646	1107.626	64.55439	1095.704	76.37003	1072.094	40.98237	103.3142659
012-91500	0.009631	6.485514	6.235973	33.27502	0.187407	1.89662	4.96548	0.183421	3.476582	0.70015	0.074994	3.54533	1085.638	37.74311	1079.905	53.62247	1068.354	37.87666	101.6179081
012-91500	0.018527	5.966631	118.018	29.74039	3.968275	1.946318	6.750591	0.185945	5.342696	0.791441	0.075915	4.126266	1099.372	58.73611	1097.178	74.06603	1092.83	45.09306	100.5986556
012-91500	0.014414	6.582439	4.217703	31.60079	0.133468	2.010495	6.354589	0.193272	4.761473	0.749297	0.075445	4.208228	1139.076	54.2368	1119.058	71.11157	1080.392	45.46534	105.4317949
012-91500	0.013271	7.261859	4.198266	36.17678	0.116049	1.917528	6.151084	0.183603	3.87228	0.629528	0.075746	4.779255	1086.63	42.07737	1087.208	66.87507	1088.365	52.01576	99.84056218
012-91500	0.019002	5.969732	3.916536	29.67938	0.131961	1.954757	6.659129	0.186735	5.45709	0.81949	0.075922	3.816302	1103.666	60.22802	1100.083	73.25593	1093.003	41.71229	100.9755336
012-91500	0.002682	9.441448	19.663	44.92839	0.437652	1.922687	4.818485	0.18475	4.190815	0.869737	0.075479	2.377996	1092.87	45.80015	1089.002	52.47339	1081.275	25.71267	101.0723461
012-91500	0.025914	4.625964	10.51357	21.27085	0.494271	2.104767	9.327857	0.199696	7.766245	0.832586	0.076442	5.166659	1173.689	91.15158	1150.367	107.3046	1106.671	57.17794	106.0558042
012-91500	0.003693	11.4477	18.6438	55.76288	0.334341	1.929789	4.947299	0.184519	4.546394	0.918965	0.075852	1.950915	1091.617	49.62921	1091.466	53.99809	1091.165	21.2877	100.0414389
012-91500	0.00283	10.546	22.49904	52.06992	0.432093	1.908628	3.115533	0.183301	2.658026	0.853153	0.075519	1.625253	1084.985	28.83917	1084.106	33.77567	1082.339	17.59075	100.2444196

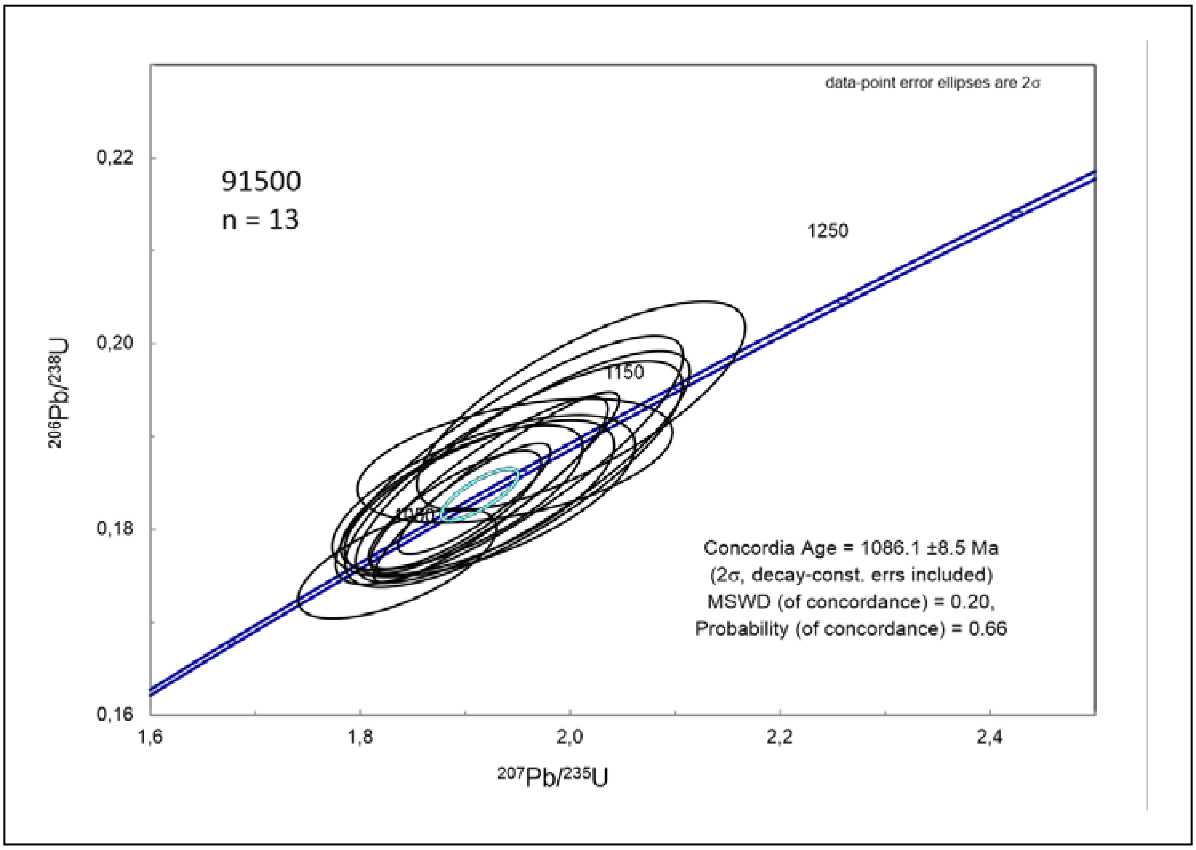

FIGURE 8. Concordia diagram of 91500 (reference material) U-Pb isotopic results obtained in the laboratory during the analysis of unknown samples reported herein.

TABLE 6 - Configuration of the Faraday collectors used for the Lu and Hf analyzes.

Faraday collectors	H3	H2	H1	C	L1	L2	L3	L4
Isotopes	^{179}Hf	^{178}Hf	^{177}Hf	^{176}Hf	^{175}Lu	^{174}Hf	^{173}Yb	^{171}Yb
Interferers				^{176}(Yb+Lu)		^{174}Yb		

TABLE 7. Operating conditions of the LA-MC-ICP-MS for the Lu-Hf method.

ICP-MC-MS – NEPTUNE PLUS (Termo Scientific	
RF Energy	1200W
Gas flow:	Ar Coll: 15L/min Ar Aux: 0,73 L/min Ar carrier: 0,85 L/min
Analysis Mode:	Static
Detectors:	Faradys
Aquisition time:	1,045s
Laser ablation – Machines In. 193 mm	
Crater diameter:	40 - 50 μm
Laser pulse energy:	4-7 j/cm^2
Frequence:	10 Hz
Abration time	50 s
Gas flow (He) (A):	0,80 L/min
Gas flow (He) (B):	0,22 L/min

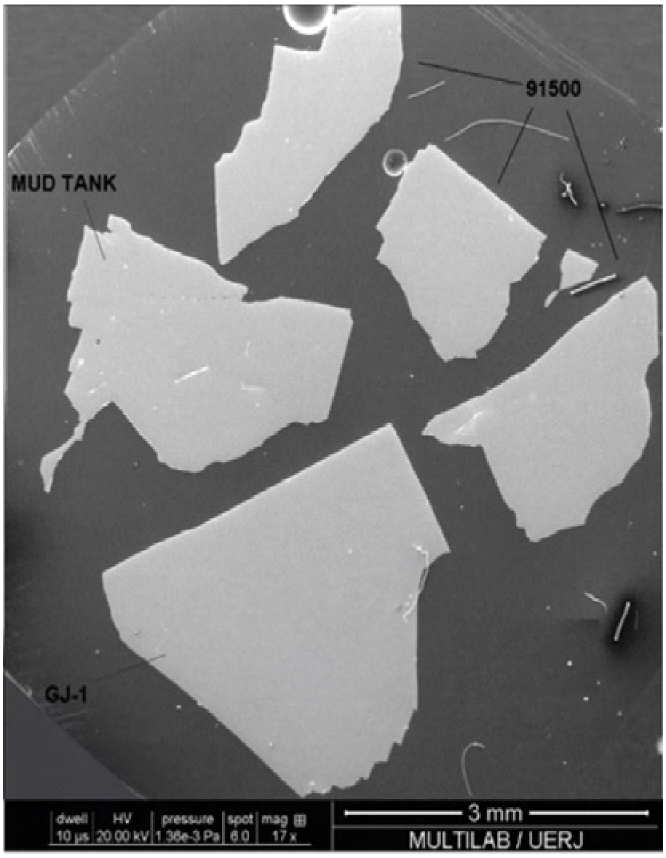

FIGURE 9. SEM images of the reference materials used for calibration of the Lu-Hf method in LA-ICP-MS in the MultiLab laboratory (UERJ).

obtained at the upper intercept of 2209 ± 22 Ma (MSWD = 5.00) is interpreted as the crystallization age of the magmatic orthogneiss protolith because the analyses correspond to the nucleus of the zircon grains. The CL images also show zircon grains with core and rims, and the analysis performed in some grains result in different ages, suggesting an isotopic re-homogenization process of the oldest nucleus during the growth of the edge in the reworking event (metamorphism in granulite facies). In cases where the core is light gray, the best Paleoproterozoic ages were obtained, suggesting the preservation of the original isotopic composition. The Neoproterozoic zircon grains are light gray or dark gray in color and do not show very light oscillatory zoning but tend to have complex gray color variation patterns. Neoproterozoic ages were obtained in white rims but in several cases all the grain was completely re-homogeneized.

The results obtained in the white border of the grains yielded an age of 596 ± 19 Ma (obtained in the lower

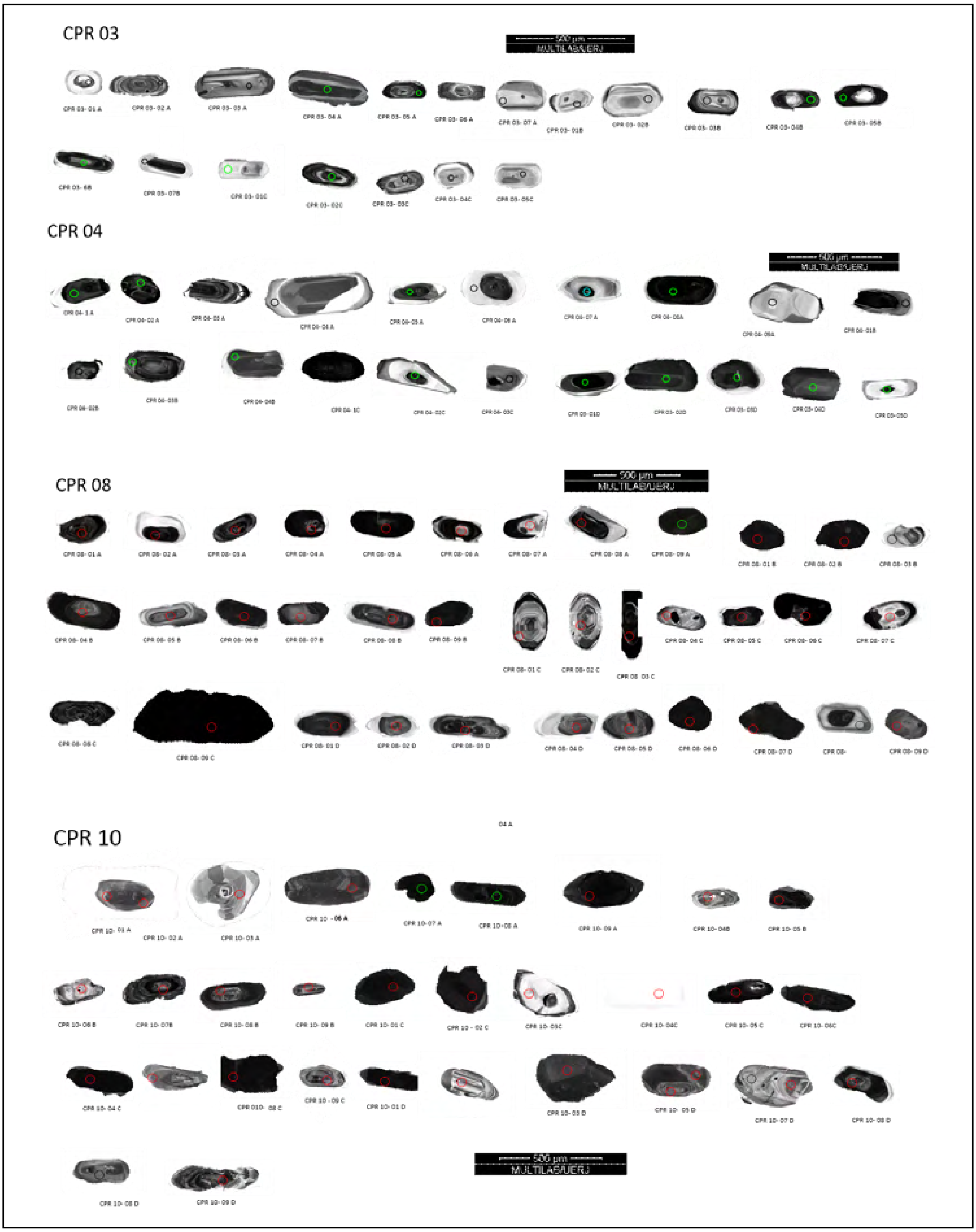

FIGURE 10. Cathodoluminescence images of the zircon grains of samples (A) CPR-3; (B) CPR 04; (C) CPR 08; and (D) CPR 10.

TABLE 8. U-Pb isotopes results obtained by LA-ICP-MS for the zircon grains of samples CPR-3, CPR 04, CPR 08, and CPR 10.

									Isotope ratios						Ages (Ma)				
Spot number	ƒ 206a	Pb ppm	Th ppm	U ppm	Th/Ub	^{207}Pb/^{235}U	1 s [%]	^{206}Pb/^{238}U	1 s [%]	Rhod	^{207}Pb/^{206}Pbe	1 s [%]	^{206}Pb/^{238}U	1 s abs	^{207}Pb/^{235}U	1 s abs	^{207}Pb/^{206}Pb	1 s abs	% Concord
CPR-03																			
CPR 03 1a	0.000608728	55.3119592	89.07579078	154.7662139	0.575550623	5.484032993	7.125965526	0.312234677	6.445686509	0.90453518	0.127384812	3.038504584	1751.69408	112.908709	1898.09889	135.2578726	2062.19293	62.65982672	84.94326858
CPR 03 2a	0.000300615	103.0703507	154.5617136	270.3703234	0.571666711	5.520856001	6.798342204	0.306641072	6.154664723	0.905318464	0.130579446	2.887483138	1724.156501	106.116052	1903.848968	129.4301679	2105.771686	60.80380236	81.87765619
CPR 03 3a	0.003678443	10.68163603	117.0310013	79.65708553	1.469185076	0.833341325	10.32989734	0.099946418	8.822561323	0.854080252	0.060472011	5.373005748	614.0948785	54.17889724	615.4644491	63.57684576	620.5061507	33.33983114	98.96676734
CPR 03 4a	0.000902864	53.80819921	117.1030607	154.7914337	0.756521585	4.990312316	5.096265225	0.284317907	4.397028746	0.862794331	0.127298193	2.57644279	1613.071816	70.92723144	1817.681424	92.6338663	2060.993138	53.10030911	78.26672423
CPR 03 5a	0.005851948	7.846249226	93.24156672	56.66919618	1.645365966	0.810454769	10.92559071	0.095263504	9.445909982	0.864567439	0.061702244	5.49029298	586.5913115	55.40888725	602.7091105	65.84953059	663.8046353	36.44481929	88.36806499
CPR 03 6a	0.000559624	94.92089942	156.838811	245.6130412	0.6385606	5.435938036	5.38767659	0.299489815	4.677065955	0.868104438	0.131640998	2.674343487	1688.778321	78.98527592	1890.539271	101.8561417	2119.970589	56.69529535	79.66045993
CPR 03 7a	0.001004404	47.30435281	82.91665607	113.7734713	0.728787257	6.704611491	4.452794264	0.362391235	3.690081564	0.828711444	0.134182123	2.49212255	1993.498254	73.56171156	2073.228456	92.31659775	2153.410757	53.66563508	92.57398978
CPR 03 1b	0.002719257	13.240814	117.6066156	100.2198548	1.17348619	0.832063797	6.962321385	0.099932879	6.577257234	0.944693137	0.060387486	2.283332291	614.015528	40.38538073	614.7566524	42.80133388	617.4874148	14.09928954	99.43773967
CPR 03 2b	0.001400509	29.18320531	123.7748289	242.527828	0.5103531	0.875479463	6.705946608	0.103888448	6.424365785	0.95801028	0.061119168	1.922821929	637.1564796	40.93326287	638.5381942	42.82003038	643.4305152	12.37202304	99.0249086
CPR 03 3b	0.000674911	52.73408861	108.138424	178.7303791	0.605036618	4.098703807	8.021953017	0.249373972	7.712672341	0.961445713	0.119204908	2.205995369	1435.246434	110.6958548	1654.045136	132.6867237	1944.339878	42.89204766	73.81664341
CPR 03 4b	0.005396147	5.333897102	47.5599136	42.1999411	1.127013744	0.817306085	7.435796212	0.099691022	6.849987639	0.921217775	0.059460343	2.892876536	612.5979131	41.96288133	606.5443789	45.10140395	583.9926986	16.89418775	104.8982144
CPR 03 5b	0.003916325	11.67931461	153.0172883	79.64278951	1.921294937	0.813999296	9.507865765	0.097685136	8.725071369	0.917668758	0.060435799	3.777914902	600.8286273	52.42272654	604.6950944	57.49359786	619.213576	23.39336196	97.03091964
CPR 03 6b	0.000577657	39.98212388	97.05934112	169.9198389	0.571206645	2.886944541	5.810463427	0.183737177	4.970172204	0.855383097	0.113956769	3.009796256	1087.358795	54.04360457	1378.507777	80.09769021	1863.448895	56.08601506	58.35195147
CPR 03 7b	0.023491103	1.523549819	19.54514764	11.29603535	1.730266154	0.811821713	11.6812216	0.094255787	7.712242566	0.660225688	0.062467103	8.77338319	580.6574418	44.78171039	603.4754637	70.4933062	690.1389548	60.54853505	84.13630874
CPR 03 1c	0.002016904	14.94297444	79.6238413	123.2822961	0.645865983	0.789391115	12.50844248	0.094435592	10.86908324	0.868939778	0.060625488	6.190651244	581.7166128	63.22726283	590.8264232	73.90318328	625.9728819	38.751798	92.93000217
CPR 03 2c	0.001021049	78.08664186	84.30032483	194.7928363	0.432769122	6.7790895	4.62104735	0.36724664	3.589615653	0.776796986	0.133878939	2.910109633	2016.43169	72.38214759	2082.9967	96.25626384	2149.46089	62.55166842	93.81104349
CPR 03 3c	0.000822487	33.14103324	64.93622596	119.2861194	0.544373698	3.479576224	6.398670791	0.208435503	5.241816718	0.819204002	0.121074695	3.669651943	1220.477359	63.97518626	1522.595775	97.42589113	1972.122173	72.37001965	61.88649849
CPR 03 4c	0.000656337	45.15983944	76.48883155	123.9084413	0.617301216	5.43887342	6.120595464	0.301985403	5.300223776	0.86596538	0.130623623	3.060933967	1701.146381	90.16456497	1891.002274	115.7405994	2106.36534	64.47445215	80.76217118
CPR 03 5c	0.000601473	55.14195639	80.73434098	123.0540745	0.65608832	6.748254986	6.656329567	0.362213593	5.982471557	0.898764326	0.135121813	2.918348398	1992.657653	119.2101773	2078.963959	138.3826927	2165.585694	63.1993354	92.01472189
CPR-04																			
CPR 04 1a	0.000608728	55.3119592	89.07579078	154.7662139	0.575550623	5.484032993	7.125965526	0.312234677	6.445686509	0.90453518	0.127384812	3.038504584	1751.69408	112.908709	1898.09889	135.2578726	2062.19293	62.65982672	84.94326858
CPR 04 2a	0.000300615	103.0703507	154.5617136	270.3703234	0.571666711	5.520856001	6.798342204	0.306641072	6.154664723	0.905318464	0.130579446	2.887483138	1724.156501	106.116052	1903.848968	129.4301679	2105.771686	60.80380236	81.87765619
CPR 04 3a	0.003678443	10.68163603	117.0310013	79.65708553	1.469185076	0.833341325	10.32989734	0.099946418	8.822561323	0.854080252	0.060472011	5.373005748	614.0948785	54.17889724	615.4644491	63.57684576	620.5061507	33.33983114	98.96676734
CPR 04 4a	0.00502862	9.040504781	77.11845535	69.4674013	1.110138769	0.881088872	10.07871672	0.103819424	8.530867012	0.84642393	0.061551668	5.367013948	636.7533878	54.32058471	641.5705906	64.66208238	658.5682102	35.3454477	96.6875379
CPR 04 5a	0.000902864	53.80819921	117.1030607	154.7914337	0.756521585	4.990312316	5.096265225	0.284317907	4.397028746	0.862794331	0.127298193	2.57644279	1613.071816	70.92723144	1817.681424	92.6338663	2060.993138	53.10030911	78.26672423
CPR 04 6a	0.005851948	7.846249226	93.24156672	56.66919618	1.645365966	0.810454769	10.92559071	0.095263504	9.445909982	0.864567439	0.061702244	5.49029298	586.5913115	55.40888725	602.7091105	65.84953059	663.8046353	36.44481929	88.36806499
CPR 04 7a	0.000559624	94.92089942	156.838811	245.6130412	0.6385606	5.435938036	5.38767659	0.299489815	4.677065955	0.868104438	0.131640998	2.674343487	1688.778321	78.98527592	1890.539271	101.8561417	2119.970589	56.69529535	79.66045993
CPR 04 8a	0.001004404	47.30435281	82.91665607	113.7734713	0.728787257	6.704611491	4.452794264	0.362391235	3.690081564	0.828711444	0.134182123	2.49212255	1993.498254	73.56171156	2073.228456	92.31659775	2153.410757	53.66563508	92.57398978
CPR 04 9a	0.002719257	13.240814	117.6066156	100.2198548	1.17348619	0.832063797	6.962321385	0.099932879	6.577257234	0.944693137	0.060387486	2.283332291	614.015528	40.38538073	614.7566524	42.80133388	617.4874148	14.09928954	99.43773967
CPR 04 1b	0.001400509	29.18320531	123.7748289	242.527828	0.5103531	0.875479463	6.705946608	0.103888448	6.424365785	0.95801028	0.061119168	1.922821929	637.1564796	40.93326287	638.5381942	42.82003038	643.4305152	12.37202304	99.0249086
CPR 04 2b	0.000674911	52.73408861	108.138424	178.7303791	0.605036618	4.098703807	8.021953017	0.249373972	7.712672341	0.961445713	0.119204908	2.205995369	1435.246434	110.6958548	1654.045136	132.6867237	1944.339878	42.89204766	73.81664341
CPR 04 3b	0.003916325	11.67931461	153.0172883	79.64278951	1.921294937	0.813999296	9.507865765	0.097685136	8.725071369	0.917668758	0.060435799	3.777914902	600.8286273	52.42272654	604.6950944	57.49359786	619.213576	23.39336196	97.03091964
CPR 04 4b	0.023491103	1.523549819	19.54514764	11.29603535	1.730266154	0.811821713	11.6812216	0.094255787	7.712242566	0.660225688	0.062467103	8.77338319	580.6574418	44.78171039	603.4754637	70.4933062	690.1389548	60.54853505	84.13630874
CPR 04 5c	0.002016904	14.94297444	79.6238413	123.2822961	0.645865983	0.789391115	12.50844248	0.094435592	10.86908324	0.868939778	0.060625488	6.190651244	581.7166128	63.22726283	590.8264232	73.90318328	625.9728819	38.751798	92.93000217

TABLE 8. U-Pb isotopes results obtained by LA-ICP-MS for the zircon grains of samples CPR-3, CPR 04, CPR 08, and CPR 10.(continued)

									Isotope ratios						Ages (Ma)				
Spot number	ƒ 206a	Pb ppm	Th ppm	U ppm	Th/Ub	$^{207}Pb/^{235}U$	1 s [%]	$^{206}Pb/^{238}U$	1 s [%]	Rhod	$^{207}Pb/^{206}Pb^{e}$	1 s [%]	$^{206}Pb/^{238}U$	1 s abs	$^{207}Pb/^{235}U$	1 s abs	$^{207}Pb/^{206}Pb$	1 s abs	% Concord
CPR-03																			
CPR 04 1c	0.001021049	78.08664186	84.30032483	194.7928363	0.432769122	6.7790895	4.62104735	0.36724664	3.589615653	0.776796986	0.133878939	2.910109633	2016.43169	72.38214759	2082.9967	96.25626384	2149.46089	62.55166842	93.81104349
CPR 04 2c	0.000656337	45.15983944	76.48883155	123.9084413	0.617301216	5.43887342	6.120595464	0.301985403	5.300223776	0.86596538	0.130623623	3.060933967	1701.146381	90.16456497	1891.002274	115.7405994	2106.36534	64.47445215	80.76217118
CPR 04 3c	0.000601473	55.14195639	80.73434098	123.0540745	0.65608832	6.748254986	6.656329567	0.362213593	5.982471557	0.898764326	0.135121813	2.918348398	1992.657653	119.2101773	2078.963959	138.3826927	2165.585694	63.1993354	92.01472189
CPR 04 1d	0.001039663	38.35933965	68.75556976	126.4979787	0.543530975	4.709592057	5.169913869	0.278804261	3.200606808	0.619083197	0.122513123	4.060064712	1585.337437	50.74041796	1768.947126	91.45304282	1993.144549	80.92295848	79.5395115
CPR 04 2d	0.000311805	69.89297104	123.1382853	264.0115765	0.466412446	3.666281914	7.92076769	0.223745357	6.731842816	0.849897772	0.118842164	4.17382955	1301.634945	87.62401852	1564.05807	123.8854063	1938.888933	80.92591921	67.13303288
CPR 04 3d	0.000953462	43.25726667	69.62522131	121.656361	0.57231057	5.817535341	4.942570401	0.329266944	3.63191107	0.734822324	0.128141447	3.352346067	1834.82753	66.63930418	1949.02576	96.33197031	2072.631916	69.48179451	88.52645354
CPR 04 4d	0.000334307	78.8132863	108.5635719	238.4305051	0.455325848	4.534128863	5.013308533	0.257423056	3.669741277	0.731999887	0.127745363	3.41559093	1476.644207	54.189022	1737.253558	87.09388087	2067.176561	70.60629513	71.43290202
CPR 04 5d	0.000365577	73.5576419	118.6024368	224.3140804	0.528733803	4.356566948	5.76368509	0.250677892	4.493312992	0.779590301	0.126045424	3.609737411	1441.970787	64.7922607	1704.141011	98.22132139	2043.530066	73.7660693	70.56273898
CPR-08																			
CPR 08 A 01	0.000777565	141.9290487	163.8170982	319.9841303	0.511953821	6.60623512	1.221745904	0.349392396	0.923460393	0.755853071	0.137132155	0.799927469	1931.696466	17.83845177	2060.180049	25.17016536	2191.296716	17.52878436	88.15312195
CPR 08 A 02	0.001050055	79.81956804	202.0688878	543.8894702	0.371525648	1.572428457	1.519090678	0.129654743	0.86062861	0.56654196	0.087959188	1.251780685	785.8955625	6.763642053	959.3850615	14.57392904	1381.592946	17.29451365	56.88329291
CPR 08 A 03	0.000671613	108.8153961	108.7961792	301.377335	0.360996553	6.30431925	1.930996715	0.34443954	1.035952017	0.536485644	0.132746758	1.629586369	1907.991795	19.76587948	2019.054527	38.9878766	2134.615903	34.78540978	89.38337769
CPR 08 A 04	0.005726151	92.7750207	142.9396688	279.6565328	0.511125799	5.263846156	2.761074633	0.295420129	1.766622821	0.639831607	0.129229549	2.121927647	1668.558042	29.47712714	1863.019138	51.43934884	2087.515089	44.29555982	79.93034639
CPR 08 A 05	0.000950587	36.84830289	63.28780308	214.552535	0.294975788	2.195085018	2.327520979	0.157508088	1.741018601	0.748014139	0.101075805	1.544735622	942.9137449	16.41630369	1179.482862	27.45271107	1643.961934	25.39486561	57.35617871
CPR 08 A 06	0.002765791	39.66388466	55.80677664	92.32508344	0.604459531	7.18461352	2.175171379	0.380966465	1.980489259	0.910498032	0.136777729	0.899462519	2080.796721	41.20995556	2134.595107	46.43110183	2186.796546	19.66941529	95.15273493
CPR 08 A 08	0.000565085	112.9283477	118.4159453	254.8224581	0.4646998	6.919135751	3.096758884	0.367826544	2.943947262	0.950654336	0.136429256	0.960775783	2019.16529	59.44316127	2101.113954	65.06643304	2182.358415	20.96757114	92.52216668
CPR 08 A 09	0.002046717	48.91136763	82.73835635	100.0706937	0.826799069	6.80981356	3.18356795	0.360071432	2.975277963	0.934573412	0.137165623	1.132619061	1982.512309	58.98525184	2086.999128	66.44103538	2191.720942	24.82384916	90.45459533
CPR 08 B 01	0.000329692	157.4987785	59.34724093	470.4727858	0.126143834	5.99747181	1.589862485	0.334710328	1.336950317	0.840921985	0.129956446	0.860364208	1861.171866	24.88294317	1975.477396	31.40737403	2097.374198	18.04505691	88.73818835
CPR 08 B 02	0.000403242	143.5213175	89.28907334	349.1560328	0.255728285	7.554910215	3.512480944	0.406984219	3.358993744	0.95630234	0.134632671	1.026977802	2201.118852	73.93544453	2179.525219	76.555408	2159.260862	22.17512975	101.9385332
CPR 08 B 03	0.003397821	22.12533423	1.747979644	226.9525933	0.007701959	0.885484605	2.709257885	0.106683842	2.284751095	0.84331252	0.060197865	1.456018792	653.4602039	14.92993917	643.9405722	17.44601073	610.6942478	8.891823009	107.0028425
CPR 08 B 04	0.001488283	21.90418687	34.04913931	56.30306139	0.604747566	5.815888985	2.003265275	0.322766778	1.527983786	0.762746604	0.130685079	1.295506586	1803.226991	27.55301604	1948.780527	39.03924359	2107.190782	27.29879536	85.57492781
CPR 08 B 05	0.002936423	13.81607759	15.66266616	41.82404295	0.374489529	4.913917428	3.174849365	0.278985984	2.599829032	0.818882641	0.127745084	1.822239691	1586.253434	41.2398773	1804.64889	57.29488382	2067.17271	37.66884161	76.73540899
CPR 08 B 06	0.00263785	29.21782172	37.76861965	64.75282951	0.583273657	6.610737375	4.314225033	0.348546247	4.111577835	0.953028135	0.137558749	1.306700171	1927.652915	79.25694999	2060.780893	88.90672517	2196.694867	28.70421559	87.7524204
CPR 08 B 07	0.004520322	10.76061964	11.3285607	23.34886122	0.485186862	7.693714649	6.202122934	0.40956135	5.907461821	0.952490282	0.136243513	1.888974252	2212.915757	130.7271535	2195.867706	136.1904146	2179.987286	41.17939855	101.5104891
CPR 08 B 08	0.001208735	71.92584511	54.88326657	151.9033778	0.361303793	7.492016436	3.059671741	0.394049146	2.948617709	0.963703939	0.137894535	0.816850518	2141.579805	63.1470014	2172.032776	66.45707306	2200.929939	17.97830761	97.30340651
CPR 08 B 09	0.000398067	234.4032898	101.1976774	532.989377	0.189868095	5.708783921	4.341093224	0.307763975	4.174318287	0.961582273	0.134531674	1.191703492	1729.69405	72.20293505	1932.698077	83.90022523	2157.951511	25.71638351	80.15444468
CPR 08 C 01	0.001149608	54.26483821	62.84781986	129.3962673	0.485700408	6.686386657	2.510830491	0.360142039	2.256993362	0.89890312	0.134653112	1.100113956	1982.846958	44.75272423	2070.823778	51.99487483	2159.525712	23.75724375	91.81863159
CPR 08 C 02	0.002556377	32.74272242	57.84912032	98.71362593	0.586029738	5.099433701	3.07238681	0.291978597	2.525153873	0.821886705	0.126668801	1.750188169	1651.409117	41.70062128	1836.011505	56.40937532	2052.245614	35.91815995	80.46839546
CPR 08 C 03	0.000632737	101.7735522	33.95816277	298.316882	0.113832521	5.884573152	2.623672139	0.329608152	2.177931133	0.830107962	0.129483892	1.462966669	1836.482041	39.99731412	1958.961399	51.39672444	2090.972357	30.59022864	87.82909225
CPR 08 C 06	0.004284301	19.95352023	27.40602643	61.44744113	0.446007611	4.775175147	4.427848789	0.276508751	3.939482499	0.889705744	0.125250408	2.021465443	1573.755444	61.9978203	1780.543823	78.83978812	2032.339306	41.08303675	77.4356644
CPR 08 C 07	0.000452422	115.3249134	8.107657177	1103.794171	0.007345262	0.853155675	2.6197339	0.102471681	2.334062169	0.890953913	0.060384177	1.189604766	628.8776256	14.67839475	626.3796073	16.40947892	617.3690956	7.344252182	101.8641247
CPR 08 C 08	0.000302812	185.0328425	181.1668835	412.296433	0.439409291	6.956407115	5.071947157	0.37684768	5.02137413	0.990028873	0.133880668	0.714457703	2061.541313	103.5177022	2105.881637	106.8092038	2149.483446	15.35715005	95.90868528
CPR 08 D 01	0.000751693	89.9906593	90.83178658	203.1264486	0.447168683	7.385025503	2.047286275	0.392930916	1.849691168	0.903484379	0.136312136	0.877509929	2136.406768	39.5169273	2159.158691	44.20415954	2180.863753	19.13729597	97.96149644
CPR 08 D 02	0.003037953	17.46663058	19.51137112	47.32069646	0.412322146	5.701148056	3.927332181	0.317040917	3.077491304	0.783608608	0.130420461	2.439874039	1775.261825	54.63352829	1931.54172	75.85805957	2103.633272	51.32600209	84.39027127

TABLE 8. U-Pb isotopes results obtained by LA-ICP-MS for the zircon grains of samples CPR-3, CPR 04, CPR 08, and CPR 10. (continued)

									Isotope ratios						Ages (Ma)				
Spot number	ƒ 206a	Pb ppm	Th ppm	U ppm	Th/Ub	$^{207}Pb/^{235}U$	1 s [%]	$^{206}Pb/^{238}U$	1 s [%]	Rhod	$^{207}Pb/^{206}Pb$e	1 s [%]	$^{206}Pb/^{238}U$	1 s abs	$^{207}Pb/^{235}U$	1 s abs	$^{207}Pb/^{206}Pb$	1 s abs	% Concord
CPR-03																			
CPR 08 D 03	0.003714505	15.3961245	50.15605089	96.12666417	0.52177043	1.51253652	4.591976091	0.128739977	3.927455983	0.855286679	0.085210118	2.37935578	780.6733023	30.66060032	935.4651048	42.95633396	1320.324593	31.41521952	59.12737719
CPR 08 D 04	0.001743067	34.75887735	70.70764291	92.11437799	0.767607017	6.306794646	3.562057105	0.35029384	2.635434745	0.739863137	0.130579474	2.396400327	1936.00147	51.02205539	2019.398577	71.9321305	2105.77207	50.46272879	91.93784536
CPR 08 D 05	0.001403466	37.89710107	19.89496769	106.7648086	0.186343871	6.625166301	1.954330824	0.363668348	1.266691307	0.648145796	0.132126523	1.488254716	1999.538327	25.32797817	2062.704099	40.31206201	2126.4192	31.64653403	94.03312042
CPR 08 D 06	0.000335139	148.7250774	99.91093346	334.6471831	0.298556027	8.213990236	2.031038159	0.435292659	1.815614019	0.893933977	0.136858433	0.910308595	2329.532776	42.29532366	2254.884507	45.79756479	2187.822477	19.91593605	106.4772302
CPR 08 D 07	0.000473628	171.693352	31.02128723	563.5330436	0.055047858	5.392780331	1.646521774	0.308223192	1.403193133	0.852216567	0.126895477	0.861442385	1731.95729	24.30270577	1883.707448	31.01565329	2055.402046	17.7061044	84.26367453
CPR 08 D 08	0.000492386	104.3736742	26.90604488	936.7029724	0.028724201	0.952319961	3.08895259	0.113596467	2.802981359	0.907421295	0.060801849	1.298046073	693.6008919	19.4415037	679.3099343	20.98356181	632.231493	8.206656065	109.7067925
CPR 08 D 09	0.001399292	27.95449462	43.82268064	82.11502607	0.533674319	5.124858949	4.533144134	0.29755823	4.097288513	0.903851365	0.124913298	1.93949029	1679.189132	68.80122341	1840.235292	83.42051821	2027.568259	39.3244895	82.81788414
CPR-10																			
CPR 10 A 01	0.000295324	98.51838534	138.6679523	385.2136262	0.359976758	3.842326165	3.602036893	0.236316894	2.899050865	0.804836527	0.117922909	2.137796497	1367.521116	39.64513275	1601.660373	57.69239752	1924.984602	41.15225339	71.04062624
CPR 10 A 02	0.000130185	36.18941489	39.37173032	130.3670761	0.302006699	4.529221737	5.625892577	0.264382487	5.347702374	0.95055181	0.124248063	1.747211093	1512.224658	80.86927394	1736.352816	97.68534419	2018.107697	35.26060155	74.93280265
CPR 10 A 03	0.000448369	89.45572356	98.43485414	251.0641677	0.392070502	6.66084081	3.623536678	0.363791362	3.357977207	0.926712631	0.132793066	1.361619306	2000.119821	67.16356768	2067.443513	74.914574	2135.226047	29.07365009	93.67250946
CPR 10 A 05	0.000524727	63.18555781	12.25336719	238.7971119	0.051312878	3.679551428	2.032625032	0.228618545	1.891435943	0.930538547	0.116729909	0.744335	1327.254818	25.1041747	1566.941419	31.85004352	1906.742467	14.19255155	69.60849937
CPR 10 A 07	0.000704359	28.84586366	0.907987399	305.3146656	0.00297394	0.825559402	2.052266282	0.098747691	1.603796082	0.781475628	0.060634543	1.280482339	607.0657089	9.736096055	611.145313	12.5423292	626.2947931	8.019594218	96.92970716
CPR 10 A 08	0.00126651	7.343040835	2.006488741	79.59071795	0.025210085	0.79053599	4.621054202	0.100753033	2.531488711	0.547816277	0.056906548	3.865967776	618.820441	15.6653696	591.4758702	27.33242055	487.913531	18.86257988	126.8299405
CPR 10 A 09	0.000913991	36.56306841	22.43249955	93.0670882	0.241035795	6.853704924	1.721423995	0.363321454	1.538707052	0.893857096	0.136814801	0.771803846	1997.898264	30.74180148	2092.689633	36.02406148	2187.267907	16.88141783	91.34218346
CPR 10 B 04	0.001784899	56.55461208	72.49054848	231.8201894	0.312701619	4.14651785	5.601875395	0.255172938	4.778256851	0.852974498	0.117854902	2.923913371	1465.098225	70.00615633	1663.522709	93.18846934	1923.950739	56.2546529	76.15050612
CPR 10 B 05	0.000446855	123.2231379	127.0398729	337.9290993	0.37593647	6.347521091	4.652831374	0.343365267	4.325942226	0.929744037	0.134074602	1.713202749	1902.838735	82.31570432	2025.042382	94.22180729	2152.011201	36.86831506	88.42141406
CPR 10 B 06	0.000191347	111.8298628	109.3978482	272.2490983	0.401829974	7.909872081	3.219727396	0.417924036	2.441472033	0.758285324	0.137268484	2.099013773	2251.048223	54.95871281	2220.805082	71.50386963	2193.023992	46.03187565	102.6458548
CPR 10 B 07	0.000196277	121.7477506	85.93059753	324.7484519	0.264606643	6.814428863	3.276010614	0.368870016	2.69185219	0.82168604	0.133984584	1.867130775	2024.081186	54.48527374	2087.599004	68.38996495	2150.838443	40.15896648	94.10661192
CPR 10 B 08	0.000825619	34.82190455	4.77758678	341.612063	0.013985416	0.887151079	6.14646717	0.104807672	5.154237017	0.838569031	0.061390792	3.348566775	642.5222701	33.11712069	644.837616	39.63473237	652.9543741	21.86461323	98.40232267
CPR 10 B 09	0.002003792	15.97720409	22.43458904	42.89747937	0.522981522	5.664300839	3.746293827	0.31038749	3.120632975	0.83299205	0.132355145	2.072768022	1742.613294	54.38056507	1925.943086	72.15148693	2129.445892	44.13847351	81.83411938
CPR 10 C 01	0.012230573	4.692347553	66.78425957	30.80644079	2.167866779	0.809640184	6.837866939	0.102181515	5.937646439	0.86834776	0.057466989	3.391279852	627.1807364	37.23977466	602.2521521	41.18120079	509.4994978	17.27855382	123.0974199
CPR 10 C 02	0.000446376	66.4723385	81.87629544	246.8300592	0.331711201	4.007677965	7.890139939	0.239334655	7.507496403	0.951503581	0.121446766	2.427304268	1383.237175	103.8464812	1635.754001	129.0632797	1977.588732	48.0020957	69.94564405
CPR 10 C 03	0.000198638	190.1539284	63.78313571	741.1656809	0.086057864	2.876967605	3.946761523	0.190486568	3.563039534	0.902775481	0.109539143	1.69754994	1124.010339	40.04893275	1375.89816	54.30341918	1791.760389	30.41602742	62.73217925
CPR 10 C 06	0.000263266	152.5648495	33.15612068	1498.646752	0.02212404	0.898539091	5.97539744	0.107573822	5.208517454	0.871660422	0.060579977	2.928603848	658.6422385	34.30549595	650.9465307	38.89664233	624.3537595	18.28484822	105.4918351
CPR 10 C 07	0.000896817	55.48048483	49.57838988	143.9716794	0.3443621	6.922393404	3.737951881	0.373735576	3.308893962	0.885215772	0.134335427	1.738822882	2046.953922	67.73153472	2101.531561	78.5542385	2155.403955	37.47865716	94.96845902
CPR 10 C 08	0.000359865	77.41097559	62.629102	280.2623338	0.223465998	4.866509653	2.845588944	0.284377673	2.14640162	0.754290821	0.124114013	1.868244235	1613.371796	34.62943838	1796.476468	51.12033575	2016.193944	37.66742712	80.02066475
CPR 10 C 09	0.001978981	26.04617443	41.69690603	73.13875386	0.57010687	5.789509936	4.787730981	0.32378329	4.28431609	0.894853137	0.12968391	2.137054888	1808.178988	77.46810332	1944.843138	93.11385746	2093.685478	44.74320783	86.36344893
CPR 10 D 01	0.001330995	48.09590989	73.50585986	238.6266595	0.308037082	2.638852563	4.885818933	0.180492202	4.331567009	0.886559053	0.106036506	2.260255272	1069.662996	46.33316943	1311.538206	64.07938198	1732.357074	39.1556921	61.74610373
CPR 10 D 02	0.000510683	96.54213202	100.2691894	247.7403698	0.404734963	6.385039458	2.170926085	0.345193142	2.074805726	0.955723799	0.134152927	0.638828043	1911.604209	39.66207359	2030.214001	44.07444533	2153.030856	13.75416489	88.78666109
CPR 10 D 03	0.000370119	131.486557	150.2638823	362.5310527	0.414485549	5.599331576	3.789087572	0.309444469	3.643085813	0.961467832	0.131235759	1.041686321	1737.972461	63.31582814	1915.995702	72.59875504	2114.566492	22.02714989	82.19048526
CPR 10 D 05	0.004889155	12.86251576	41.91062304	123.1354108	0.340362068	0.887657521	2.710888195	0.107306791	1.484419114	0.547576664	0.059995262	2.268350656	657.087847	9.753937598	645.1100712	17.48821277	603.4037256	13.68731237	108.8968827
CPR 10 D 07	0.008265085	7.771881219	24.08840704	79.76779891	0.301981594	0.801485572	3.045479436	0.095588488	1.31438451	0.431585416	0.060811938	2.747241954	588.5037948	7.735202719	597.6662868	18.20180386	632.5887646	17.37874394	93.03102231
CPR 10 D 08	0.001263444	20.33078077	1.152871763	193.5134653	0.005957579	0.878279761	2.128113802	0.105358237	1.571667684	0.738526146	0.060459299	1.434827183	645.733946	10.14879176	640.0531422	13.62105926	620.0525287	8.896682228	104.1418132
CPR 10 D 09	0.003824425	13.96396349	2.552699238	145.9637746	0.017488581	0.822239451	2.140671173	0.099283597	1.179882906	0.551174286	0.060064731	1.78615492	610.2091336	7.199753258	609.2970625	13.04304657	605.9072639	10.82244241	100.7099881

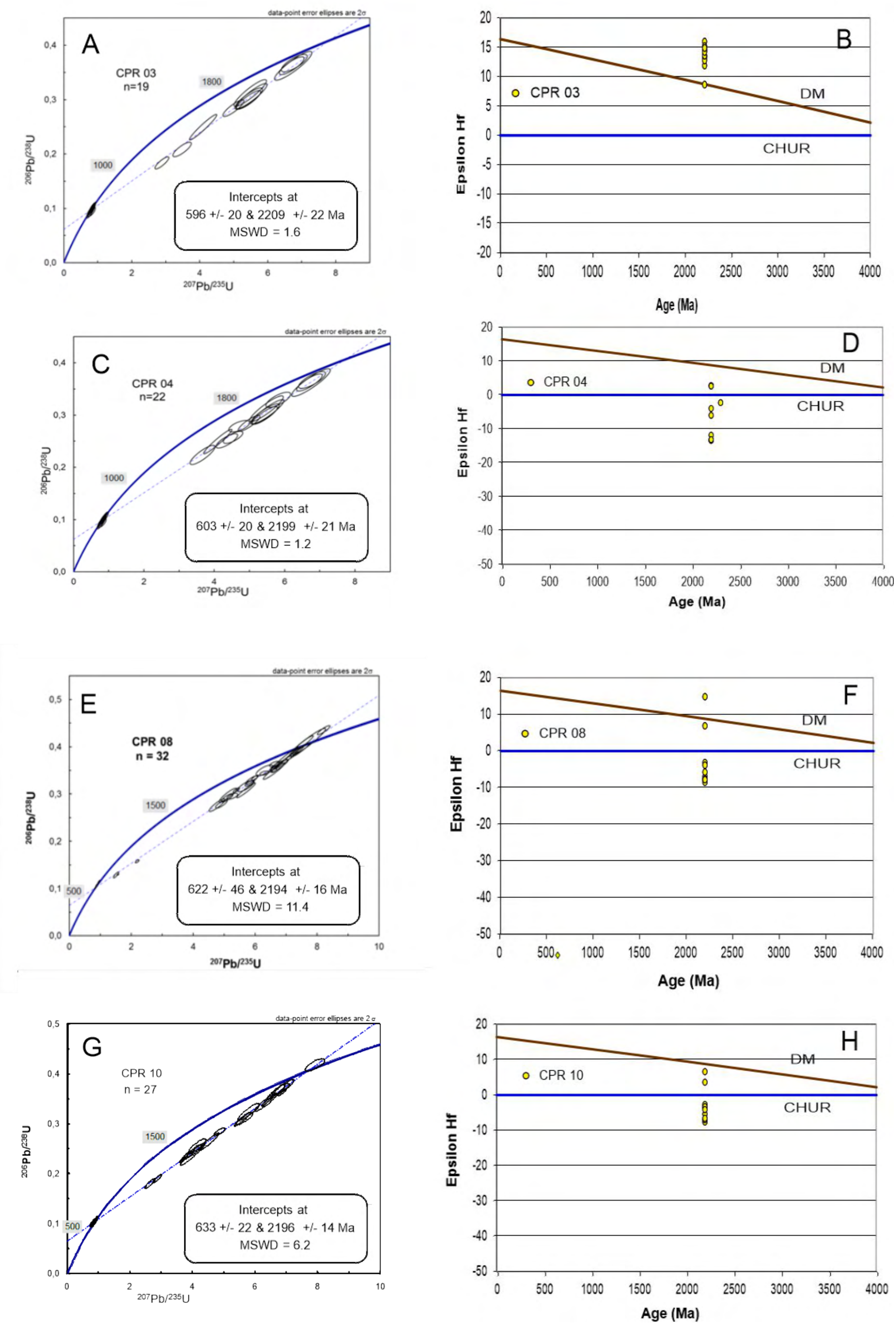

FIGURE 11. Cathodoluminescence images of the zircon grains of samples (A) CPR-3; (B) CPR 04; (C) CPR 08; and (D) CPR 10.

Table 9. Lu-Hf isotopes results obtained by LA-ICP-MS for the zircon grains of samples studied herein.

				Sample (Present day ratios)				Chur	DM	Sample Initial Ratios				DM Model Ages (Ga)				
CPR-03		**U-Pb Age (Ma)**	**±2s**	**176Hf/177Hf**	**±2SE**	**176Lu/177Hf**	**±2SE**	**176Hf/177Hf (t)**	**176Hf/177Hf (t)**	**176Hf/177Hf (t)**	**εHf(0)**	**εHf(t)**	**±2SE**	**T DM**	**T DM Crustald**	**T DM Crustale**	**Mafic**	**Felsic**
	003-Mud Tank	732	5	0.282266152	3.96392E-05	5.37413E-05	4.35013E-07	0.282322656	0.282716102	0.282265412	-18.34780491	-2.027588093	0.030546851	1.343067171	1.736793449	1.642087394	2.149957235	1.563696793
	004 samplecpr-	2212	0.6	0.281834978	6.4672E-05	0.000377936	1.28026E-05	0.281368334	0.281614089	0.281819043	-33.59519903	16.0184674	0.550648637	1.937140069	1.748751995	1.792959704	1.554543219	1.829464948
	005 Sample 2	2212	0.6	0.281737817	9.50304E-05	0.000807963	6.20853E-05	0.281368334	0.281614089	0.281703751	-37.03106388	11.92091277	0.923277846	2.090568568	2.009833406	2.029083616	1.925371594	2.044986557
	006 sample 5	2212	0.6	0.281758718	9.27251E-05	0.000381002	2.92652E-05	0.281368334	0.281614089	0.281742654	-36.29194704	13.30354678	1.029848702	2.039735054	1.921879135	1.949524852	1.800530104	1.972360203
	007 Sample 4	2212	0.6	0.281732228	5.00154E-05	7.78967E-05	7.93802E-07	0.281368334	0.281614089	0.281728944	-37.22870105	12.81627535	0.136355295	2.059338015	1.952892689	1.977576643	1.844560273	1.997966607
	008 sample 5	2212	0.6	0.281768425	4.22863E-05	0.000396795	1.06769E-05	0.281368334	0.281614089	0.281751695	-35.94867724	13.62487914	0.372355399	2.02752381	1.90141734	1.931017987	1.771474481	1.955467294
	009 Sample 6	2212	0.6	0.281826443	4.0219E-05	0.00114991	4.05177E-05	0.281368334	0.281614089	0.281777959	-33.89703776	14.55831507	0.518996279	1.987836933	1.841933653	1.877221239	1.686981519	1.906364974
	010 Sample 7	2212	0.6	0.281820142	3.72508E-05	0.00056097	1.77069E-05	0.281368334	0.281614089	0.28179649	-34.11984615	15.21690369	0.486456966	1.966281906	1.799924969	1.839232239	1.627286948	1.871693574
	011 Sample 8	2212	0.6	0.281785442	4.20335E-05	0.000374617	9.55887E-06	0.281368334	0.281614089	0.281769647	-35.34692327	14.26289662	0.36993412	2.003531282	1.860766492	1.894252946	1.713736691	1.92190999
	012 Sample 9	2212	0.6	0.281640822	5.35815E-05	0.000676884	2.34126E-05	0.281368334	0.281614089	0.281612282	-40.4610684	8.670058947	0.303887884	2.21443485	2.21606455	2.2156782	2.217758022	2.215358921
	013 Sample 10	2212	0.6	0.281773514	5.25177E-05	0.000473696	5.71692E-05	0.281368334	0.281614089	0.281753541	-35.76874013	13.69048637	1.658533954	2.024668977	1.897238643	1.927238608	1.765540184	1.952017572
	014-91500	1065	0.6	0.282140129	5.98874E-05	0.000327374	8.99804E-07	0.282110227	0.282470797	0.282133555	-22.80427627	0.826920037	0.002914224	1.52330174	1.818636815	1.747452689	2.129549188	1.68855544
CPR-04		**U-Pb Age (Ma)**	**±2s**	**176Hf/177Hf**	**±2SE**	**176Lu/177Hf**	**±2SE**	**176Hf/177Hf (t)**	**176Hf/177Hf (t)**	**176Hf/177Hf (t)**	**εHf(0)**	**εHf(t)**	**±2SE**	**T DM**	**T DM Crustald**	**T DM Crustale**	**Mafic**	**Felsic**
	003-Mud Tank	732	5	0.282343091	3.23525E-05	3.39686E-05	2.56686E-07	0.282322656	0.282716102	0.282342624	-15.62703238	0.707277215	0.010256774	1.238616516	1.565986496	1.48726639	1.909684431	1.422125545
	002 D	2199	0.6	0.28132636	7.83218E-05	0.000316348	6.65192E-05	0.281376832	0.281623902	0.281313102	-51.58123993	-2.264950829	0.477504695	2.612573027	2.893926729	2.82825549	3.180839439	2.773924679
	003 A	2199	0.6	0.281455779	3.94922E-05	2.38323E-05	3.46053E-07	0.281376832	0.281623902	0.28145478	-47.00465173	2.770229701	0.041369261	2.422744286	2.578261628	2.542325426	2.735498131	2.512609942
	002 D	2199	0.6	0.28100996	4.86727E-05	0.000842296	1.31602E-05	0.281376832	0.281623902	0.280974659	-62.76996269	-14.29304285	0.229692328	3.071151427	3.640545205	3.50517281	4.229923711	3.393043791
	004 D	2199	0.6	0.281026708	4.63682E-05	0.000667878	2.21522E-05	0.281376832	0.281623902	0.280998717	-62.17771384	-13.43804318	0.451597891	3.035273167	3.587815138	3.457336538	4.156025666	3.349270088
	008 A	2199	0.6	0.281078528	4.33741E-05	0.000865438	2.90323E-05	0.281376832	0.281623902	0.281042258	-60.34519504	-11.89060884	0.403966579	2.981476366	3.492248618	3.370650542	4.022020352	3.269954496
	009 A	2199	0.6	0.281279145	4.03384E-05	0.000358203	3.32882E-06	0.281376832	0.281623902	0.281264133	-53.25088184	-4.00528935	0.0388889	2.677963283	3.002600686	2.926729254	3.333908258	2.863948739
	006 D	2199	0.6	0.281231739	3.4268E-05	0.000578931	8.82717E-06	0.281376832	0.281623902	0.281207476	-54.92726739	-6.018828432	0.094146901	2.75618429	3.128059905	3.040436106	3.5104619	2.967916439
	007 D	2199	0.6	0.281026099	3.89481E-05	0.000603542	3.87534E-06	0.281376832	0.281623902	0.281000805	-62.19923475	-13.36384557	0.091307754	3.031109057	3.583236729	3.45318325	4.149607919	3.34546968
	009 D	2199	0.6	0.281031298	3.4016E-05	0.000604779	3.94826E-05	0.281376832	0.281623902	0.281005952	-62.01537442	-13.180908	0.865698728	3.024314172	3.571946781	3.442941753	4.133781388	3.336098452
	003 A	2199	0.6	0.281450896	3.43811E-05	2.13452E-05	2.53354E-07	0.281376832	0.281623902	0.281450002	-47.17731126	2.600410408	0.03189239	2.429037631	2.588938294	2.551993775	2.750578451	2.521443993
	014-91500	1065	0.6	0.282137211	4.61057E-05	0.000324396	4.51558E-07	0.282110227	0.282470797	0.282130696	-22.90747692	0.725592437	0.001537379	1.527134096	1.82497973	1.753200331	2.13848276	1.693809954
CPR-08		**U-Pb Age (Ma)**	**±2s**	**176Hf/177Hf**	**±2SE**	**176Lu/177Hf**	**±2SE**	**176Hf/177Hf (t)**	**176Hf/177Hf (t)**	**176Hf/177Hf (t)**	**εHf(0)**	**εHf(t)**	**±2SE**	**T DM**	**T DM Crustald**	**T DM Crustale**	**Mafic**	**Felsic**
	003-Mud Tank	732	5	0.282353396	3.5928E-05	3.77196E-05	2.38563E-07	0.282322656	0.282716102	0.282352877	-15.26261075	1.070467431	0.014218479	1.224818845	1.5432623	1.466672453	1.877694967	1.403296701
	004 sample 1	2194	0.6	0.281219814	7.61706E-05	0.000867902	3.75155E-05	0.2813801	0.281627675	0.281183525	-55.34896696	-6.986104441	0.305780571	2.792631859	3.184346798	3.090991027	3.591647298	3.013719873
	005 Sample 2	2194	0.6	0.281188514	3.50616E-05	0.000634803	8.1537E-06	0.2813801	0.281627675	0.281161972	-56.45581009	-7.75209432	0.102658023	2.817701978	3.231942984	3.13413979	3.658552368	3.053181328
	006 sample 5	2194	0.6	0.281238343	6.99235E-05	0.000493373	2.03188E-05	0.2813801	0.281627675	0.281217714	-54.69373673	-5.771060449	0.240685424	2.741411319	3.108760948	3.022475342	3.48534806	2.951064828
	007 Sample 4	2194	0.6	0.281185166	3.57126E-05	0.000549151	1.98651E-06	0.2813801	0.281627675	0.281162205	-56.57421943	-7.743816373	0.031113853	2.816003986	3.231428844	3.133673673	3.65782978	3.052755029
	008 sample 5	2194	0.6	0.281162461	4.14694E-05	0.000533784	3.20026E-05	0.2813801	0.281627675	0.281140142	-57.3771197	-8.527890428	0.51487351	2.8450471	3.280105426	3.177805543	3.726228882	3.093118359
	009 Sample 6	2194	0.6	0.28131133	3.77961E-05	0.000487214	2.92593E-05	0.2813801	0.281627675	0.281290958	-52.1127363	-3.168020952	0.191545433	2.643947438	2.946470294	2.875395651	3.256906175	2.816589098
	010 Sample 7	2194	0.6	0.281284947	0.000113563	0.00032363	2.32232E-05	0.2813801	0.281627675	0.281271416	-53.04569336	-3.862553966	0.279787314	2.667931757	2.989820184	2.914678411	3.317953525	2.852502433
	011 Sample 8	2194	0.6	0.281578825	2.58862E-05	0.000144325	5.5816E-06	0.2813801	0.281627675	0.28157279	-42.65342985	6.848040097	0.267342022	2.266947298	2.317375967	2.305660429	2.368698863	2.295976904
	012 Sample 9	2194	0.6	0.281190527	4.40735E-05	0.000724931	2.10461E-05	0.2813801	0.281627675	0.281160216	-56.38462513	-7.814481677	0.230230382	2.821512571	3.235817674	3.137652585	3.663997887	3.056394054

Table 9. Lu-Hf isotopes results obtained by LA-ICP-MS for the zircon grains of samples studied herein. (continued)

				Sample (Present day ratios)				Chur	DM	Sample Initial Ratios				DM Model Ages (Ga)				
CPR-03		U-Pb Age (Ma)	±2s	176Hf/177Hf	±2SE	176Lu/177Hf	±2SE	176Hf/177Hf (t)	176Hf/177Hf (t)	176Hf/177Hf (t)	εHf(0)	εHf(t)	±2SE	T DM	T DM Crustald	T DM Crustale	Mafic	Felsic
	013 Sample 10	2194	0.6	0.281815705	3.80214E-05	0.000432566	1.63736E-05	0.2813801	0.281627675	0.281797619	-34.27673971	14.8382348	0.567721453	1.965791162	1.810170696	1.846774903	1.649426452	1.877005347
	014-91500	1065	0.6	0.282225901	5.29709E-05	0.000307542	6.8278E-07	0.282110227	0.282470797	0.282219725	-19.77117317	3.881396038	0.01153237	1.406396657	1.627078968	1.573902388	1.859548764	1.529917976
CPR-10		U-Pb Age (Ma)	±2s	176Hf/177Hf	±2SE	176Lu/177Hf	±2SE	176Hf/177Hf (t)	176Hf/177Hf (t)	176Hf/177Hf (t)	εHf(0)	εHf(t)	±2SE	T DM	T DM Crustald	T DM Crustale	Mafic	Felsic
	003-Mud Tank	732	5	0.282347559	3.51008E-05	3.87866E-05	2.33186E-07	0.282322656	0.282716102	0.282347025	-15.46902752	0.863192531	0.011192965	1.232735267	1.55623232	1.47842651	1.895953892	1.414043249
	004 sample 1	2196	0.6	0.28131745	7.32122E-05	0.000341581	6.5115E-06	0.281378793	0.281626166	0.281303155	-51.89630724	-2.688135478	0.052677458	2.626062244	2.918047374	2.849828821	3.216051138	2.793388125
	005 Sample 2	2196	0.6	0.281576606	4.41323E-05	0.000279865	1.06594E-05	0.281378793	0.281626166	0.281564893	-42.73189432	6.613871661	0.254749929	2.277713867	2.333716274	2.320640593	2.390993713	2.309832586
	006 sample 5	2196	0.6	0.281300317	5.56874E-05	0.000479301	5.83232E-06	0.281378793	0.281626166	0.281280257	-52.50218868	-3.50188442	0.0442624	2.658064798	2.96886331	2.895875002	3.28762709	2.835483127
	007 Sample 4	2196	0.6	0.28132298	6.69959E-05	0.000913983	4.09573E-05	0.281378793	0.281626166	0.281284728	-51.70076995	-3.34299329	0.151515188	2.657328736	2.95894487	2.886887219	3.273658813	2.827266333
	008 sample 5	2196	0.6	0.28149668	4.69993E-05	0.000382694	3.9574E-05	0.281378793	0.281626166	0.281480663	-45.55829765	3.620398103	0.375974942	2.39035915	2.522456065	2.491509559	2.657894359	2.465922209
	009 Sample 6	2196	0.6	0.281247249	4.52581E-05	0.000474288	7.95481E-06	0.281378793	0.281626166	0.281227399	-54.37880237	-5.380420479	0.092576983	2.728253545	3.085987906	3.002021495	3.452495523	2.932533112
	010 Sample 7	2196	0.6	0.281183447	4.9289E-05	0.000484451	6.02199E-06	0.281378793	0.281626166	0.281163172	-56.63500512	-7.663014677	0.098692562	2.813651488	3.227961253	3.1307168	3.652145286	3.050221615
	011 Sample 8	2196	0.6	0.281204961	4.10734E-05	0.000539003	2.0558E-05	0.281378793	0.281626166	0.281182403	-55.87421641	-6.979564174	0.269132559	2.788977692	3.185491289	3.092215491	3.592444505	3.015010636
	012 Sample 9	2196	0.6	0.281295006	5.72355E-05	0.000782929	6.29415E-05	0.281378793	0.281626166	0.281262239	-52.68999692	-4.142238281	0.33497902	2.685888654	3.008817427	2.93208177	3.343884338	2.868585206
	013 Sample 10	2196	0.6	0.281214036	4.86834E-05	0.000500966	1.10406E-06	0.281378793	0.281626166	0.28119307	-55.55329235	-6.600461239	0.017492537	2.774228707	3.16191911	3.070847273	3.559300383	2.995469484
	014-91500	1065	0.6	0.28213189	5.88268E-05	0.000327452	5.44618E-07	0.282110227	0.282470797	0.282125314	-23.09562282	0.534821102	0.001302336	1.534452206	1.836919615	1.764019848	2.155298116	1.703701325
CPR-13		U-Pb Age (Ma)	±2s	176Hf/177Hf	±2SE	176Lu/177Hf	±2SE	176Hf/177Hf (t)	176Hf/177Hf (t)	176Hf/177Hf (t)	εHf(0)	εHf(t)	±2SE	T DM	T DM Crustald	T DM Crustale	Mafic	Felsic
	003-Mud Tank	732	5	0.282319893	5.1441E-05	3.7019E-05	4.33614E-07	0.282322656	0.282716102	0.282319384	-16.4473748	-0.115895372	0.002170267	1.270025479	1.617455348	1.533913369	1.982118077	1.464776737
	004 sample 1	2176	0.6	0.281292449	7.41563E-05	0.000213562	7.08366E-06	0.281391862	0.281641257	0.281283594	-52.78042989	-3.84759276	0.129696376	2.65059855	2.974932797	2.89949911	3.304336076	2.837081278
	005 Sample 2	2176	0.6	0.281056497	0.000277693	0.000535649	2.64571E-05	0.281391862	0.281641257	0.281034288	-61.12428462	-12.70734438	0.643707941	2.985651459	3.524856527	3.398089335	4.077006588	3.293103445
	006 sample 5	2176	0.6	0.281771739	9.38478E-05	0.000360087	7.3775E-06	0.281391862	0.281641257	0.281756809	-35.83149887	12.96934992	0.273613398	2.021177759	1.915317847	1.94015216	1.806324717	1.960666274
	007 Sample 4	2176	0.6	0.281311389	4.20734E-05	1.95414E-05	7.99063E-07	0.281391862	0.281641257	0.281310579	-52.11063373	-2.888595456	0.119345514	2.612749701	2.915067884	2.845251273	3.220028189	2.787486845
	008 sample 5	2176	0.6	0.281050639	4.9896E-05	0.000858191	1.45567E-05	0.281391862	0.281641257	0.281015056	-61.33144047	-13.39078475	0.233205309	3.018149493	3.567043945	3.436358404	4.136149796	3.328120176
	009 Sample 6	2176	0.6	0.281007915	4.64102E-05	0.000325334	1.4813E-05	0.281391862	0.281641257	0.280994426	-62.84226506	-14.1239368	0.649312411	3.033721582	3.612263054	3.477380691	4.199522407	3.3656585
	010 Sample 7	2176	0.6	0.280817779	4.78006E-05	0.000333778	1.23537E-05	0.281391862	0.281641257	0.28080394	-69.56594378	-20.89334446	0.782616361	3.28395696	4.027990598	3.8546745	4.781144919	3.711023564
	011 Sample 8	2176	0.6	0.280818712	4.72248E-05	0.000483215	6.18477E-06	0.281391862	0.281641257	0.280798676	-69.53298304	-21.08041267	0.279170522	3.295153198	4.039433269	3.865063128	4.797128345	3.720535957
	012 Sample 9	2176	0.6	0.280925082	4.72649E-05	0.000964218	9.10292E-05	0.281391862	0.281641257	0.280885103	-65.77146094	-18.00901518	1.708177628	3.194089099	3.851250548	3.694240872	4.534097277	3.564141586
	013 Sample 10	2176	0.6	0.280793191	6.24913E-05	0.000820949	7.76131E-06	0.281391862	0.281641257	0.280759153	-70.43543715	-22.48497799	0.223778689	3.357379975	4.125270346	3.942999827	4.916984691	3.791903997
	014-91500	1065	0.6	0.281785198	6.85035E-05	0.000301614	7.44897E-07	0.282110227	0.282470797	0.281779141	-35.35555691	-11.73604347	0.038449525	2.000129325	2.599382976	2.455405069	3.225959434	2.336130563
CPR-18		U-Pb Age (Ma)	±2s	176Hf/177Hf	±2SE	176Lu/177Hf	±2SE	176Hf/177Hf (t)	176Hf/177Hf (t)	176Hf/177Hf (t)	εHf(0)	εHf(t)	±2SE	T DM	T DM Crustald	T DM Crustale	Mafic	Felsic
	003-Mud Tank	732	5	0.282290279	2.73607E-05	3.47013E-05	1.86756E-07	0.282322656	0.282716102	0.282289801	-17.49461319	-1.16371917	0.014324597	1.309894797	1.682899049	1.593232022	2.074178043	1.519018738
	004 sample 1	2060	0.6	0.281695215	3.79064E-05	0.000107756	5.99569E-06	0.281467565	0.281728677	0.28169099	-38.53758474	7.937845279	0.445052593	2.110177994	2.144746766	2.136696755	2.180018383	2.130043402
	005 Sample 2	2060	0.6	0.281352113	3.97041E-05	0.000555337	6.10044E-06	0.281467565	0.281728677	0.281330338	-50.67056148	-4.875416504	0.055665051	2.594154252	2.949040769	2.865163045	3.315162891	2.795748164
	006 sample 5	2060	0.6	0.281452481	5.10112E-05	0.000483453	6.68882E-06	0.281467565	0.281728677	0.281433525	-47.12129318	-1.209397904	0.017304094	2.455555338	2.72015396	2.657750474	2.992834679	2.606126002
	007 Sample 4	2060	0.6	0.281440281	5.03955E-05	0.000816956	8.56796E-06	0.281467565	0.281728677	0.281408249	-47.55269797	-2.107402619	0.023092913	2.493048241	2.776311141	2.708631268	3.071969719	2.652636764
	008 sample 5	2060	0.6	0.281620641	3.72706E-05	0.000112728	6.42697E-06	0.281467565	0.281728677	0.281616221	-41.17471136	5.281449164	0.303349209	2.209609454	2.312485189	2.288535822	2.417337089	2.268736246
	009 Sample 6	2060	0.6	0.281546551	3.26092E-05	8.81091E-05	1.01465E-05	0.281467565	0.281728677	0.281543096	-43.79471357	2.683478673	0.310116971	2.306512984	2.476027783	2.436620109	2.64842349	2.40403215

Table 9. Lu-Hf isotopes results obtained by LA-ICP-MS for the zircon grains of samples studied herein. (continued)

				Sample (Present day ratios)				Chur	DM	Sample Initial Ratios				DM Model Ages (Ga)				
CPR-03		U-Pb Age (Ma)	±2s	176Hf/177Hf	±2SE	176Lu/177Hf	±2SE	176Hf/177Hf (t)	176Hf/177Hf (t)	176Hf/177Hf (t)	εHf(0)	εHf(t)	±2SE	T DM	T DM Crustald	T DM Crustale	Mafic	Felsic
	010 Sample 7	2060	0.6	0.281451031	3.95783E-05	0.000263603	1.53402E-05	0.281467565	0.281728677	0.281440695	-47.1725467	-0.954633839	0.055966592	2.443785638	2.704211433	2.643306779	2.97036275	2.592923535
	011 Sample 8	2060	0.6	0.281421153	3.35803E-05	0.000621574	5.16923E-06	0.281467565	0.281728677	0.281396782	-48.22910319	-2.514800884	0.021946511	2.506195144	2.801768597	2.731698457	3.107832437	2.673724015
	012 Sample 9	2060	0.6	0.281418813	3.57438E-05	0.000530053	1.28026E-05	0.281467565	0.281728677	0.28139803	-48.31186207	-2.470454939	0.060703537	2.503465355	2.798998099	2.729188039	3.103929887	2.671429037
	013 Sample 10	2060	0.6	0.281408005	3.28051E-05	0.000821954	1.77502E-05	0.281467565	0.281728677	0.281375777	-48.69405251	-3.261062122	0.071753221	2.536800546	2.848369524	2.773926567	3.173462591	2.712329558
	014-91500	1065	0.6	0.282132729	3.22135E-05	0.000313373	3.93688E-07	0.282110227	0.282470797	0.282126435	-23.06597582	0.574561502	0.001111116	1.532765	1.834432585	1.761766168	2.151795672	1.701640961
CPR-20		U-Pb Age (Ma)	±2s	176Hf/177Hf	±2SE	176Lu/177Hf	±2SE	176Hf/177Hf (t)	176Hf/177Hf (t)	176Hf/177Hf (t)	εHf(0)	εHf(t)	±2SE	T DM	T DM Crustald	T DM Crustale	Mafic	Felsic
	003-Mud Tank	732	5	0.28228663	2.59518E-05	3.77148E-05	1.79865E-07	0.282322656	0.282716102	0.282286111	-17.62364633	-1.294432378	0.015133999	1.314915363	1.691057368	1.600627258	2.085651184	1.52578143
	004 sample 1	629	0.6	0.281677945	5.51067E-05	4.2113E-05	1.30929E-06	0.282388095	0.282791669	0.281677448	-39.14828597	-25.16561722	0.811326561	2.129614104	3.079626401	2.851440484	4.068528393	2.662133786
	005 Sample 2	629	0.6	0.281455147	4.19481E-05	0.001072329	0.0001115	0.282388095	0.282791669	0.28144248	-47.02699084	-33.48634848	3.518805617	2.489390865	3.58240446	3.308563501	4.766492214	3.081203028
	006 sample 5	629	0.6	0.28140892	4.46768E-05	0.000427124	0.000133065	0.282388095	0.282791669	0.281403874	-48.66172074	-34.85347833	10.89691127	2.510083293	3.664563381	3.38329891	4.88030554	3.149745267
	007 Sample 4	629	0.6	0.281383504	3.76244E-05	0.000942772	4.22658E-05	0.282388095	0.282791669	0.281372367	-49.56049012	-35.96921316	1.65167214	2.57775431	3.731521218	3.444214394	4.973011384	3.205618671
	008 sample 5	629	0.6	0.281564771	4.26492E-05	0.000565759	3.89962E-05	0.282388095	0.282791669	0.281558088	-43.15042013	-29.39242446	2.058425102	2.310268007	3.335619905	3.084139667	4.42422011	2.875424432
	009 Sample 6	629	0.6	0.281658923	3.12581E-05	4.7249E-05	2.42675E-06	0.282388095	0.282791669	0.281658365	-39.82095035	-25.84137553	1.354754466	2.155150954	3.120635467	2.888711089	4.125553264	2.696290593
	010 Sample 7	629	0.6	0.281425866	4.93526E-05	0.001052063	0.000103061	0.282388095	0.282791669	0.281413438	-48.06245143	-34.51478686	3.42008823	2.52773259	3.644221147	3.364793744	4.852132061	3.132772849
	011 Sample 8	629	0.6	0.28146028	5.60642E-05	0.000840651	6.03833E-05	0.282388095	0.282791669	0.281450349	-46.84549618	-33.20768475	2.423572492	2.467627457	3.565642435	3.29331729	4.743263806	3.067221212
	012 Sample 9	629	0.6	0.281484937	3.72791E-05	0.00044924	7.53279E-05	0.282388095	0.282791669	0.28147963	-45.97355432	-32.170785	5.429298214	2.410096596	3.503225306	3.236548428	4.656742975	3.015163197
	013 Sample 10	629	0.6	0.281523143	4.42087E-05	0.000735659	8.90823E-05	0.282388095	0.282791669	0.281514453	-44.62249288	-30.93763752	3.780662231	2.376423367	3.428900052	3.168956846	4.553664598	2.953186538
	014-91500	1065	0.6	0.28203358	4.44019E-05	0.000321407	1.10595E-06	0.282110227	0.282470797	0.282027126	-26.57212129	-2.945689415	0.012259277	1.667032426	2.054289822	1.961032857	2.461161253	1.883843615

intercept). This age is interpreted as regional metamorphism. The lower intercept may result from episodic Pb loss due to heating (metamorphism or hydrothermal alteration) according to Wetherill (1956) or continuous Pb loss (Tilton 1960; Wasserburg 1963).

Figure 11B shows the Lu and Hf isotope analytical results (Table 9) of the zircon grains from sample CPR 03. Ten Lu-Hf analyses resulted in T_{DM} 'crustal model age values ranging between 1.83 and 2.22 Ga and ε_{Hf} values ranging from 8.7 to 16, calculated for the U-Pb age of 2209 ± 22 Ma. These results indicate that the analyzed rock was generated from a magma whose epoch of mantle extraction is close to the U-Pb age suggesting a juvenile character for this sample.

5.2. Banded charno-enderbite (Sample CPR 04)

The zircon grains morphology of the sample CPR 04 shows a length to width ratio ranging from 1:1 to 1:5. CL images present grains with whitish rims involving dark gray cores (Figure 10B).

In the sample CPR 04 a total of 22 grains were used, and the Concordia diagram obtained for these analytical data (Table 8) is presented in Figure 11C. In the construction of the concordia diagram and age calculation, the selected data presented concordances ranging from 70 to 99% and errors smaller than 10.87 (%), which resulted in small ellipses. The age obtained in the upper intercept of 2199 ± 20 Ma (MSWD = 1.2) is interpreted as the age of crystallization of the orthogneiss protolith and the age 600 ± 20 Ma obtained in the lower intercept is interpreted as representing the metamorphic peak. When the core has a lighter gray color, the oscillatory zoning is observed, and the ages indicate Paleoproterozoic isotopic inheritance. The rims of light gray grains have Neoproterozoic ages.

The analytical results (Table 9) of the Lu and Hf isotopes of the sample CPR 04 are shown in Figure 11D. Ten Lu-Hf analyses resulted in T_{DM} 'crustal model' age values between 2.51 and 3.39 Ga and the ε_{Hf} values ranging from -14.3 to 2 calculated for the U-Pb age of 2109 ± 20 Ma. The Lu-Hf results show positive and negative ε_{Hf} values, indicating that the magmatic sources of the protolith are mantle-derived with important contribution from older crust.

5.3. Granitic gneiss (Sample CPR 08)

The cathodoluminescence images of the CPR 08 sample (Figure 10C) show that the zircon grains have in general rounded shapes; in this sample, subeuhedral, grains predominate (length /width ratio ranging from 1:2 to 1:3, more homogeneous compared to the other samples). The oscillatory zoning pattern predominates and a small region with contrast in the luminescence at the center of some grains is common. Again, the metamorphic overgrowth is seen in the grains where the CL images show light gray shades.

A total of 32 spots on zircon grains were analyzed and the results are presented in Table 8 and are plotted in Figure 11E. The analytical errors are smaller than 4.6% and concordances vary between 76 and 110%. Concordia diagram plot described a clear discordance related to lead loss, yielding metamorphic age at the lower intercept of 622 ± 46 Ma. The magmatic crystallization age of the orthogneiss protolith is given by the upper intercept at 2194 ± 16 Ma, with MSWD of 11.4. The rims of the zircon grains are thick enough and the analyzes carried out confirm the Neoproterozoic ages.

In Figure 11F the Lu and Hf isotopes analytical results (Table 9) of the sample CPR 08 are presented, which resulted in T_{DM} 'crustal' model age values between 1.88 and 3.06 and ε_{Hf} values ranging from -7, 8 and 14.8 calculated for the U-Pb age of 2194 ± 16 Ma.

The results indicate that the analyzed rock crystallized in the Paleoproterozoic was generated from a magma whose period of mantle extraction was in the Archean-Paleoproterozoic limit. In addition, the values of ε_{Hf} suggest a juvenile character for this sample, but with partial crustal contribution in its formation.

5.4. Granulitic gneiss (Sample CPR 10)

The zircons observed in sample CPR 10 mostly present the prismatic habit preserved (Figure 10D) but are rounding in the rims. The cores show growth with oscillatory zoning, characterized by the alternation of light and dark bands.

The U-Pb analyses (results presented in Table 8) of the sample CPR 10 are shown in Figure 11G, and they have analytical errors lower than 7.5 and concordant values ranging from 70% to 123% (MSDW = 6.2). For this sample, 27 spots were performed, which were concordant or plotted near the concordia curve, generating a population with a crystallization age of 2196 ± 14 Ma marking the upper intercept of the concordia curve and 633 ± 22 Ma, marking the inferior intercept related to the metamorphic event. The analyses in the zircon nucleus present Paleoproterozoic isotopic inheritance. Many grains have a fine metamorphic overgrowth indicated by the whitish color in the CL image. The analyses in this area of the grains were difficult due to the small size of the metamorphic border and because this region is fractured, which limits the quality of the analyses obtained. The results achieved in this portion of the zircon grains indicate Neoproterozoic age.

In Figure 11H, the Lu and Hf isotopes results of the studied zircon grains (reported in Table 9) are plotted. In the sample CPR 10, the ten Lu-Hf analyses resulted T_{DM} 'crustal' model age values ranging from 2.31 to 3.05 Ga and ε_{Hf} values ranging from -7.7 to 6.6 calculated for the U-Pb age of 2196 ± 14 Ma. As in sample CPR 03, the results of the sample CPR 10 indicate that the rock from which the zircons were extracted was generated from a mantle source, suggesting a juvenile character for this sample, however, there may have been some crustal contribution in the magmatic process (ε_{Hf} value reaches -7.7). The mantle extraction age of the sample yielded values from the Archaean to the Paleoproterozoic. The negative ε_{Hf} values for the lower intercept age may be interpreted as result of the magma generation by anatexis process during the metamorphic peak, as indicated by petrographic studies.

5.5. Mylonitic granite (Sample CPR 13)

The cathodoluminescence images (Figure 12A) of the sample CPR 13 show a homogeneous family of magmatic, prismatic zircon crystals (ratio width/length ranging from 1: 2 to 1: 3), and euhedral to subhedral features. Most of these grains occur with oscillatory zoning and some with thin metamorphic overgrowth, with non-uniform zoning pattern. In this sample the difference between the oscillatory magmatic pattern and the irregular pattern of metamorphic zoning is well characterized. The grains with irregular zoning pattern may be related to hydrothermal fluids associated with mylonitization.

For the sample CPR 13, nineteen zircon grains (Figure 13A) were analyzed for U-Pb (results in Table 10). After discarding the grains with discordant results and/or with high individual errors, a concordia diagram plot suggests magmatic crystallization age at 2060 ± 39 Ma (MSWD = 2.1). Concordance values are between 80 and 110%, but few grains can present values up to 150%. However, the errors assume values higher than in the other samples (up to 27% in some cases), but the *rho* value for these spots remains close to 1. An age of 600 ± 18 Ma is observed in the lower intercept.

The Lu and Hf isotope results (Table 9) of the CPR 13 sample are shown in Figure 13B which resulted in T_{DM} 'crustal' model age values between 1.96 and 3.79 Ga and the

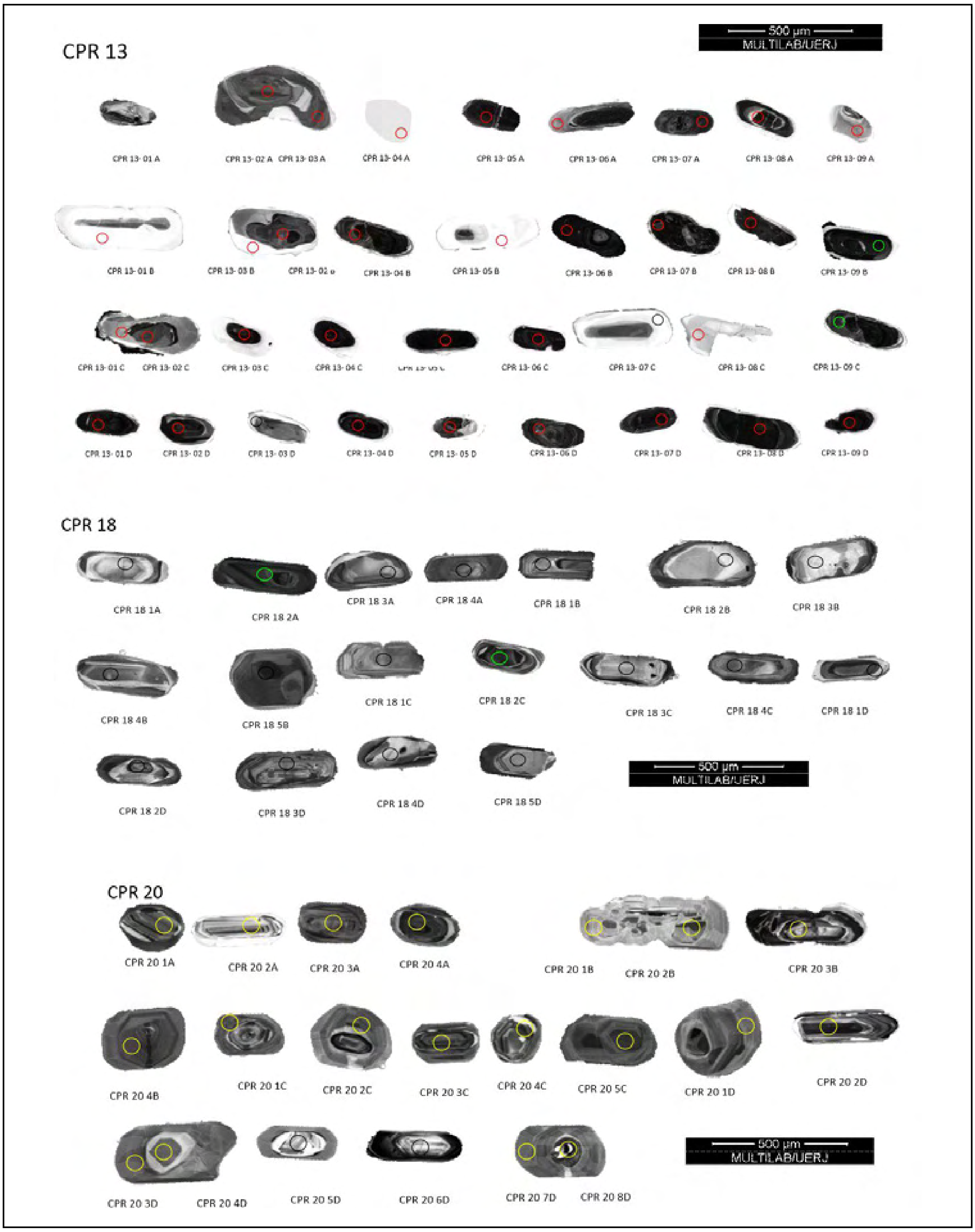

FIGURE 12. Cathodoluminescence images of the zircon grains of samples CPR-13, CPR 18 and CPR 20.

ε_{Hf} values range from -22.5 to + 13 calculated for the U-Pb age of 2092 ± 68Ma.

From the results it is possible to interpret the formation of this rock from the mixture of two sources (mantle and crust) in a period of mantle extraction that begins in the Archaean Eon going to the Paleoproterozoic Era, period when the rock was crystallized, as demonstrated by the U-Pb age. The metamorphic event that reaches this rock in the Neoproterozoic Era is characterized by crustal reworking pointed out by the age of inferior intercept of the concordia diagram.

5.6. Granitic gneiss (Sample CPR 18)

From the CL images it was possible to individualize two groups of zircon grains in the sample CPR 18 (Figure 12B). The first of prismatic zircon crystals, elongated, with width / length pattern (1: 3 to 1: 4) and the second group of zircon

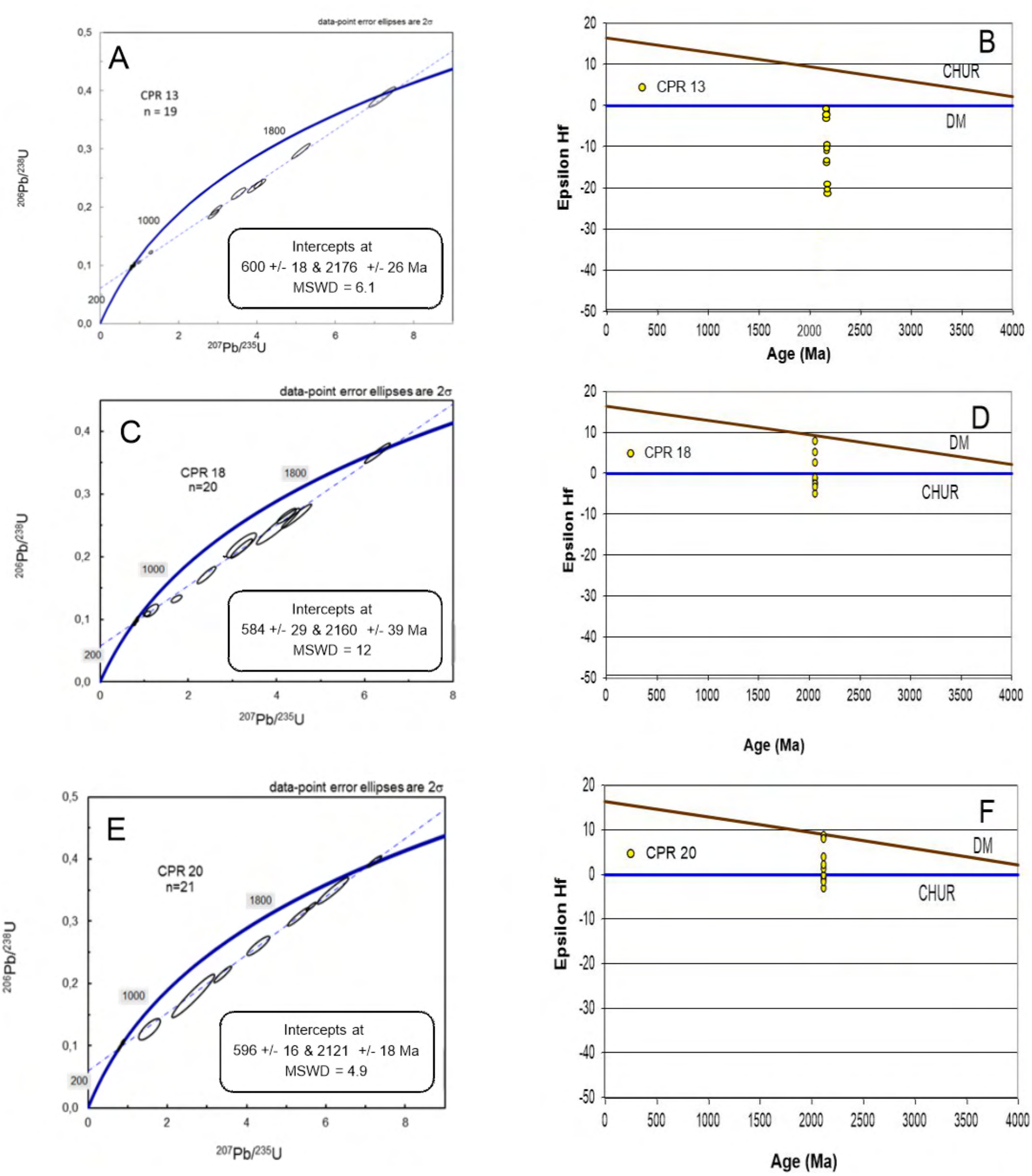

FIGURE 13. Concordia diagrams and Hf isotopic evolution for the zircon grains of samples (A) CPR-13, (B) CPR 18 and (C) CPR 20.

grains with rounded white ends. The zircon grains textures are oscillatory (boundaries between light and dark zones, straight and regular) or convolute (with boundaries between light and dark areas curved and irregular), but some regions present homogeneous light gray pattern.

The U-Pb results are presented in Table 10. In the concordia diagram it is observed that the spots with good analytical consistency are aligned in a straight discordia, characterizing events of episodic Pb loss (Figure 13C). This discordia line defines a superior intercept in 2060 ± 39 Ma, interpreted as age of magmatic crystallization, and a lower intercept in 584 ± 29 Ma, which indicates the Neoproterozoic metamorphism peak.

The analytical results (Table 9) of the Lu and Hf isotopes are shown in Figure 13D. Analyses resulted in T_{DM} 'crustal' model age values between 2.13 to 2.80 Ga and ε_{Hf} values ranging from -4.9 to +7.9 calculated for the U-Pb age of 2060 ± 39 Ma.

The results are consistent with the crystallization ages and metamorphism observed in the previous samples. The crystallization occurred in the Paleoproterozoic era from magmas originated from mixture of mantle and crustal sources and metamorphic ages point out to reworking of the rocks already formed in the Paleoproterozoic era.

5.7. Banded felsic protomylonitic gneiss (Sample CPR 20)

The sample CPR 20 shows zircon grains morphology (Figure 12C) ranging from well-formed crystals (1:4) to rounded crystals (1:1). Irregular zoning (interpreted as a result of metamorphic fluids or growth during the metamorphic event) predominates in some zircon families, and oscillatory zoning may also occur (in areas with preservation of the core with magmatic origin). Large number of nucleated grains are observed, with convolute zoning, homogeneous of low luminescence and oscillatory zoning. The analytical results of the Paleoproterozoic cores present a greater analytical error, probably due to the isotopic re-homogenization, while the rims grown during the metamorphic event present a more accurate analytical result with lower error and higher agreement.

The U/Pb analytical data (Table 10) obtained in the analysis of the sample CPR 20 are illustrated in Figure 13E with errors lower than 15% and concordant values ranging from 90 to 100%. The measurements of the 21 spots with better analytical coherence were selected, resulting in the concordance age of 2121 ± 18 Ma in the upper intercept, interpreted as the age of magmatic crystallization and 592 ± 16 Ma in the lower intercept, indicating the metamorphic event age.

Lu and Hf isotopes obtained for sample CPR 20, plotted in Figure 13F (results presented in Table 9), resulted in T_{DM} crustal model ages between 2.13 and 2.74 Ga and ε_{Hf} values ranging from -2.9 to 8.8 calculated for the U-Pb age of 2121 ± 18 Ma. Results for the U-Pb age of 596 ± 16 Ma, show ε_{Hf} values ranging from -36.0 to -25.2. Like sample CPR 13, the sample CPR 20 was crystallized in the Paleoproterozoic era and was formed from mantle and crustal sources, extracted from the mantle in the Archean eon to the Paleoproterozoic era. The metamorphism of this rock marks a period of crustal reworking evidenced by the negative ε_{Hf} values.

6. Discussion

Compositionally, the rocks of the Serra do Caparaó region are composed of an association of Paleoproterozoic enderbitic, charnockitic, dioritic, and gabbroic quartz granulites as reported in this work and data from literature (Silva et al. 2002). Some authors consider that the rocks of the Serra do Caparaó region are part of Juiz de Fora Complex (Seidensticker and Wiedmann 1992; Campos Neto and Figueiredo 1990). But such interpretation is not consensual and is still a matter of debate as noted by Noce et al. (2007), because some crystallization ages of charnockitic gneiss zircons have an age of 2195 ± 15 Ma, which is older than those found for Juíz de Fora Complex (2134-2084 Ma). Therefore, this work (i) discusses issues related to crystallization age and sources of Paleoproterozoic photolith and (ii) the Neoproterozoic metamorphic event and; (iii) propose a model for the evolution of the basement of the Ribeira-Araçuaí orogen.

6.1 The Ribeira-Araçuai belt basement evolution (ages and sources)

The obtained U/Pb data allowed to identify two age groups in the studied rocks. The first group is associated with Paleoproterozoic magmatic rocks represented by the samples (CPR 03, CPR 04, CPR 08 and CPR 10) characterized by zircon grains with Paleoproterozoic nucleus and Neoproterozoic borders, interpreted as metamorphic ages. The second group of rocks is represented by samples CPR 13, CPR 18 and CPR 20 and presents Neoproterozoic ages. The ages obtained in most of the samples may be correlated with two thermal events reported in the literature, the oldest (see results in Tables 8 and 10) related to the Paleoproterozoic magmatic event from 2.2 Ga to 2.0 Ga Ma (Ávila et al. 2010) and a younger event linked to the isotopic re-homogenization of the Brasiliano Orogeny (Heilbron et al. 2004).

The group of ages ranging from 2209 ± 22 Mato 2060 ± 39 Ma can be correlated to the implantation of the Juiz de Fora magmatic arc (as proposed by Heilbron et al. 2010; Ávila et al. 2010). It has the same age range of the rocks of the Serrinha and Ritapolis magmatic arcs (of about 2230 – 2180 Ma) and represents magmatic arcs originated by an oceanic lithosphere subduction related to the Paleoproterozoic grown of the São Francisco craton. Juíz de Fora magmatic arc developed after the consolidation of the Serrinha arc (very close to 2192 – 2121 Ma, reported to Ritapolis magmatic arc) in the Mineiro Belt, according to Ávila et al. (2010). Serrinha and Ritapolis present an intra-oceanic signature according to Ávila et al. (2006) and Juíz de Fora is marked by an important older continental crust participation in the magma generation (Noce et al. 1998).

The results obtained in this work suggest a possible regional correlation between the Caparaó complex and uíz de Fora complex. The Paleoproterozoic ages determined in this work are similar to those obtained in granulitic rocks by U-Pb in zircons by other authors (Silva et al. 2002; Heilbron et al. 2004). It is also emphasized that the ages obtained in the above-mentioned works also present strong crustal reworking associated with the Brasiliano event.

The εHf values results suggest that rocks crystallized from 2209 to 2060 Ma of the Caparaó Complex present juvenile (mantle source) magmatism with important continental

TABLE 10. U-Pb isotopes results obtained by LA-ICP-MS for the zircon grains of samples CPR-13, CPR 18 and CPR 20.

									Isotope ratios						Ages (Ma)				
Spot number	ƒ 206a	Pb ppm	Th ppm	U ppm	Th/Ub	207Pb/ 235U	1 s [%]	$^{206}Pb/^{238}U$	1 s [%]	Rhod	$^{207}Pb/^{206}Pb^{e}$	1 s [%]	$^{206}Pb/^{238}U$	1 s abs	$^{207}Pb/^{235}U$	1 s abs	$^{207}Pb/^{206}Pb$	1 s abs	% Concord
CPR-13																			
CPR 13 A 01	0.002628395	12.60289818	33.96020794	115.599489	0.293774724	0.842540002	5.045724107	0.099975707	4.727451756	0.936922363	0.061121608	1.763669942	614.2665259	29.03915366	620.5463322	31.31105588	643.5163334	11.34950414	95.45469074
CPR 13 A 02	0.000940029	68.66851424	205.0380739	271.7134111	0.754611534	3.452677414	5.472256852	0.220396478	4.432683997	0.810028498	0.113618769	3.208879499	1283.969621	56.91431593	1516.480257	82.98569478	1858.084569	59.62369479	69.10178596
CPR 13 A 03	0.000584513	123.4127722	298.9392384	325.2554898	0.919090524	5.00559285	2.427196908	0.279519628	2.151645605	0.886473445	0.129879897	1.12325688	1588.942576	34.18841311	1820.268241	44.18149445	2096.339059	23.54727271	75.79606789
CPR 13 A 04	0.001027738	38.6137742	13.2492776	393.5479556	0.033666234	0.795193919	2.264852029	0.096633054	1.887803602	0.833521827	0.059682371	1.251300233	594.6470629	11.22576868	594.1138742	13.45580014	592.0784176	7.408678621	100.4338353
CPR 13 A 05	0.032626095	1.532974481	11.62032328	12.70912296	0.914329283	0.871478009	7.875925633	0.096492742	3.347104719	0.424979218	0.065502898	7.129312349	593.8222026	19.87585097	636.3694954	50.11998821	790.5306409	56.3593986	75.11691159
CPR 13 A 06	0.004712561	5.923879172	3.335952088	59.60305266	0.055969484	0.819761039	3.31940348	0.098606331	1.740779705	0.524425463	0.060294986	2.826327207	606.236293	10.55323836	607.915109	20.17915528	614.1772192	17.35865784	98.70706272
CPR 13 A 07	0.001932253	38.06558208	31.47623346	112.5101736	0.279763442	5.865597019	2.192795739	0.335930165	1.902401668	0.867569028	0.126637388	1.090514121	1867.060771	35.51899524	1956.158807	42.89456697	2051.807665	22.37525233	90.99589608
CPR 13 A 08	0.002445363	28.93450497	18.92870768	96.92783341	0.195286607	5.229187032	2.859111836	0.317775386	2.183126774	0.763568164	0.119347313	1.846206374	1778.85577	38.8346766	1857.385218	53.1047206	1946.474295	35.93593251	91.38860835
CPR 13 A 09	0.008776935	4.670847936	2.266238511	46.91101981	0.0483093	0.86106131	3.183486935	0.099120272	2.071073071	0.650567479	0.063004318	2.417694233	609.2512972	12.61803955	630.7020578	20.07831761	708.3764553	17.12637671	86.00671192
CPR 13 B 01	0.008533073	3.590799017	3.116493149	37.93873949	0.082145406	0.785065681	4.040587688	0.094723364	2.187593619	0.541404812	0.060110122	3.397172798	583.411413	12.76267084	588.3690009	23.77356541	607.5409572	20.63921613	96.02832633
CPR 13 B 02	0.001435019	60.64431609	182.7333013	297.1548353	0.614943052	3.144268742	30.02991634	0.245437779	9.865576838	0.328524952	0.092913104	28.36311459	1414.904741	139.5885144	1443.596846	433.5109251	1486.117003	421.5090685	95.20816586
CPR 13 B 03	0.006866649	6.948359699	2.380866394	72.45997394	0.032857677	0.786365839	2.9613079	0.096101171	1.699299787	0.573834212	0.059346441	2.425226735	591.5197029	10.05169305	589.108289	17.4453103	579.828682	14.06216021	102.0162888
CPR 13 B 04	0.003812834	9.137355338	1.309334801	98.6445386	0.013273262	0.778283822	2.585949132	0.09600502	1.641288526	0.634694823	0.058795324	1.998325521	590.9541877	9.699263279	584.50399	15.11497586	559.5255172	11.18114121	105.6170218
CPR 13 B 05	0.018463981	3.204740252	33.42092127	23.97142377	1.394198425	0.68931076	6.764803496	0.092483289	3.941751793	0.582685335	0.054056823	5.497741276	570.2069403	22.47614229	532.3862636	36.01488457	373.417597	20.52953336	152.6995366
CPR 13 B 06	0.000452126	117.5414112	87.55352262	361.429742	0.242242163	5.075484195	3.903540995	0.285783828	3.757998472	0.962715257	0.12880673	1.055973385	1620.425559	60.89556776	1832.016743	71.51352459	2081.749648	21.98272222	77.83959811
CPR 13 B 07	0.000435126	87.21386355	129.2257904	412.4016236	0.313349373	2.3731879	10.20313419	0.15635934	7.770523413	0.761582007	0.110079645	6.612330392	936.5129399	72.77195726	1234.561874	125.9640047	1800.719581	119.0695281	52.0077057
CPR 13 B 08	0.000704738	78.07776768	143.64778	261.2275433	0.54989523	3.564945574	12.6072496	0.197235077	11.62659745	0.922215219	0.13108937	4.874933252	1160.449933	134.9208423	1541.764321	194.3740762	2112.609398	102.988298	54.92969664
CPR 13 B 09	0.003212427	50.40645377	97.20665151	228.407079	0.425585109	3.246674067	15.18182949	0.228679672	9.151372913	0.602784593	0.102969797	12.11364192	1327.575541	121.4913885	1468.382093	222.9272657	1678.330656	203.3069659	79.10095286
CPR 13 C 01	0.005681731	9.963157496	13.76905116	26.819067	0.513405301	4.928713095	4.036093872	0.285770969	3.719654537	0.921597628	0.12508757	1.566596267	1620.361093	60.2718349	1807.186042	72.93972509	2030.036624	31.80247798	79.81930344
CPR 13 C 02	0.00521309	7.369130991	34.36177015	52.46153953	0.65498974	1.288332673	5.071456087	0.125290228	3.024357841	0.596349015	0.074577797	4.070985936	760.9410643	23.01358075	840.5579143	42.62852551	1057.145294	43.03623624	71.98074556
CPR 13 C 03	0.001363934	22.991356	28.20075625	85.33859791	0.330457225	3.495431128	13.14803478	0.211071182	12.50938425	0.951426161	0.120107612	4.047977782	1234.522108	154.4311142	1526.183252	200.6631048	1957.818045	79.2520395	63.05601846
CPR 13 C 04	0.000781713	69.3392876	61.98938077	207.9123679	0.298151483	6.452764148	11.32645762	0.382640713	7.956743198	0.702491765	0.122307571	8.060947825	2088.607449	166.1851311	2039.48316	231.0011957	1990.158741	160.4256577	104.9467767
CPR 13 C 05	0.000211018	75.7586165	71.59604427	205.4504759	0.348483224	2.977219039	9.554948785	0.170675711	8.836363208	0.924794408	0.126513769	3.635344761	1015.83312	89.76270408	1401.820421	133.9432232	2050.082907	74.52758154	49.55083118
CPR 13 C 06	0.001159399	32.2148929	38.42250102	138.3788634	0.277661632	3.682141663	7.500452163	0.239787033	5.66075499	0.754721831	0.11137136	4.920633658	1385.589797	78.43484356	1567.5033	117.5698352	1821.914436	89.64973495	76.05131008
CPR 13 C 07	0.001820064	24.00200115	73.1216264	213.1859309	0.342994616	0.87001694	2.301400459	0.104406526	1.389834728	0.603908252	0.060436428	1.834340073	640.1812125	8.89746081	635.5764732	14.62715987	619.2360299	11.35889464	103.3824231
CPR 13 C 08	0.032366875	1.319365858	9.879611703	11.04744523	0.894289268	0.762512561	31.18234295	0.095820599	4.526632537	0.14516653	0.057714753	30.85203575	589.869386	26.70121956	575.4585801	179.441468	518.9502557	160.1067184	113.6658821
CPR 13 C 09	0.008077747	9.481982461	16.02562474	84.19672865	0.19033548	0.909500128	7.54343313	0.099800328	3.930813712	0.521090814	0.066095139	6.438329515	613.2386351	24.10526835	656.7918916	49.54465715	809.3900871	52.11120087	75.7655233
CPR 13 D 01	0.000872749	37.62410903	35.32514628	119.2592389	0.296204693	6.320706773	4.774637613	0.374386434	3.785865987	0.792911692	0.122445905	2.909361281	2050.007423	77.61053375	2021.330027	96.51118375	1992.168824	57.95938841	102.9032981
CPR 13 D 02	0.001122346	27.18111201	36.98924506	142.2247323	0.260076039	3.398552278	11.36576846	0.235500803	4.188214908	0.368493773	0.104664713	10.56596179	1363.26444	57.09644449	1504.061998	170.9482042	1708.431361	180.5122048	79.79626637
CPR 13 D 03	0.002167941	15.0196097	20.06742704	142.2282783	0.141093088	0.910301307	3.669169327	0.109291009	3.048910741	0.830953949	0.060408695	2.04131008	668.6290452	20.38590277	657.2178324	24.11443511	618.2454209	12.6203061	108.1494537
CPR 13 D 04	0.00068704	103.9540627	70.74742221	370.6633313	0.190867065	4.631725613	6.653898325	0.27345155	6.403826849	0.962417298	0.122846039	1.807031987	1558.297953	99.79070268	1755.004212	116.7761959	1997.967637	36.10391429	77.99415386
CPR 13 D 05	0.001180872	46.29146133	59.58115676	134.0398356	0.444503356	2.626155594	27.31949142	0.16321561	25.32138325	0.926861443	0.116696408	10.2558355	974.6220612	246.7877874	1307.989056	357.335958	1906.226938	195.499499	51.12833324
CPR 13 D 06	0.000403278	90.53751523	53.61787283	224.342336	0.239000243	7.198111701	3.871265884	0.389048358	3.653502147	0.9437487	0.134188012	1.280086561	2118.413398	77.39627897	2136.268312	82.70062636	2153.487384	27.5665026	98.37129365
CPR 13 D 07	0.000464916	123.95649	117.9549783	572.7227357	0.205954768	2.902770711	6.558166324	0.186490316	5.751838439	0.877049796	0.112889922	3.150539654	1102.33447	63.40449777	1382.633639	90.67541372	1846.450722	58.17316218	59.70018355
CPR 13 D 08	0.000776715	59.32830655	154.9056767	552.0383555	0.280606728	0.86328256	2.495001674	0.101622664	1.453399514	0.582524464	0.061611406	2.027970219	623.9113076	9.067923914	631.9132348	15.76624579	660.647731	13.39773923	94.43933254
CPR 13 D 09	0.000377708	142.0028686	170.9993515	519.4114794	0.329217505	3.49798678	5.741460653	0.21133966	5.11998381	0.891756318	0.120042736	2.598102424	1235.951034	63.28049284	1526.760333	87.6583438	1956.853477	50.84105762	63.16012152
CPR-18																			
CPR 18 A 01	0.00068833	30.9142901	6.21219852	312.9211318	0.019852282	0.817887463	1.246858964	0.098613717	0.879545548	0.705409011	0.060152675	0.883774238	606.2796292	5.332505487	606.8691599	7.566802517	609.0710184	5.382812753	99.54169725
CPR 18 A 02	0.00145367	14.19162081	13.24100866	37.03679583	0.357509562	6.285975047	3.778446029	0.365377415	3.615839141	0.956964613	0.124775604	1.096522552	2007.612473	72.59203759	2016.501268	76.19241209	2025.615041	22.21132573	99.11125423
CPR 18 A 03	0.001130709	16.14072718	23.88326945	162.0548755	0.147377667	0.795700316	4.267610745	0.095366497	1.798280633	0.421378786	0.060513521	3.870231031	587.1974719	10.55945841	594.4002581	25.36668928	621.9865782	24.07231756	94.40677541

TABLE 10. U-Pb isotopes results obtained by LA-ICP-MS for the zircon grains of samples CPR-13, CPR 18 and CPR 20. (continued)

									Isotope ratios						Ages (Ma)				
Spot number	ƒ 206a	Pb ppm	Th ppm	U ppm	Th/Ub	207Pb/ 235U	1 s [%]	^{206}Pb/ ^{238}U	1 s [%]	Rhod	^{207}Pb/ ^{206}Pbe	1 s [%]	^{206}Pb/ ^{238}U	1 s abs	^{207}Pb/ ^{235}U	1 s abs	^{207}Pb/ ^{206}Pb	1 s abs	% Concord
CPR 18 A 03	0.001262677	15.43529507	40.27678665	65.10020778	0.618689065	3.205840572	8.600904676	0.21820142	7.382447918	0.858333884	0.106557267	4.413051549	1272.364382	93.93163781	1458.57153	125.450347	1741.340259	76.84624329	73.06810802
CPR 18 B 01	0.000336016	41.41634873	37.40315345	409.3635586	0.091369035	0.850107945	1.584175041	0.102787235	1.255376794	0.792448285	0.05998375	0.966250312	630.7224836	7.917943693	624.7083169	9.896473236	602.9884677	5.826377954	104.5994272
CPR 18 B 02	0.002257372	6.14127304	31.02154402	55.84170559	0.555526442	0.839044375	2.867285293	0.097726754	1.631329007	0.56894548	0.062268755	2.35798444	601.073031	9.805478706	618.61814	17.73754694	683.3518056	16.11332925	87.9595292
CPR 18 B 03	0.00110165	20.45298967	83.56806866	191.2755741	0.436898799	0.807940571	1.65097021	0.097911897	0.849441814	0.514510685	0.05984704	1.415680486	602.1601975	5.115000504	601.2980567	9.927251789	598.0487765	8.466459827	100.6874725
CPR 18 B 04	0.001833133	10.49578607	20.60613995	52.23180982	0.394513229	2.414252274	7.202405014	0.170660018	6.538214193	0.907782078	0.102600526	3.02099208	1015.746706	66.41169529	1246.848267	89.80306208	1671.691445	50.50166614	60.76161418
CPR 18 B 05	0.000351946	74.32952299	68.83125733	254.1418513	0.270837947	4.038125457	9.9435046	0.248402124	9.499960215	0.955393556	0.117902558	2.936671525	1430.230025	135.8712833	1641.909001	163.2632971	1924.675303	56.52139157	74.31019781
CPR 18 C 01	0.00103312	12.89021706	29.93035034	119.1705735	0.251155545	0.834473011	3.270305296	0.101313232	2.831020054	0.865674546	0.059737198	1.637138413	622.1003374	17.61178531	616.091032	20.14805765	594.0687624	9.725727912	104.7185741
CPR 18 C 02	0.000847177	24.36167501	22.68959556	100.3164952	0.226180107	3.204924234	6.318377846	0.213165773	5.914369892	0.936058279	0.109043308	2.223089604	1245.661783	73.67304547	1458.350282	92.14408113	1783.493849	39.64866633	69.84390691
CPR 18 C 03	0.001517775	15.58218193	34.93638561	147.4306637	0.236968245	0.810245141	1.808295716	0.098309446	1.181606957	0.653436795	0.059775045	1.368845644	604.4939887	7.142743024	602.5915352	10.89663692	595.4412354	8.150671413	101.5203437
CPR 18 C 04	0.00245796	5.701565699	18.42255679	46.90715187	0.392745158	1.062473504	6.283426188	0.108859325	3.017472087	0.480227188	0.070786623	5.511470481	666.1199172	20.09998257	735.0418769	46.18581378	951.2580407	52.42830611	70.02515498
CPR 18 D 01	0.006338707	5.208554124	18.07294912	41.83664453	0.431988495	1.168468669	10.74331909	0.114224012	7.174552292	0.667815247	0.074192223	7.996543283	697.2326164	50.02331866	785.9280458	84.43475778	1046.70092	83.69989212	66.61240122
CPR 18 D 02	0.000751488	26.26731155	43.03566918	80.84727125	0.532308246	4.455981897	6.233247498	0.26463508	5.982016804	0.959695056	0.122122231	1.751813155	1513.51237	90.5385643	1722.813223	107.3872121	1987.461333	34.81660907	76.15304737
CPR 18 D 03	0.000752255	32.10144848	44.37456189	117.8143729	0.376648119	4.227614704	4.234807035	0.265104161	3.744901951	0.884314662	0.115658507	1.977194983	1515.903043	56.76908262	1679.397974	71.11926353	1890.165717	37.37226172	80.19947825
CPR 18 D 04	0.000964406	21.71305873	29.71647327	136.2069837	0.218171436	1.733651614	5.621051805	0.132807413	3.627386795	0.645321716	0.094675637	4.293982817	803.861326	29.15915959	1021.108091	57.39701476	1521.628617	65.33847136	52.82900945
CPR 18 D 04	0.003368686	8.16763884	39.75474542	79.93170067	0.497358934	0.776623596	3.252214474	0.091738318	1.485922165	0.456895502	0.061398609	2.892911043	565.8095923	8.407490145	583.5555737	18.97847883	653.2276186	18.89729392	86.61752447
CPR 18 D 05	0.001638807	11.39242032	64.11912568	109.2264789	0.587029137	0.764727827	2.216158267	0.092103203	1.413605695	0.637863151	0.060218632	1.706773683	567.9637781	8.028768314	576.7339926	12.78133806	611.439628	10.43589066	92.88959237
CPR-20																			
CPR 20 a1	0.001892133	14.82468953	43.8190363	141.2169521	0.310295865	0.807607063	3.148468909	0.097897547	2.727298972	0.866230238	0.059831105	1.573116901	602.0759363	16.42041082	601.1107334	18.92578455	597.472011	9.398933186	100.7705675
CPR 20 a2	0.000987652	21.45733552	59.48603176	200.6660843	0.296442879	0.797305682	3.336654515	0.097138608	2.975549582	0.891776349	0.059529428	1.50975761	597.6182097	17.78242614	595.3076104	19.86335826	586.5130186	8.85492493	101.8934262
CPR 20 a3	0.001089527	25.72939591	91.05774721	241.1512477	0.377596003	0.80149162	3.052654821	0.097554579	2.706038771	0.886454228	0.059586799	1.412818326	600.0618526	16.23790638	597.6696955	18.24479277	588.6029371	8.315890165	101.9467989
CPR 20 a4	0.000607589	50.91929903	39.08854075	168.5761872	0.231874628	4.296333537	5.470506967	0.26046416	4.864132535	0.889155715	0.11963238	2.503330013	1492.216175	72.58337247	1692.658573	92.59700516	1950.737745	48.83340343	76.49496603
CPR 20 b1	0.002939665	16.8058165	87.6280365	148.5452153	0.589908172	0.810406607	2.183608848	0.098061356	1.258106008	0.576159054	0.059938215	1.784745605	603.0376861	7.586853359	602.6820988	13.16021964	601.3448662	10.73247607	100.2815057
CPR 20 b2	0.001778648	20.32249935	54.97864659	196.9023765	0.279217791	0.800774803	2.002538158	0.096969364	0.970309546	0.484539854	0.059892794	1.751758676	596.623718	5.789096889	597.2655922	11.96047139	599.7037043	10.50536167	99.48641533
CPR 20 b3	0.001552083	19.58951794	105.7346897	175.6537011	0.601949683	0.795367881	2.111264215	0.096581345	1.264155009	0.598766843	0.059727388	1.690960881	594.3430929	7.51341798	594.2122642	12.5453909	593.7128138	10.03945142	100.1061589
CPR 20 b4	0.001492879	32.4634264	39.59625187	96.64054685	0.409727109	5.303348038	4.192752309	0.30728185	3.960290105	0.94455618	0.12517337	1.376689582	1727.317053	68.40676635	1869.402373	78.37941115	2031.250367	27.96401218	85.03713186
CPR 20 c1	0.001572576	17.08994676	88.0553941	155.947175	0.564648857	0.77961296	2.225058809	0.094831441	1.236886826	0.555889499	0.059624593	1.849593924	584.0478055	7.224010361	585.2626314	13.02243774	589.978229	10.91220148	98.99480638
CPR 20 c2	0.002795503	14.71924137	66.66603968	136.8671299	0.487085831	0.777166934	2.079145782	0.094677417	1.40319847	0.674891815	0.059534216	1.534236369	583.1408448	8.182623414	583.8660571	12.1394265	586.6875383	9.001173584	99.39547148
CPR 20 c3	0.000845699	32.3462297	23.735273	76.26016268	0.311240786	7.220959056	2.073719098	0.395955301	1.913702006	0.922835696	0.132265764	0.79878378	2150.388299	41.15202401	2139.094152	44.35880395	2128.263339	17.00022236	101.0395781
CPR 20 c4	0.001632945	20.23253898	97.44407707	183.1117977	0.532156193	0.768657201	2.245405852	0.092760398	1.633545727	0.727505776	0.060099218	1.54057645	571.8418726	9.341298478	578.992349	13.00072809	607.148669	9.353589411	94.18481861
CPR 20 c5	0.00064754	55.41333871	47.20441535	222.4289112	0.212222481	3.39677405	5.407612608	0.214630197	5.049993501	0.933867469	0.114782204	1.933866529	1253.43862	63.29856887	1503.651421	81.3116438	1876.468187	36.28839019	66.79775489
CPR 20 d1	0.002117537	15.83860856	58.79260455	149.7990039	0.392476605	0.797687386	2.004113376	0.097137774	0.963298494	0.480660678	0.059558439	1.757420393	597.6133102	5.756800017	595.52323	11.93496071	587.5701702	10.32607799	101.7092665
CPR 20 d2	0.000600537	62.756375	47.16273842	166.0150274	0.284087165	5.624557019	1.857170654	0.323655916	1.708565934	0.919983272	0.126038579	0.727932199	1807.558687	30.88333197	1919.869528	35.65525346	2043.434087	14.87481468	88.45691175
CPR 20 d3	0.002141373	15.60939064	92.6447052	133.9653763	0.691557085	0.813048622	2.092517589	0.099127087	1.152964413	0.550993893	0.059487114	1.746225336	609.2912641	7.024911446	604.1628168	12.64221321	584.9698206	10.21489122	104.1577262
CPR 20 d4	0.002694552	11.44424706	5.204583399	109.1125757	0.047699208	0.877658721	4.170122933	0.105855509	3.262797242	0.782422316	0.060132731	2.596936548	648.6333732	21.16359181	639.7173573	26.67700023	608.3540981	15.79856991	106.6210247
CPR 20 d5	0.001746136	18.41682142	32.74734945	174.2929945	0.18788678	0.874809027	3.596407355	0.10430267	2.522378038	0.701360494	0.060829823	2.563543426	639.574974	16.13249868	638.1751555	22.95137823	633.2219688	16.23292015	101.0032825
CPR 20 d6	0.000529696	79.68637657	172.1274201	171.2544783	1.005097337	6.174268107	5.251000777	0.348898729	4.998639445	0.951940336	0.128346734	1.608295016	1929.337653	96.44063297	2000.813068	105.0627098	2075.451431	33.37938194	92.95990376
CPR 20 d7	0.000991395	31.25574384	15.10187536	211.5489126	0.071387157	1.551267942	14.34309302	0.126426648	11.02307645	0.768528548	0.08899117	9.176933205	767.4479549	84.59637477	950.9980887	136.4025405	1403.96961	128.8413533	54.66271846
CPR 20 d8	0.000426171	61.08817425	36.8725753	314.1979852	0.117354589	2.654346304	16.54372214	0.180087613	15.82081775	0.956303401	0.106898711	4.836989539	1067.453242	168.879832	1315.852391	217.6909634	1747.200945	84.51192692	61.09504721

crust participation in the genesis of these rocks. Such a contamination would explain the variability of ε_{Hf} values from positive to negative (Figure 14).

The obtained T_{DM} 'crustal' ages from 2.13 to 3.87 Ga can be interpreted as the age of the mantle extraction of the studied rocks. Similar Lu-Hf model age has been reported in Paleoproterozoic crust (Teixeira et al. 2015; Martínez Dopico et al. 2017; Barbosa et al. 2018). The Neoproterozoic ages (633 to 583 Ma) that marked the lower intercept of some samples, corroborate the idea of crustal reworking occurred in the Brasiliano Orogeny related to the formation of the Ribeira – Araçuaí belts.

The U-Pb and Lu-Hf results reported here define two groups of ε_{Hf} values. The first group with positive ε_{Hf} values is correlated to rocks formed in magmatic arc. The second group indicates granulite facies metamorphism during paleoproterozoic rocks (from high amphibolite to granulite facies). In this way, the sin-collisional stage of the Mineiro Belt occurred during the process of plate convergence and compressive tectonics between opposite continental margins (São Francisco craton Archean core) and crustal duplication with increased pressure and temperature resulting in processes of metamorphism and anatexis. The collisional orogen was preceded by the pre-collisional stage, formed by the subduction of oceanic lithosphere, in which the calcium-alkaline magmatic arcs were built.

6.2 The Neoproterozoic metamorphic event time constraints

Metamorphism in the Ribeira-Araçuai belts is associated with crustal thickening, corresponding to the M1 event represented by the collision of the Oriental Terrane with the Rio Negro magmatic arc (630-600 Ma), and with a later event M2, related to the collision (540-500 Ma) of the Costeiro Terrane and the Congo craton (Schmitt et al. 2004). The M1 event was responsible for the production of the main Ribeira Belt foliation and the intermediate to high pressure paragenesis. In the Paleoproterozoic enderbite and charnockite orthogranulites of Juiz de Fora Complex, it was reported that the M1 geothermobarometric event was associated with pressures between 4-6 kbar and temperatures between 750°C and 850°C (Heilbron et al. 2004). This event is characterized by the infiltration of fluids rich in CO_2, providing a granulitic metamorphism. According to Heilbron et al. (2004), the metamorphic degree of the Northern Ribeira Belt increases in the NW-SE direction, going from the greenschist facies to the granulite facies. In the NW area of the Ribeira Orogen, the Oriental Terrane, the metamorphism varies from the greenschist facies, on the edge of the São Francisco Craton, to the medium pressure granulite facies, close to the contact with the Oriental and Paraíba do Sul Terranes (700°C and 7 kbar).

A number of Neoproterozoic ages associated with the Brasiliano event were also recorded in the analyzed samples reported here. These ages are associated with metamorphic reworking processes and crystallization/generation of zircon grains. The obtained U/Pb ages can be associated with the time interval that the Rio Negro magmatic arc was developed in the Ribeira Orogeny, given by ages between ≈790-620 Ma (Tupinambá et al. 1996, 2012).

6.3 Th/U ratios and zircon growth

The U/Pb method is an important tool for the investigation of metamorphic events since the isotopic results allow to characterize the discordance of the ages $^{235}U/^{207}Pb$ ages and $^{238}U/^{206}Pb$ ages, commonly attributed to the episodic loss of radiogenic Pb in an open system (Wetherill, 1956; Tilton 1960; Wasserburg 1963) caused by a thermal event. Thus, metamorphic growth of zircon from aqueous fluid versus anhydrous melt can be distinguished by the concentrations of Th and U. For example, a zircon grain crystallized with kyanite, garnet, titanite and quartz in granulite facies is interpreted as having grown from hydrothermal solutions and it has very low Th/U ratios from 0.003 to 0.068 (Zheng et al.,

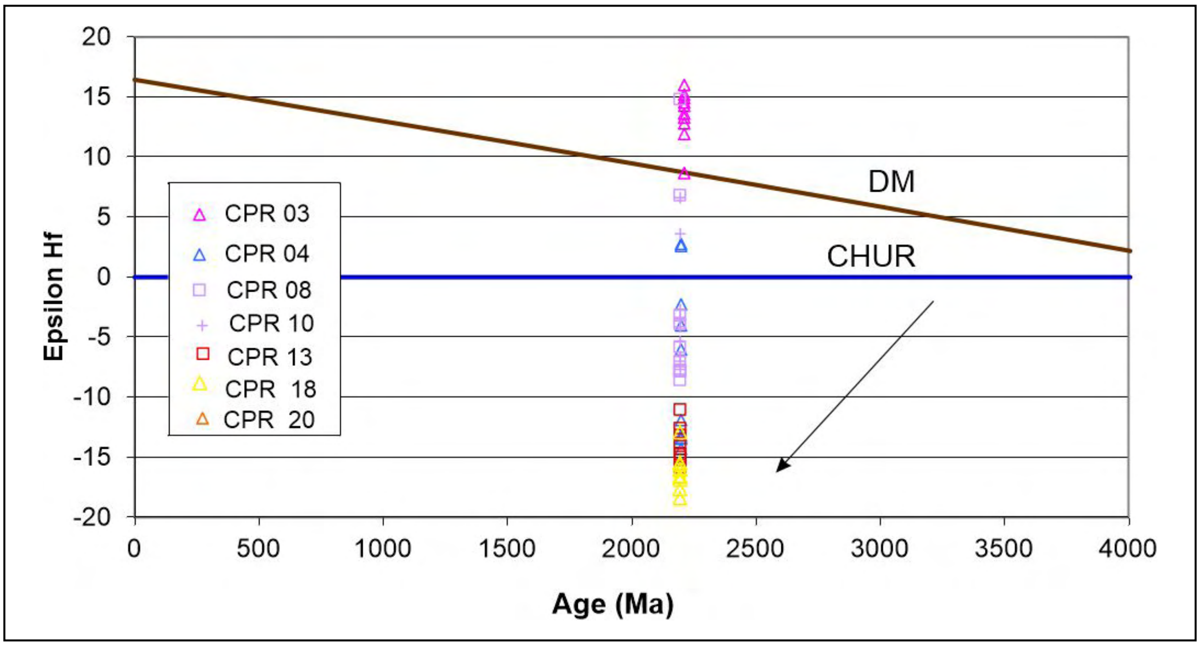

FIGURE 14. Hf isotopic evolution diagram for the studied samples. It is observed the variation of Hf isotope values in the Paleoproterozoic zircon grains, indicating a mantle source with an important crustal contribution for the magma formation of the Caparaó Complex rocks. The arrow indicates the isotopic evolution of Hf for the ratio ^{176}Lu / ^{177}Hf = 0.015 (Belousova et al. 2010).

2006). In contrast, zircon grains grown in anhydrous metamorphic environments present Th/U ratios preserving the original protolith compositions. While partial loss of radiogenic Pb is frequently observed, examples of almost complete loss of this element are interpreted as chemical leaching during extreme mylonitization process (Wayne and Sinha 1988).

Thus, the hydrothermal fluid is a facilitating medium for the isotopic homogenization and conditions for zircon growth (Rowley et al. 1997) and the distribution of U and Th in zircon allows the identification of fluid availability (fluid inclusions, structural hydroxyl, and crystalline water) within the crystals of high-grade metamorphic rocks (Chen et al. 2010).

Since fluid availability controls zircon growth during high-grade metamorphism, the concentrations of U and Th in metamorphic domains of different zircon grains or among distinct grains reflect the activity of the fluid involved responsible for the metamorphism.

The CL images of the zircon grains studied in this work indicate that most grains nuclei are of igneous origin, but some of them underwent different degrees of metamorphic modification. Such domains are present in zircon grains as edges where no oscillatory zoning typical of magmatic domains is observed. Figure 15 presents the relationship between the $^{207}Pb/^{206}Pb$ apparent age and the Th/U ratios for the studied samples. It shows that the inherited nuclei with the isotopic signature of the protolith and the edges that underwent metamorphic re-homogenization show equivalent values of U and Th. The values of U and Th in these domains suggest the non-interference of fluids during the metamorphic process, since this should have been an anhydrous event, as corroborated by petrographic analyzes and the mineralogy composed of orthopyroxene + K-feldspar + garnet and amphibole associated only to mylonitic zones.

7. Conclusion and final remarks

The analytical techniques U-Pb and Lu-Hf were applied to understand the crustal evolution of the Caparaó Complex rocks. The Lu-Hf isotopic analyses contributed to the understanding of the magmatism origin involved in the rocks formation of the Caparaó Complex (ε_{Hf} petrogenetic parameter) and to the understanding of the period of mantle extraction (T_{DM} 'crustal age') of such magmatism. The present investigation provided robust Lu-Hf isotopic data (model ages and ε_{Hf} parameter) poorly observed in the literature. It also provided intervals of U-Pb ages for the Caparaó Complex, between 2209 and 2060 Ma, like those reported in the literature for the same rocks of 2195 ± 15 Ma. The results reported herein allow to correlate the Caparaó Complex to the Juiz de Fora Complex, with granulitic rocks with age of 2199 ± 17 Ma and important rework associated with the Brasiliano Orogeny.

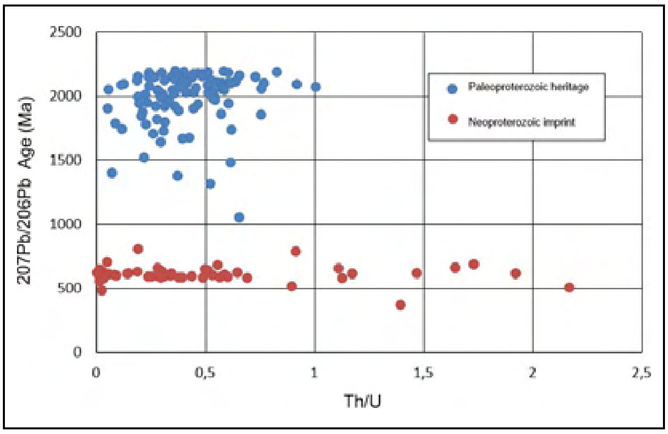

FIGURE 15. Relationship between the $^{207}Pb/^{206}Pb$ apparent age and the Th/U ratios for the studied samples. The results show little variation in the isotopic signatures for the inherited domains and newly formed domains in the zircon grains.

It is noteworthy that the data obtained in this work corroborate the proposals of Horn (2006) and Novo et al. (2011) that the Caparaó Complex configures a tectonic Paleoproterozoic fragment reworked in Brasiliano Orogeny, during collisional events. With the obtained geochronological data, it is possible to propose a geological evolution of the Caparaó Complex in 3 evolutionary stages:

First stage: 2209 – 2060 Ma (Magmatic Arc)

The Paleoproterozoic ages obtained in the Caparaó Complex represent a period of crustal accretion with juvenile sources (mantle-derived) in a magmatic arc environment (Figure 16 A) with signature of intraoceanic environments (medium-high-K calcium-alkaline rocks similar to that reported by Novo et al. 2011). This event has a strong correlation with the ages obtained in Mineiro Belt (Ávila et al. 2010) and in Juiz de Fora Terrane rocks (Heilbron et al. 2004). This event may be responsible for the amalgamation of São Francisco craton in a global paleocontinent. Supercontinent collage during the Paleoproterozoic times is indicated by paleomagnetic data during the Columbia amalgamation which includes Laurentia (Superior and Wyoming cratons), Baltica (Karelia craton), Australia, and Kalahari and Kaapvaal cratons at about 2.45 Ga (Rogers 1996; D'Agrella Filho et al. 2020). A second continental mass is proposed at that period of time (Pesonen et al. 2003). The break-up of Columbia supercontinent resulted in formation of platform sedimentary basins (Figure 16B).

Second stage: Rio Negro Magmatic Arc

The set of ages from 640-580 Ma represents the oldest stage of rework generated during the Brasiliano event (Figure 16 C). It can be correlated with the end of the implantation of the Rio Negro magmatic arc (Pedrosa-Soares 2001; Tupinambá et al. 1996, 2012). In this way, at this time interval the Rio Negro magmatic arc developed in the Ribeira Orogeny (790-620 Ma). Such a segment would have developed over a prolonged period of subduction and collision between the blocks of western Gondwana in SE Brazil and West Africa. This event is also discussed by Pedrosa Soares (2001) in the Araçuaí belt as pre-collisional or pre-orogenic stage that occurred at about 630 to 585 Ma.

Third Stage: 633 - 584 Ma (Brasiliano collisional stage)

This stage represents the peak of the metamorphic deformation of the Caparaó Complex rocks and is correlated with the acting of the thrusting zones that controlled the regional structure (Figure 16 D). As several

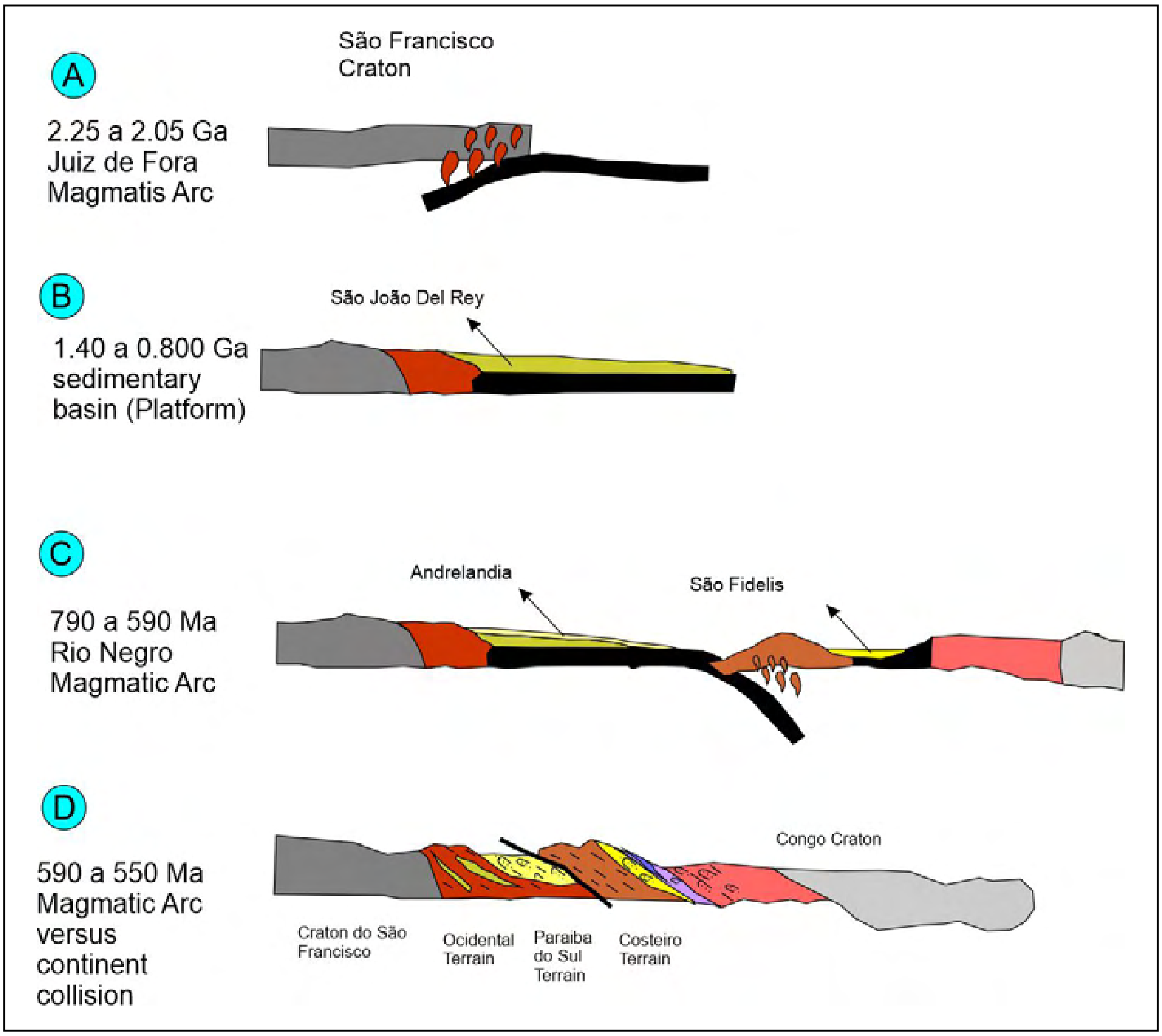

FIGURE 16. Schematic model for the formation of the studied rocks.

studies suggest, the lithosphere of the Brazilian margin represented by the São Francisco Craton was compressed against the rigid lithosphere of the Congo craton, resulting in thrust and nappe systems with NW direction and SW striking tangential tectonics. In this model, it is also possible to characterize a crustal thickening with variable uplift, high pressure and high temperature metamorphism simultaneously with the main transcurrent movement in the collision zone, represented by the probable region of suture, defined as central tectonic boundary.

High-grade metamorphism occurred within a relatively dry rock system. This may be the reason for the non-existence of a change in the isotopic signature of the U/Th ratios of the newly formed zircon grains. In this sense, the metamorphism occurred without the influence of hydrothermal solutions that allowed anhydrous recrystallization in the zircon grains, resulting in the opening of the U/Pb isotopic system with age distribution from 540 and 500 Ma.

The tectonics models should incorporate some important features, such as several approximately parallel shear zones that mark the block boundaries, accentuated crustal thickening and uplift. This model, associated with the evolution of the continental margin of the collisional oblique type, is the best answer to describe the metamorphic peak in Ribeira-Araçuai belt.

Acknowledgments

This work is part of the Master's degree research of the first author. MCG thanks the Conselho Nacional de Desenvolvimento Científico e Tecnológico (CNPq) for the fellowship grant (process # 301470/2016-2). We thank CNPq for financial support in the field trips. We also thank to Professor Marcio Martins Pimentel (*in memory)* to the development of the geochronology in Brazil, and in particular for the contribution and incentive to UERJ isotopic laboratory facilities construction.

Authorship credits

Author	A	B	C	D	E	F
TGF	■	■		■		
MIA		■	■			
GLP	■					
LFR	■		■			
SWOR					■	■
MVAM					■	■
MCG			■	■	■	

A - Study design/Conceptualization **B** - Investigation/Data acquisition
C - Data Interpretation/ Validation **D** - Writing
E - Review/Editing **F** - Supervision/Project administration

References

Almeida F.F.M., Hasui Y., Neves B.B.B., Fuck, R.A. 1977 Províncias estruturais brasileiras. In: Simpósio de Geologia do Nordeste, 8, 363-91.

Almeida F.F.M.A., Hasui Y., Brito Neves B.B., Fuck R.A. 1981. Brazilian structural provinces: an introduction. Precambrian Res. 17, 1-29. https://doi.org/10.1016/0012-8252(81)90003-9

Alves M.I., Almeida B.S., Cardoso L.M.C., Santos A.C., Appi C. Bertotti A.L., Chemale F., Tavares Jr. A.D., Martons M.V.A., Geraldes M.C. 2019. Isotopic composition of Lu, Hf and Yb in GJ-01, 91500 and Mud Tank reference materials measured by LA-ICP-MS: application of the Lu-Hf geochronology in zircon. Journal of Sedimentary Environments 4 (2), 220-248. https://doi.org/10.12957/jse.2019.43877

Andersen T., Griffin W.L., Pearson N.J. 2002. Crustal evolution in the SW part of the Baltic Shield: the Hf isotope evidence. Journal of Petrology, 43(9), 1725-1747. https://doi.org/10.1093/petrology/43.9.1725

Amelin Y., Lee D.-C., Halliday A. N., Pidgeon R. T. 1999. Nature of the Earth's earliest crust from hafnium isotopes in single detrital zircons. Nature, 399, 252-255. https://doi.org/10.1038/20426

Amorim LE.D., Rios F.J., Freitas M.E., Cutts K., Geraldes M.C., Diniz A.C. 2021. Zircon U–Pb geochronology of Paleoproterozoic Statherian intraplate A-Type magmatic associations of the Lagoa Real Uranium Province, São Francisco Craton (Bahia, Brazil). Journal of South American Earth Sciences, 109, 103245. https://doi.org/10.1016/j.jsames.2021.103245

Angeli N. 1978. Pesquisa de calcário e caulim no norte do Estado do Rio de Janeiro, Sul do Estado do Espírito Santo e Serra do Caparaó (Minas Gerais). In: Congresso Brasileiro de Geologia, 30, 1714-1728. Available online at: http://www.sbgeo.org.br/home/pages/44.

Ávila C.A., Teixeira W., Cordani U.G., Barrueto H.R., Pereira R.M., Martins V.T.S., Dunyl L. 2006. The Gloria quartz-monzodiorite isotopic and chemical evidence of arc related magmatism in the central part of the Mineiro Belt, Minas Gerais State, Brazil. Anais da Academia Brasileira de Ciências, 78(3), 543-556. https://doi.org/10.1590/S0001-37652006000300013

Ávila C.A., Teixeira W., Cordani U.G., Moura C. A. V., Pereira R.M. 2010. Rhyacian (2.23-2.20) juvenile accretion in the Southern São Francisco craton, Brazil: geochemical and isotopic evidence from the Serrinha magmatic suíte, Mineiro belt. Journal oh South American Earth Sciences, 29(2), 464-482. https://doi.org/10.1016/j.jsames.2009.07.009

Barbosa N.S., Teixeira W., Ávila C.A., Montecinos P.M., Bongiolo E.M., Vasconcelos F.F. 2018. U-Pb geochronology and coupled Hf-Nd-Sr isotopic-chemical constraints of the Cassiterita Orthogneiss (2.47–2.41-Ga) in the Mineiro belt, São Francisco craton: geodynamic fingerprints beyond the Archean-Paleoproterozoic transition. Precambrian Research, 326, 399-416. https://doi.org/10.1016/j.precamres.2018.01.017

Belousova E., Griffin W., O'Reilly S.Y. 2006. Zircon crystal morphology, trace element signatures and Hf isotope composition as a tool for petrogenetic modelling: examples from Eastern Australian Granitoids. Journal of Petrology, 47(2), 329-353. https://doi.org/10.1093/petrology/egi077

Belousova E.A., Kostitsyn Y.A., Griffin L., Begg G.C., O'Reilly S.Y., Pearson N.J. 2010. The growth of the continental crust: constraints from zircon Hf-isotope data. Lithos 119(3-4), 457-466. https://doi.org/10.1016/j.lithos.2010.07.024

Bertotti A. L., Chemale Jr. F., Kawashita K. 2013. Lu-Hf em zircão por LA-MC-ICP-MS: aplicação em gabro do Ofiolito Aburrá, Colômbia. Pesquisas em Geociências, 40(2), 117-127. https://doi.org/10.22456/1807-9806.43075

Bouvier A., Vervoort J.D., Patchett P.J. 2008. The Lu–Hf and Sm–Nd isotopic composition of CHUR: constraints from unequilibrated chondrites and implications for the bulk composition of terrestrial planets. Earth and Planetary Science Letters, 273(1-2), 48-57. https://doi.org/10.1016/j.epsl.2008.06.010

Campos Neto M.C, Figueiredo M.C.H. 1990. Evolução geológica dos terrenos costeiro, Paraíba do Sul e Juiz de Fora (RJ-MG-ES). In: Congresso Brasileiro de Geologia, 36, 6, 2631-2648. Available on line at: http://www.sbgeo.org.br/home/pages/44

Chauvel C., Garçon M., Bureau S., Besnault A., Jahn B.-M. Ding Z. L. 2014. Constraints from loess on the Hf-Nd isotopic composition of the upper continental crust. Earth and Planetary Science Letters, 388, 48-58. https://doi.org/10.1016/j.epsl.2013.11.045

Chen R., Zheng Y., Xie L. 2010 Metamorphic growth and recrystallization of zircon: distinction by simultaneous in-situ analyses of trace elements, U–Th–Pb and Lu–Hf isotopes in zircons from eclogite-facies rocks in the Sulu orogen. Lithos, 114(1-2), 132-154. https://doi.org/10.1016/j.lithos.2009.08.006

Choi S.H., Mukasa S.B., Andronikov A., Osanai Y., Harley S., Kelly N. 2006. Lu–Hf systematics of the ultra-high temperature Napier Metamorphic Complex in Antarctica: evidence for the early Archean differentiation of Earth's mantle. Earth and Planetary Science Letters, 246(3-4), 305-316. https://doi.org/10.1016/j.epsl.2006.04.012

Correia-Neves J.M; Marciano V.R.P.R.O., Lena J.C., Pedrosa-Soares, A.C. 1987. Fosfatos do tipo crandalita (plumbogumita, goyazita, gorceixcita) resultantes do intemperismo de ambligonita de pegmatitos de Coronel Murta (nordeste Minas Gerais) e seu significado paleoclimático. Revista Brasileira de Geociencias, 17(1), 42-52. https://doi.org/10.25249/0375-7536.19874252

D'Agrella Filho M.S., Teixeira W., Trindade R.I.F., Patroni O.A.L., Prieto R.F. 2020. Paleomagnetism of 1.79 Ga Pará de Minas mafic dykes: testing a São Francisco/Congo North China-Rio de la Plata connection in Columbia. Precambrian Research, 338, 105584. https://doi.org/10.1016/j.precamres.2019.105584

De Campos C. P., Medeiros S.R., Mendes J.C., Pedrosa-Soares A.C., Dussin I., Ludka I.P., Dantas E.L. 2016. Cambro-Ordovician magmatism in the Araçuaí Belt (SE Brazil): snapshots from a post-collisional event. Journal of South American Earth Sciences, 68, 248-268. https://doi.org/10.1016/j.jsames.2015.11.016

De Campos C. P. 2014. Chaotic flow patterns from a deep plutonic environment: a case study on natural magma mixing. Pure and Applied Geophysics, 171(9). https://doi.org/10.1007/s00024-014-0940-6

De Campos C. P., Mendes J. C., Ludka I. P., Medeiros S. R., Costa-de-Moura J., Walfass C.M. 2004. A review of the Brasiliano magmatism in southern Espírito Santo, Brazil, with emphasis on post-collisional magmatism. Journal of the Virtual Explorer, 17, 1-39. https://10.3809/jvirtex.2004.00106

Duchene S., Blichert-Tof J., Luai B., Telou P., Albared F. 1997. The Lu–Hf dating of garnets and the ages of the Alpine high-pressure metamorphism. Nature, 387, 586-589. https://doi.org/10.1038/42446

Elhlou S., Belousova E., Griffin W.L., Pearson N.J., O'reilly S.Y. 2006. Trace element and isotopic composition of GJ-red zircon reference material by laser ablation. Geochimica et Cosmochimica Acta, 70(18), A158. https://doi.org/10.1016/j.gca.2006.06.1383

Freitas N.C., Almeida J., Heilbron H., Cutts K., Dussin I. 2021 The Cabo Frio Thrust: a folded suture zone, Ribeira belt, SE Brazil. Journal of Structural Geology, 149, 104379. https://doi.org/10.1016/j.jsg.2021.104379

Geraldes M.C. 2010. Introdução à geocronologia. São Paulo, Sociedade Brasileira de Geologia, 146p.

Gerdes A., Zeh A. 2009. Zircon formation versus zircon alteration: new insights from combined U-Pb and Lu-Hf in-situ LA-ICP-MS analyses, and consequences for the interpretation of Archean zircon from the Central Zone of the Limpopo Belt. Chemical Geology, 261(3-4), 230-243.

Gerdes A., Zeh A. 2006. Combined U-Pb and Hf isotope LA-(MC)-ICP-MS analyses of detrital zircons: comparison with SHRIMP and new constraints for the provenance and age of an Armorican metasediment in Central Germany. Earth and Planetary Science Letters, 249(1-2), 47-61. https://doi.org/10.1016/j.epsl.2006.06.039

Griffin W.L., Belousova E.A., Walters S.G., O'Reilly S.Y. 2006. Archaean and Proterozoic crustal evolution in the Eastern Succession of the Mt Isa district, Australia: U–Pb and Hf-isotope studies of detrital zircons. Australian Journal of Earth Sciences, 53 (1), 125-149. https://doi.org/10.1080/08120090500434591

Griffin W.L., Pearson N.J., Belousova E., Jackson S.E., O'Reilly S.Y., Van Achterberg E., Shee S.R., 2000. The Hf isotope composition of cratonic mantle: LAM-MC-ICPMS analysis of zircon megacrysts in kimberlites. Geochimica et Cosmochimica Acta, 64(1), 133-147. https://doi.org/10.1016/S0016-7037(99)00343-9

Griffin W.L., Wang X., Jackson S.E., Pearson S.E., O'Reilly S.Y., Xu X.S., Zhou X.M. 2002. Zircon chemistry and magma genesis, SE China: in-situ analysis of Hf isotopes, Tonglu and Pingtan Igneous Complexes. Lithos, 61(3-4), 237-269. https://doi.org/10.1016/S0024-4937(02)00082-8

Hawkesworth C.J., Kemp A.I.S. 2006. Using hafnium and oxygen isotopes in zircons to unravel the record of crustal evolution. Chemical Geology, 226, (3-4), 144-162. https://doi.org/10.1016/j.chemgeo.2005.09.018

Heilbron M., Duarte B.P., Valeriano C.M., Simoneti A., Machado N., Nogueira J.R. 2010. Evolution of reworked Paleoproterozoic basement rocks within the Ribeira belt (Neoproterozoic), SE-Brazil, based on U–Pb geochronology: Implications for paleogeographic reconstructions of the São Francisco-Congo paleocontinent. Precambrian Research, 178(1-4), 136-148. https://doi.org/10.1016/j.precamres.2010.02.002

Heilbron M., Mohriak W.E., Valeriano C.M., Milani E., Almeida J.C.H, Tupinamba M. 2000. From collision to extension: the roots of the outheastern Continental Margin of Brazil. In: Mohriak W., M. Taiwani. Atlantic rifts and continental margins. Geophysical Monograph Series, 115. Washington DC, American Geophysical Union, Geophysical. p. 1-34.

Heilbron M., Silva L.G.E., Almeida J.C.H., Tupinamba M., Peixoto C., Valeriano C.M., Lobato M., Rodrigues S., Ragatky C.D., Silva M.A., Monteiro T., Freitas N., Miguens D., Girao R. 2020. Proterozoic to Ordovician geology and tectonic evolution of Rio de Janeiro State, SE-Brazil: insights on the central Ribeira Orogen from the new 1: 400,000 scale geologic map. Brazilian Journal of Geology, 50(2), 1-25. https://doi.org/10.1590/2317-4889202020190099

Heilbron M., Soares A.C.P., Campos N., Silva L.C., Trouw R., Janasi V. 2004. Província Mantiqueira. In: Mantesso-Neto V., Bartorelli A., Carneiro C.D.R., Brito Neves B.B. (eds.). Geologia do Continente Sul-Americano: evolução da obra de Fernando Flávio Marques de Almeida. São Paulo, Beca, p. 180-211. Available on line at: https://geologia.ufc.br/wp-content/uploads/2016/02/geologia-do-continente.pdf

Heilbron M., Valeriano C., Tassinari C.C.G., Almeida J.C.H., Tupinamba M., Siga O., Trouw R., 2008. Correlation of Neoproterozoic Terranes between the Ribeira Belt, SE Brazil and its African Counterpart: comparative tectonic evolution and open questions. In: Pankhurst R.J., Trouw R.A.J., Brito Neves B.B., Wit M.J. West Gondwana: Pre-Cenozoic correlations across the South Atlantic Region. Geological Society, London, 294, 211-237. https://doi.org/10.1144/SP294.12

Horn A.H. 2006. Folha Espera Feliz 1:100.000: SE 24-V-A-IV. Belo Horizonte, CPRM/UFMG, Programa Geologia do Brasil. Available on line at: https://rigeo.cprm.gov.br/handle/doc/10251

Jackson S.E., Pearson N.J., Griffin W.L., Belousova E. 2004. The application of laser ablation inductively coupled plasma mass spectrometry to in-situ U–Pb zircon geochronology. Chemical Geology, 211(1-2), 47-69. https://doi.org/10.1016/j.chemgeo.2004.06.017

Ludwig K. R. 2003. Isoplot 3.00: a geochronological toolkit for Microsoft Excel. Special publication, Berkeley Geochronology Center, 4, 70 p.

Machado M.S., Cardoso L.M.C., Bonifácio J.F., Cruz R.H.V., Alves M.I., Nogueira J.R., Coelho M.H.P.A, Tavares A.D., Geraldes M.C. 2021 Geocronologia U-Pb e Lu-Hf em ortognaisses da região de Espera Feliz (MG): contribuição a evolução crustal do embasamento Riaciano no limite dos orógenos Ribeira e Araçuaí. Revista Geociências Unesp, 40(3), 583-610. https://doi.org/10.5016/geociencias.v40i04.15610

Martínez Dopico C.I., Lana C., Moreira H.S., Cassino L.F., Alkmim F.F. 2017. U-Pb ages and Hf-Isotope data of detrital zircons from the late Neoarchean-paleoproterozoic Minas basin, SE Brazil. Precambrian Research, 291, 143-161. https://doi.org/10.1016/j.precamres.2017.01.026

Morel M.L.A., Nebel O., Nebel-Jacobsen Y.J., Miller J.S., Vroon P.Z. 2008. Hafnium isotope characterization of the GJ-1 zircon reference material by solution and laser-ablation MC-ICPMS. Chemical Geology, 255 (1-2), 231-235. https://doi.org/10.1016/j.chemgeo.2008.06.040

Noce C.M., Machado N., Teixeira W. 1998. U–Pb geochronology of gneisses and granitoids in the Quadrilátero Ferrífero (southern São Francisco Craton): age constraints for Archean and Paleoproterozoic magmatism and metamorphism. Revista Brasileira de Geociências, 28(1), 95-102. https://doi.org/10.25249/0375-7536.199895102

Noce C.M., Pedrosa-Soares A.C., Silva L.C. Alkmim F.F. 2007. O embasamento arqueano e paleoproterozóico do Orógeno Araçuaí. Geonomos, 15(1), 17-23. https://doi.org/10.18285/geonomos.v15i1.104

Novo T.A., Noce C. M., Pedrosa-Soares A.C., Batista G.A.P. 2011. Rochas granulíticas da Suíte Caparaó na região do Pico da Bandeira: embasamento oriental do Orógeno Araçuaí. Geonomos, 19(2), 70-77. https://doi.org/10.18285/geonomos.v19i2.42

Paciullo F.V.P., Ribeiro A., Andreis R.R., Trouw R.A.J. 2000. The Andrelândia Basin, a Neoproterozoic intraplate continental margin, Southern Brasília Belt. Revista Brasileira de Geociências, 30(1), 200-202. https://doi.org/10.25249/0375-7536.2000301200202

Patchett P. J., Tatsumoto M. 1981. Lu/Hf in chondrites and definition of a chondritic hafnium growth curve. Lunar and Planetary Science, 12, 822-824. Available on line at: https://adsabs.harvard.edu/full/1981LPI....12..822P

Patchett P. J., Tatsumoto M. 1980. Hafnium isotope variations in oceanic basalts. Geophysical Research Letters, 7(12), 1077-1080.

Patchett P.J., Kouvo O., Hedge C.E. Tatsumoto M. 1981. Evolution of continental crust and mantle heterogeneity: evidence from Hf isotopes. Contributions to Mineralogy and Petrology, 78, 279-297. https://doi.org/10.1007/BF00398923

Pedrosa-Soares A. C., Noce C. M., Alkmim F. F., Silva L. C., Babinski, M., Cordani U., Castañeda C. 2007. Orógeno Araçuaí: síntese do conhecimento 30 anos após Almeida 1977. Geonomos, 15(1), 1-16 https://doi.org/10.18285/geonomos.v15i1.103

Pedrosa-Soares A.C., Noce C.M, Wiedemann C.M., Pinto C.P. 2001. The Araçuaí-West-Congo Orogen in Brazil: an overview of a confined orogen formed during Gondwanaland assembly. Precambrian Research, 110(1-4), 307-323. https://doi.org/10.1016/S0301-9268(01)00174-7

Pedrosa-Soares A.C., Noce C.M., Vidal P.H., Monteiro R.L.B.P., Leonardos O.H. 1992. Toward a new tectonic model for the late Proterozoic Araçuai (SE Brazil) - West Congolian (SW Africa) belt. Journal of South American Earth Science, 6(1-2), 33-47. https://doi.org/10.1016/0895-9811(92)90015-Q

Pedrosa-Soares A.C., Wiedemann C.M., Fernandes M.L.S., Faria L.F., Ferreira J.C.H. 1999. Geotectonic significance of the Neoproterozoic granitic magmatism in the Araçuaí Belt: a model and pertinent questions. Revista Brasileira de Geociências, 29(1), 59-66. https://doi.org/10.25249/0375-7536.1999295966

Pedrosa-Soares A.C., De Campos C., Noce C.M., Silva L.C., Novo T., Roncato J., Medeiros S., Castañeda C., Queiroga G., Dantas E., Dussin I., Alkmim F.F. 2011. Late Neoproterozoic-Cambrian granitic magmatism in the Araçuaí orogen (Brazil), the Eastern Brazilian Pegmatite Province and related resources. In: Sial A.N., Bettencourt J.S., De Campos C.P., Ferreira V.P. Granite-related ore deposits. Geological Society, London, Special Publications, 350, p. 25-51. https://doi.org/10.1144/SP350

Pesonen L.J., Elming S.A., Mertanen S., Pisarevsky S., D'Agrella Filho M.S., Meert J.G., Schmidt P.W., Abrahamsen N., Bylund G. 2003. Palaeomagnetic configuration of continents during the Proterozoic. Tectonophysics, 375(1-4), 289-324. https://doi.org/10.1016/S0040-1951(03)00343-3

Pinto C.P., Silva M.A. 2014. Mapa geológico do estado de Minas Gerais. Escala: 1:1.000.000. Programa de Aceleração do Crescimento. Brasília, CPRM. Available on line at: https://rigeo.cprm.gov.br/handle/doc/20786

Ribeiro A., Teixeira W., Dussin I.A., Ávila C.A., Nascimento D. 2013. U–Pb LA-ICP-MS detrital zircon ages of the São João del Rei and Carandaí basins: New evidence of intermittent Proterozoic rifting in the São Francisco paleocontinent. Gondwana Research, 24(2), 713-726. https://doi.org/10.1016/j.gr.2012.12.016

Rogers J.W. 1996. A history of continents in the Past Three Billion Years. The Journal of Geology, 104(1), 91-107. http://dx.doi.org/10.1086/629803

Rowley D.B., Xue F., Tucker R.D., Peng Z.X., Baker J., Davis A. 1997. Ages of ultrahigh pressure metamorphism and protolith orthogneisses from the e https://doi.org/10.1016/S0012-821X(97)81848-1 astern Dabie Shan: U/Pb zircon geochronology. Earth and Planetary Science Letters, 151(3-4), 191-203. https://doi.org/10.1016/S0012-821X(97)81848-1

Santosh M., Wan Y.S., Liu D.Y., Dong C.Y., Li J.H. 2009. Anatomy of zircons from an ultra-hot orogen: the amalgamation of the North China Craton within the supercontinent Columbia. The Journal of Geology, 117(4), 429-443. https://doi.org/10.1086/598949

Schmidt A., Weyer S., Mezger S., Scherer E., Xiao Y., Hoefs J., Brey J. 2008. Rapid eclogitisation of the Dabie–Sulu UHP terrane: constraints from Lu–Hf garnet geochronology. Earth and Planetary Science Letters, 273(1-2), 203-213. https://doi.org/10.1016/j.epsl.2008.06.036

Schmitt R.S., Trouw R.A.J., Van Schmus W.R., Armstrong R., Stanton N.S.G., 2016. The tectonic significance of the Cabo Frio Tectonic Domain in the SE Brazilian margin: a Paleoproterozoic through Cretaceous saga of a reworked continental margin. Braz. J. Genet. 46, 3–66. https://doi.org/10.1590/2317-4889201620150025

Schmitt R.S., Trouw R.A.J., Van Schmus W.R., Passchier C.W. 2008. Cambrian orogeny in the Ribeira Belt (SE Brazil) and correlations within West Gondwana: ties that bind underwater. Geological Society, London, Special Publications, 294, 279-296. https://doi.org/10.1144/SP294.15

Schmitt R.S., Trouw R.A.J., Van Schmus W.R., Pimentel M.M. 2004. Late amalgamation in the central part of West Gondwana: new geochronological data and the characterization of a Cambrian collisional orogeny in the Ribeira Belt (SE Brazil). Precambrian Research, 133(1-2), 29-61. https://doi.org/10.1016/j.precamres.2004.03.010

Seidensticker U., Wiedemann C. 1992. Geochemistry and origin of lower crustal granulite facies rocks in the Serra do Caparaó region, Espirito Santo/Minas Gerais, Brazil. Journal of South American Earth Sciences, 6(4), 289-298. https://doi.org/10.1016/0895-9811(92)90047-3

Silva L.C., Armstrong R., Noce C.M., Carneiro M., Pimentel M., Pedrosa-Soares A.C., Leite C., Vieira V. S., Silva M., Paes V., Cardoso-Filho, J. 2002. Reavaliação da evolução geológica em terrenos pré-cambrianos brasileiros com base em novos dados U-Pb SHRIMP, parte II: Orógeno Araçuaí, Cinturão Móvel Mineiro e Cráton São Francisco Meridional. Revista Brasileira de Geociências, 32(4), 513-528.

Silva L.C., McNaughton N.J., Armstrong R., Hartmann L., Fletcher I. 2005. The neoproterozoic Mantiqueira Province and its African connections: a zircon-based U–Pb geochronologic subdivision for the Brasiliano/Pan-African systems of orogens. Precambrian Research, 136(3-4), 203-240. https://doi.org/10.1016/j.precamres.2004.10.004

Steiger R.H., Jäger E. 1977. Subcommission on geochronology: convention on the use of decay constants in geo- and cosmochronology. Earth and Planetary Science Letters, 36(3), 359-362. https://doi.org/10.1016/0012-821X(77)90060-7.

Teixeira W., Ávila C.A., Dussin I.A., Corrêa Neto A.V., Bongiolo E.M., Santos O.S., Barbosa N.S., 2015. A juvenile accretion episode (2.35–2.32 Ga) in the Mineiro belt and its role to the Minas accretionary orogeny: Zircon U–Pb–Hf and geochemical evidences. Precambrian Research, 256, 148-169. https://doi.org/10.1016/j.precamres.2014.11.009

Tilton G. R. 1960. Volume diffusion as a mechanism for discordant lead ages. Journal of Geophysical Research, 65(9), 2933-2945. https://doi.org/10.1029/JZ065i009p02933

Trouw R.A., Heilbron M., Ribeiro A., Paciullo F., Valeriano C.M., Almeida J.H., Tupinamba M., Andreis R. 2000. The central segment of the Ribeira belt. In: Cordani U.G., Milani E.J., Thomaz-Filho A., Campos D.A. (eds.). Tectonic Evolution of South America: 31st International Geological Congress, 287-310.

Tupinambá M., Heilbron M., Oliveira A., Pereira A. J., Cunha E. R. S. P., Fernandes G. A., Ferreira F. N., Castilho J. G., Teixeira W. 1996. Complexo Rio Negro: uma unidade estratigráfica relevante no entendimento da evolução da Faixa Ribeira. In: Congresso Brasileiro de Geologia, 39(6), 104-107. Available on line at: http://www.sbgeo.org.br/home/pages/44

Tupinambá, M., Heilbron, M.,Valeriano, C., Porto Jr, R., Dios, F. B. , Machado, N. , Silva, Eirado Silva, L. and Almeida, J. 2012. Juvenile contribution of the Neoproterozoic Rio Negro Magmatic Arc (Ribeira Belt, Brazil): implications for Western Gondwana amalgamation. Gondwana Research, 21(2-3), 422-438. https://doi.org/10.1016/j.gr.2011.05.012

Vervoort J.D., Blichert-Toft J., 1999. Evolution of the depleted mantle: Hf isotope evidence from juvenile rocks through time. Geochimica et Cosmochimica Acta, 63(3-4), 533-556. https://doi.org/10.1016/S0016-7037(98)00274-9

Vieira V.S., Menezes R.G. 2014. Mapa Geológico do Estado do Espírito Santo. 1:4000.000. Belo Horizonte, CPRM.

Vieira V.S (org). 1997. Cachoeira do Itapemirim. SF.24-V-A: estados do Espírito Santo, Minas Gerais e Rio de Janeiro. Escala: 1:250.000. Programa Levantamentos Geológicos Básicos do Brasil. Brasília, CPRM. 110 p.

Wasserburg G.J. 1963. Diffusion processes in lead-uranium systems. Journal of Geophysical Research, 68(16), 4823-4846. https://doi.org/10.1029/JZ068i016p04823

Wayne D. M., Sinha A. K. 1988. Physical and chemical response of zircons to deformation. Contributions to Mineralogy and Petrology, 98, 109-121. https://doi.org/10.1007/BF00371915

Wetherill G.W. 1956. Discordant uranium-lead ages, I. Eos, Transactions American Geophysical Union, 37(3), 320-326. https://doi.org/10.1029/TR037i003p00320

Wiedemann C. M., Penha H. M., Schmidt-Thomé R. 1987. Granitoids of Espírito Santo and Rio de Janeiro. Revista Brasileira de Geociências, 17(4), 674-689.

Wiedemann C.M. 1993. The evolution of the early Paleozoic, late to post collisional magmatic arc of the Coastal Mobile Belt, in the state of Espirito Santos, Eastern Brazil. Anais da Academia Brasileira de Ciências, 65, 163-181.

Wiedemann C.M., Medeiros S.R., Ludka I.P., Mendes J.C., Costa-de-Moura J.C. 2002. Architecture of Late Orogenic Plutons in the Araçuaí-Ribeira Folded Belt, Southeast Brazil. Gondwana Research, 5(2), 381-399. https://doi.org/10.1016/S1342-937X(05)70730-9

Woodhead J., Hergt J., Shelley M., Eggins S., Kemp R. 2004. Zircon Hf-isotope analysis with an excimer laser, depth profiling, ablation of complex geometries and concomitant age estimation. Chemical Geology, 209(1-2), 121-135. https://doi.org/10.1016/j.chemgeo.2004.04.026

Woodhead J.D., Hergt J.M. 2005. A preliminary appraisal of seven natural zircon reference materials for in situ Hf isotope determination. Geostandards ans Geoanalytical Research, 29 (2), 183-195. https://doi.org/10.1111/j.1751-908X.2005.tb00891.x

Zeh A., Gerdes A., Klemd R., Barton Jr. J.M. 2007. Archaean to proterozoic crustal evolution in the Central Zone of the Limpopo Belt (South Africa-Botswana): constraints from combined U-Pb and Lu-Hf Isotope Analyses of Zircon. Journal of Petrology, 48(8), 1605-1639. https://doi.org/10.1093/petrology/egm032